

AN ANALYTICAL AND EXPERIMENTAL STUDY OF THE INFLUENCE
OF COMPONENT VISCOELASTIC SHEAR MODES ON
LAUNCH VEHICLE TORSIONAL DYNAMICS

FACILITY FORM 602

N70-30379

130
(PAGES)

TMX-62955
(NASA CR OR TMX OR AD NUMBER)

7
(CODE)

32
(CATEGORY)

By

Ross L. Goble

Thesis submitted to the Graduate Faculty of the
Virginia Polytechnic Institute

in candidacy for the degree of

DOCTOR OF PHILOSOPHY

in

Engineering Mechanics



May 1970

AN ANALYTICAL AND EXPERIMENTAL STUDY OF THE INFLUENCE
OF COMPONENT VISCOELASTIC SHEAR MODES ON
LAUNCH VEHICLE TORSIONAL DYNAMICS

by :

Ross L. Goble

Thesis submitted to the Graduate Faculty of the
Virginia Polytechnic Institute
in partial fulfillment of the requirements for the degree of
DOCTOR OF PHILOSOPHY.

in

Engineering Mechanics

APPROVED:

Chairman, Dr. H. F. Brinson

Dr. J. Counts

Dr. R. P. McNitt

Dr. G. A. Gray

Prof. A. A. Pap

May 1970

Blacksburg, Virginia

ACKNOWLEDGMENTS

The author expresses his sincere appreciation to Mr. Vernon Alley of the Dynamics Analysis Branch at NASA Langley Research Center for his guidance, to the NASA for its support, and to Dr. Halbert F. Brinson of the Engineering Mechanics Department of Virginia Polytechnic Institute for his technical advice and help. The invaluable assistance of Mrs. Joy Rodgers, Mrs. Glenna Martin, and Mrs. Remona Sturgill in typing the final manuscript accurately and expediently is also appreciated. Finally the author dedicates this thesis to his wife Mabel and children, Deborah, Pamela, and Gregory for their love, encouragement, and understanding during his academic pursuits.

AN ANALYTICAL AND EXPERIMENTAL STUDY OF THE INFLUENCE
OF COMPONENT VISCOELASTIC SHEAR MODES ON
LAUNCH VEHICLE TORSIONAL DYNAMICS

By

Ross L. Goble

ABSTRACT

This research report presents an analytical investigation of the influence of viscoelastic shear modes of a solid propellant motor on the torsional dynamics of the parent launch vehicle system. The equations of motion which describe the behavior of the propellant in pure shear are derived from the theory of elasticity, with the propellant mathematically modeled as a thick-walled hollow cylinder. The resulting general solution of the governing Bessel's equation is then evaluated for free-free, free-pinned, and pinned-free boundary conditions. The frequency determinant is also established for the same boundary conditions. A correspondence principle is invoked to obtain the associated propellant frequency characteristics in the viscoelastic regime. The composite system problem consisting of the combined propellant and launch vehicle components is then developed using Lagrange's equations for dissipative systems with coupling constraint conditions expressed as Lagrange Multiplier relations. Small damping assumptions are made, and the problem is expressed in matrix form. A frequency scaling technique is used to circumvent the singularity problems which arise in the solution of the system eigenvalue problem due to the presence of the

Lagrange multiplier relations. A simplified experimental technique is then employed to verify the method of systems analysis.

Application of the analysis to the torsional dynamics of a contemporary axisymmetric launch vehicle with a small solid propellant segment attached as an upper stage is presented. Comparisons of system dynamic characteristics for the assumptions of elastic, viscoelastic and rigid propellant inertias are provided. Results indicate the necessity for considering propellant shear flexibility about the rotational axis of symmetry in assessing composite system dynamic response to oscillatory torsional excitations during flight.

TABLE OF CONTENTS

CHAPTER	PAGE
I. INTRODUCTION	1
II. DERIVATION OF THEORY	6
Pure Shear Elasticity Solution	6
Viscoelastic Solution.	13
III. SYSTEMS ANALYSIS	18
Solution of System Equations	36
IV. VERIFICATION OF SYSTEMS ANALYSIS	41
Test Method	47
Test Results	53
V. EXAMPLE SYSTEMS PROBLEM.	59
Discrete Vehicle Model.	62
Propellant Model	67
Vehicle Systems Analysis	67
Discussion of Results.	77
VI. CONCLUDING REMARKS	81
VII. BIBLIOGRAPHY	84
VIII. VITA	88
IX. APPENDICES	89
A. General Frequency and Modal Relations for Propellant Shear Dynamics.	89
B. Orthogonality of the Component Modes	94
Thick-Walled Cylinder Component.	94
Elastic Thin-Walled Cylinder Component	96

CHAPTER	PAGE
C. Asymptotic Approximations.	97
D. Method of Obtaining Higher Modes	103
E. Computer Programs.	107
Propellant Cylinder Shear Modes.	108
Systems Eigenvalue Program	113

LIST OF TABLES AND FIGURES

TABLE	PAGE
I. Shaft-disc physical parameters	44
II. Results of shaft-disc experiment and analysis	56
III. Atlas discrete torsional stiffness and inertias	65
IV. Propellant physical data.	70
V. Launch vehicle system modes and frequencies for various propellant assumptions.	79
FIGURE	
1. Propellant section coordinates.	7
2. Launch vehicle system physical components schematic	19
3. Disc-shaft experimental model schematic	43
4. Analytical disc free-free mode shapes	45
5. Analytical neoprene disc characteristics at system frequencies	46
6. Free-free suspension for experiment	48
7. Vibration shaker mounting for experiment.	49
8. Radial accelerometer orientation schematic	50
9. Neoprene disc	51
10. Neoprene disc location in system.	52
11. Complete test setup	54
12. Experimental steel disc	55
13. Analytical vs experimental mode shapes for neoprene disc at system frequencies	57
14. Atlas FIRE configuration.	60

FIGURE	PAGE
15. Booster torsional input	61
16. Solid propellant mounting schematic	63
17. Atlas math model	64
18. Launch vehicle torsional modes and frequencies without solid propellant	68
19. Propellant shear mode shapes	71
20. Elastic propellant shear deflections at system frequencies	73
21. Launch vehicle deflections at system frequencies with elastic propellant	74
22. Viscoelastic propellant shear deflections at system frequencies	75
23. Launch vehicle deflections at system frequencies with viscoelastic propellant	76
24. Launch vehicle deflections at system frequencies with rigid propellant	78

LIST OF SYMBOLS

A listing of all major symbols used in the body of this report is contained in this section.

a_1, a_2, a_3, a_4	Coefficients
a_n, c_i	Modal coefficients and generalized coordinates
$a_{l,k}$	Coefficients of Lagrange multipliers
\bar{a}_n, \bar{c}_i	Modal time dependent coefficients
A, B	Coefficients
e	Exponential
F_ϕ	Body force per unit volume
γ	Dissipation function
$\bar{G}(\omega_v)$	Transformed viscoelastic shear modulus
G^0	Shear modulus, at zero frequency
G_1	Shear storage modulus
G_2	Shear loss modulus
G_F	Elastic shear modulus, thick-walled cylinder
h	Thickness, thin-walled cylinder
I_{F_n}	Generalized inertia-propellant nth mode
I_{V_j}	Generalized inertia-vehicle jth mode
J_n	Bessel's function of the first kind of order n
J_{IV}	Rotational polar moment of inertia, vehicle
k_n	Propellant modal damping coefficient
K_1, K_2	Coefficients
l	Propellant length

L	Vehicle length
M_{Pn}	Generalized mass, propellant nth mode
$p(r)$	Circumferential shear deflection at the rth station
$p_n(r)$	Nth shear mode
$\bar{p}_n(r)$	Nth shear mode normalized
q_k	Generalized coordinate
r	radial coordinate
R_i	Cylinder inside radius
R_o	Cylinder outside radius
s	Vehicle longitudinal coordinate
t	Time
T	Kinetic energy
u	Vector displacement
u, v	Arbitrary variables
U	Potential energy
u	Vector
Y_n	Bessel's function of the second kind of order n
$Z(x)$	Rotational mass moment of inertia of the vehicle
α, β, μ	Trigonometric functions
δ	Mass density, propellant
∇	Del operator
ϵ, κ	Exponents
$\gamma_{r\phi}$	Shear strain
λ	Eigenvalue
λ'	Scaled eigenvalue

ρ	Circumferential deflection
ρ_s	Density, thin-walled cylinder
φ	Angular coordinate
$\tau_{r\varphi}$	Shear stress
ω	Natural frequency
ω_e	Elastic natural frequency
ω_v	Viscoelastic natural frequency
ζ	Vehicle angular displacement
Subscripts	
e	Elastic element
F	Propellant
i, j	Modal coefficient range, vehicle
g, h	General modes
n, m	Modal coefficient range, propellant
v	Viscoelastic element
x	Length index
Superscripts	
g, h, q	General modes

I. INTRODUCTION

Various analytical methods have been developed for examining the dynamical behavior of viscoelastic propellants to include the effects of temperature and pressure [1-4], angular oscillation effects on ablation [5], thermomechanical behavior during cyclic loading [6], free and forced multiaxis vibrations [7-18], and other dynamic phenomena [19, 20]. In short, the viscoelastic cylinder, case bonded at its outer boundary to an elastic cylinder, has been rigorously treated analytically for a wide range of significant boundary conditions and motion characteristics. These analytical methods deal in general with highly idealized structures, but have application to launch vehicles wherein the solid propellant motor is the prime mover. Even so, Baltrukonis [21] has pointed out the lack of well-founded methods to quantitatively evaluate the contributions of the propellant to the dynamic responses of the composite structure. Achenbach [22] also has stated that the interaction of the combustion process and the mechanical vibrations of the solid rocket should be further investigated.

An equally important interaction is that arising in launch vehicle systems where small solid propellant rocket motors are used in upper stages of launch vehicles in which the main stage is liquid-fueled. In this case the solid propellant prior to its ignition is generally treated as a rigid body in analyzing the overall vehicle modal characteristics. Otherwise, the coupled system thus described has received little attention in the literature. The rigid body simulation

of the solid propellant, however, is not thought to be sufficient for analysis of the vehicle system response to oscillatory torsional excitations which can occur in the flight profile. The purpose of the present paper is to investigate the torsional response characteristics of a more realistic launch vehicle system comprised of a long elastic thin-walled vehicle cylinder containing a concentric viscoelastic solid propellant upper stage attached over a short portion of the elastic vehicle cylinder. Comparisons of the response frequencies and mode shapes of the total system for various assumptions concerning the viscoelastic cylinder are presented. The primary value of the investigation lies in the fact that the majority of the work done to date involving elastic and viscoelastic cylinders with application to solid propellants has pertained to the solid propellant and its bonded container per se without relation to the overall systems problem.

As pointed out by Achenbach [23], analytical methods for determination of propellant dynamics are important, not only to ensure propellant structural integrity, but also to provide information on propellant natural frequencies and mode shapes for analysis of the complete launch vehicle dynamics. It is a problem in this latter category to which the present investigation is addressed.

As previously mentioned, while the dynamics of solid propellants have been examined considerably in the literature, natural vibration characteristics of propellants in twist or torsion appear to have received the least attention.

There have been some recent works, however, which treat the torsion problem well. An example is the work by Kelkar [24] which provides a closed-form solution for a hollow elastic cylinder bonded to a thin casing of a different material. Three-dimensional elasticity theory is utilized, and the approach represents a higher degree of sophistication than torsional solutions such as Achenbach's [25] which involved only one displacement component.

Other investigators such as Sam and Shaffer [26] and Baltrukronis, Chi, and Gottenberg [27] performed elastic transverse vibration studies for layered cylinders in which two displacement components were obtained. Since the problem under consideration, however, is one of total vehicle torsional response in which the encased propellant represents but one entity, it was important to survey the literature for studies pertinent to dynamics of vehicle systems. It was found that even when launch vehicle systems have been considered, attention has generally been directed analytically and experimentally toward modes of vibration and response characteristics which do not pertain to torsion [28-33]. Matrix methods for discrete mass launch vehicle representation are, of course, plentiful and practical since such vehicles are generally composite axisymmetric bodies, discontinuous with regard to distribution of physical characteristics along the axis of symmetry. (An example is provided in reference [34].) While many analytical methods exist for motion analysis of such vehicles, using single beam discrete mass representation [35] as well as branched-beam methods [36], recourse to discrete analogies and numerical methods of solution via computer are

commonplace; therefore, existing analogies will be used for the discontinuous elastic cylinder portion of the system investigated herein.

Governing equations for the pure shear natural modes and frequencies of a thick-walled cylindrical propellant are derived from basic linear elasticity theory considering free-free, free-pinned, and pinned-free boundary conditions. A dynamical correspondence principle is then used to obtain the natural frequencies in the viscoelastic medium. The short viscoelastic cylindrical propellant - long elastic cylindrical vehicle system is coupled through the use of Lagrange Multiplier constraint relations. Lagrange's equations are then used to develop the total system eigenvalue problem. Variations in the elastic restraints at the viscoelastic disc - elastic cylinder interface then permit system dynamic characteristics to be examined on a parametric constraint condition basis.

The eigenvectors obtained define the modal coefficients of the component modes which are subsequently used to establish system modes at the composite system frequencies. The analytical method thus developed is sufficiently general to handle a wide array of linear non-homogeneous systems of equations wherein the physical dynamics problem includes elastic or viscoelastic elements separately or in combination. As previously mentioned, the method has particular application to the launch vehicle system problem at hand.

A simplified disc-shaft experimental model used to verify the method of systems analysis is discussed, and analytical system natural

frequency characteristics are compared against the experimentally determined data.

The method of analysis is then applied to a characteristic launch vehicle. Elastic, viscoelastic, and rigid propellant shear modes are used, respectively, in combination with launch vehicle torsional modes to provide a comparative study as to the effects of such propellant assumptions on launch vehicle system torsional response characteristics.

II. DERIVATION OF THEORY

The approach taken in solving the systems dynamical problem is to first develop the dynamic elasticity solution for the propellant segment (figure 1) in a pure shear mode. (Justification for the assumption that the propellant segment behaves in pure shear is provided later in the discussion of the theory application to a launch vehicle system problem.)

Both the elastic and viscoelastic propellant dynamic characteristics are developed in the present chapter.

Pure Shear Elasticity Solution

The tangential equilibrium equation for plane problems in polar coordinates is [37].

$$\frac{1}{r} \frac{\partial \sigma_{\phi}}{\partial \phi} + \frac{\partial \tau_{r\phi}}{\partial r} + 2 \frac{\tau_{r\phi}}{r} + F_{\phi} = 0 \quad (2-1)$$

The body force per unit volume, F_{ϕ} , can be expressed for the shear problem as

$$F_{\phi} = -\delta \frac{d^2 \rho}{dt^2} \quad (2-2)$$

but $\rho = \phi r$, thus

$$F_{\phi} = -\delta r \ddot{\phi} \quad (2-3)$$

Now, making the assumption of pure shear motion, substituting relation (2-3) into (2-1), and simplifying, the governing equation becomes

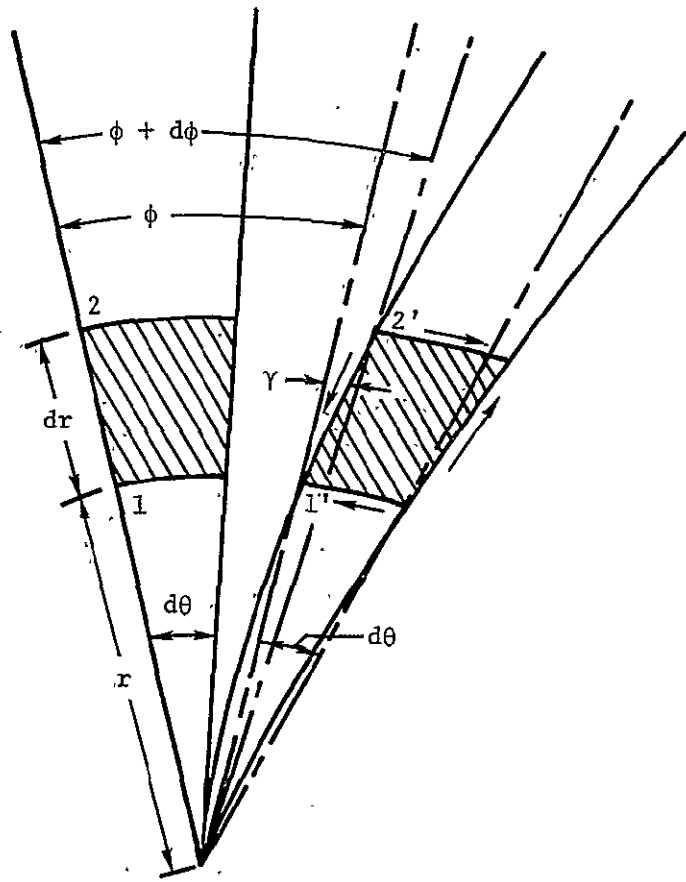
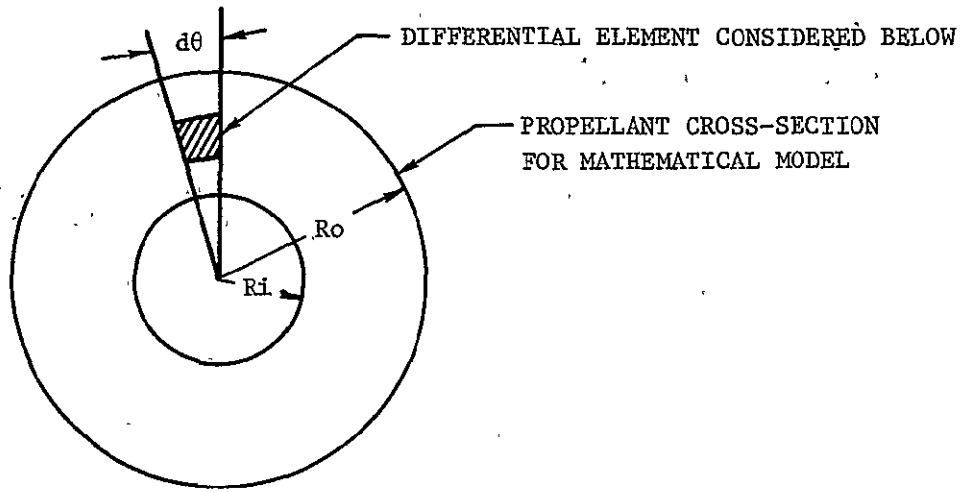


Figure 1.- Propellant section coordinates.

$$\delta r^2 \ddot{\varphi} - 2\tau_{r\varphi} - r \frac{\partial \tau_{r\varphi}}{\partial r} = 0 \quad (2-4)$$

Expressing the shear stress in terms of the shear modulus,

$$\tau_{r\varphi} = G_F \gamma_{r\varphi} \quad (2-5)$$

and it can be seen from figure 1 that the shearing strain is

$$\gamma_{r\varphi} = r \frac{\partial \varphi}{\partial r} \quad (2-6)$$

Therefore

$$\tau_{r\varphi} = G_F r \frac{\partial \varphi}{\partial r} \quad (2-7)$$

Also

$$\frac{\partial \tau_{r\varphi}}{\partial r} = \left(r \frac{\partial^2 \varphi}{\partial r^2} + \frac{\partial \varphi}{\partial r} \right) G_F \quad (2-8)$$

Making the substitution of relations (2-7) and (2-8) into (2-4) and simplifying, the governing equation takes the form

$$\frac{\partial^2 \varphi}{\partial r^2} + \frac{3}{r} \frac{\partial \varphi}{\partial r} - \frac{\delta}{G_F} \ddot{\varphi} = 0 \quad (2-9)$$

Now $\rho = \varphi r$, and if it is assumed that the cylinder oscillates with undamped harmonic motion, $\rho(r,t) = p(r)e^{i\omega t}$, and the first order derivative of equation (2-9) is obtained as

$$\frac{\partial \varphi}{\partial r} = \frac{r \frac{\partial \rho}{\partial r} - \rho}{r^2} = \frac{1}{r} \frac{\partial \rho}{\partial r} - \frac{\rho}{r^2} = e^{i\omega t} \left(\frac{p'}{r} - \frac{p}{r^2} \right) \quad (2-10)$$

where for the sake of brevity, $\rho = \rho(r,t)$ and $p = p(r)$ here and in

the following development. The second order derivative of (2-9) is developed from (2-10) as

$$\frac{\partial^2 \varphi}{\partial r^2} = \frac{r \frac{\partial^2 p}{\partial r^2} - \frac{\partial p}{\partial r}}{r^2} - \frac{r^2 \frac{\partial p}{\partial r}}{r^4} + \frac{2rp}{r^4} = e^{i\omega t} \left(\frac{p''}{r} - \frac{p'}{r^2} - \frac{p'}{r^2} + \frac{2p}{r^3} \right) \quad (2-11)$$

Also

$$\ddot{\varphi} = \frac{\ddot{p}}{r} = -\omega^2 e^{i\omega t} \frac{p}{r} \quad (2-12)$$

Making substitution of relations (2-10), (2-11), and (2-12) into equation (2-9), and multiplying through by $e^{-i\omega t}$ results in the differential equation

$$\frac{p''}{r} - \frac{p'}{r^2} - \frac{p'}{r^2} + \frac{2p}{r^3} + \frac{3p'}{r^2} - \frac{3p}{r^3} + \frac{\delta}{G_F} \omega^2 \frac{p}{r} = 0 \quad (2-13)$$

which can be simplified to

$$p'' + \frac{p'}{r} + \left[\omega^2 \frac{\delta}{G_F} - \frac{1}{r^2} \right] p = 0 \quad (2-14)$$

Making the substitution $\frac{\omega^2 \delta}{G_F} = \lambda^2$ into (2-14) yields

$$p'' + \frac{p'}{r} + \left(\lambda^2 - \frac{1}{r^2} \right) p = 0 \quad (2-15)$$

which is precisely the Bessel's equation of first order with parameter λ , for which the solution is

$$p(r) = AJ_1(\lambda r) + BY_1(\lambda r) \quad (2-16)$$

The physical boundary conditions for the free-free natural mode investigation are that the shear vanish at $r = R_0$ and $r = R_1$; therefore, $\left. \frac{\partial \phi}{\partial r} \right|_{R_1} = \left. \frac{\partial \phi}{\partial r} \right|_{R_0} = 0$ (by equation (2-7)); hence $\frac{dp}{dr} = \frac{p(r)}{r}$

(by equation (2-10)); thus

$$\left. \frac{dp}{dr} \right|_{R_0} = \frac{p(R_0)}{R_0}, \quad \left. \frac{dp}{dr} \right|_{R_1} = \frac{p(R_1)}{R_1} \quad (2-17)$$

Substituting equation (2-16) into the outer and inner radius boundary conditions of (2-17) yields

$$AJ_1'(\lambda R_0) + BY_1'(\lambda R_0) = \frac{p(R_0)}{\lambda R_0} \quad (2-18)$$

$$AJ_1'(\lambda R_1) + BY_1'(\lambda R_1) = \frac{p(R_1)}{\lambda R_1} \quad (2-19)$$

Substituting for $p(R_0)$ and $p(R_1)$ in equations (2-18) and (2-19) in terms of the exact solution (2-16) and rearranging, the resulting set of simultaneous equations is

$$\begin{aligned} A \left[J_1'(\lambda R_0) - \frac{1}{\lambda R_0} J_1(\lambda R_0) \right] + B \left[Y_1'(\lambda R_0) - \frac{1}{\lambda R_0} Y_1(\lambda R_0) \right] &= 0 \\ A \left[J_1'(\lambda R_1) - \frac{1}{\lambda R_1} J_1(\lambda R_1) \right] + B \left[Y_1'(\lambda R_1) - \frac{1}{\lambda R_1} Y_1(\lambda R_1) \right] &= 0 \end{aligned} \quad (2-20)$$

Now the recurrence relations for Bessel functions include the following:

$$\bar{x} J_n'(\bar{x}) = \bar{x} J_{n-1}(\bar{x}) - n J_n(\bar{x}) \quad (2-21)$$

where n indicates the order, and \bar{x} , the argument. Also

$$\bar{x}Y_n'(\bar{x}) = \bar{x}Y_{n-1}(\bar{x}) - nY_n(\bar{x}) \quad (2-22)$$

Making substitution of (2-21) and (2-22) into (2-20), the resulting set of equations, simplified and expressed in matrix form is

$$\begin{bmatrix} \lambda_{R_0}J_0(\lambda_{R_0}) - 2J_1(\lambda_{R_0}) & \lambda_{R_0}Y_0(\lambda_{R_0}) - 2Y_1(\lambda_{R_0}) \\ \lambda_{R_1}J_0(\lambda_{R_1}) - 2J_1(\lambda_{R_1}) & \lambda_{R_1}Y_0(\lambda_{R_1}) - 2Y_1(\lambda_{R_1}) \end{bmatrix} \begin{Bmatrix} A \\ B \end{Bmatrix} = 0 \quad (2-23)$$

The system of equations (2-23) has a solution other than the trivial solution if, and only if, the determinant of the coefficients is equal to zero. The resulting secular equation for the roots λ_n is thus

$$\begin{aligned} & \left[\lambda_{nR_0}J_0(\lambda_{R_0}) - 2J_1(\lambda_{R_0}) \right] \left[\lambda_{nR_1}Y_0(\lambda_{R_1}) - 2Y_1(\lambda_{R_1}) \right] \\ & - \left[\lambda_{nR_0}Y_0(\lambda_{R_0}) - 2Y_1(\lambda_{R_0}) \right] \left[\lambda_{nR_1}J_0(\lambda_{R_1}) - 2J_1(\lambda_{R_1}) \right] = 0 \quad (2-24) \end{aligned}$$

The mode shape can now be developed with the boundary conditions expressed in terms of the Bessel's functions.

Substituting equation (2-16) into equation (2-19) for $p(r)$ evaluated at $r = R_1$ yields, after simplifying

$$A \left[J_1'(\lambda_{R_1}) - \frac{J_1(\lambda_{R_1})}{\lambda_{R_1}} \right] = -B \left[Y_1'(\lambda_{R_1}) - \frac{Y_1(\lambda_{R_1})}{\lambda_{R_1}} \right] \quad (2-25)$$

or

$$A = -\bar{B} \frac{\left[Y_1'(\lambda R_1) - \frac{Y_1(\lambda R_1)}{\lambda R_1} \right]}{\left[J_1'(\lambda R_1) - \frac{J_1(\lambda R_1)}{\lambda R_1} \right]} \quad (2-26)$$

Thus the mode shape (2-16) eliminating the arbitrary constant A is

$$p(r) = B \left\{ Y_1(\lambda r) - \frac{\left[Y_1'(\lambda R_1) - \frac{Y_1(\lambda R_1)}{\lambda R_1} \right]}{\left[J_1'(\lambda R_1) - \frac{J_1(\lambda R_1)}{\lambda R_1} \right]} J_1(\lambda r) \right\} \quad (2-27)$$

or after use of equations (2-21) and (2-22) and further simplifying, (2-27) becomes

$$p(r) = \bar{B} \left\{ \left[\lambda R_1 J_0(\lambda R_1) - 2J_1(\lambda R_1) \right] Y_1(\lambda r) - \left[\lambda R_1 Y_0(\lambda R_1) - 2Y_1(\lambda R_1) \right] J_1(\lambda r) \right\} \quad (2-28)$$

where

$$\bar{B} = \frac{B}{\lambda R_1 J_0(\lambda R_1) - 2J_1(\lambda R_1)}$$

and since B is arbitrary, we can choose it such that $\bar{B} = 1$.

The mode shape normalized at $r = R_0$ takes the final form

$$\bar{p}(r) = \frac{\left[\lambda R_1 J_0(\lambda R_1) - 2J_1(\lambda R_1) \right] Y_1(\lambda r) - \left[\lambda R_1 Y_0(\lambda R_1) - 2Y_1(\lambda R_1) \right] J_1(\lambda r)}{\left[\lambda R_1 J_0(\lambda R_1) - 2J_1(\lambda R_1) \right] Y_1(\lambda R_0) - \left[\lambda R_1 Y_0(\lambda R_1) - 2Y_1(\lambda R_1) \right] J_1(\lambda R_0)} \quad (2-29)$$

Thus the free-free motion of the elastic propellant segment is completely defined by equation (2-24) for frequencies and (2-29) for mode shapes.

Before proceeding to the viscoelastic solution for the propellant, brief discussion of three appendices related to the propellant modes is in order. General frequency and modal relations, for which equations (2-24) and (2-29) are special cases, have been included in Appendix A. Other boundary conditions described by selection of proper coefficients in these general relations are pinned-free and free-pinned shear mode conditions. Orthogonality conditions for the free-free modes are developed in Appendix B. Also, an alternate method of solving expressions (2-24) and (2-29) using asymptotic approximations to the Bessel's functions is provided in Appendix C. This method of solution to the problem at hand was developed specifically for an early stage of the analysis and, to the author's knowledge, does not exist elsewhere in the published literature. It should also be pointed out here that a computer program has been developed for this investigation to solve relations (2-24) and (2-29) and is included in Appendix E.

Returning to the present analytical process, it is next required to establish the viscoelastic natural motion description for the propellant in shear. Equations (2-24) and (2-29) will be used in this development.

Viscoelastic Solution

It is well known that various means can be employed to obtain the viscoelastic solution directly from the elastic solution provided certain criteria are met such that the dynamical correspondence principle applies. Although many quasi-static problems have been solved through the use of Laplace transform techniques, few classes

of dynamical problems have been solved via correspondence principles. As is pointed out in the literature [38], Fourier transform techniques have been employed for some dynamical problems, with inversion of the transformed solution after substitution of viscoelastic moduli often being quite difficult. Fisher and Leitman [39] have developed a correspondence principle which utilizes the Fourier transform technique and which applies to the propellant natural motion being considered herein. The authors provide an analytical proof for the hypothesis that if the elastic mode shapes of simple free vibration are dependent upon only one relevant relaxation function, the viscoelastic mode shapes are the same as those developed for the associated elastic material (specifically, those described by equation (2-29) in the present analysis), and the frequencies are related by the expression

$$\left[\frac{\omega_v}{\omega_e}\right]^2 = 1 + \frac{\bar{G}(\omega_v)}{G^0} \quad (2-30)$$

where

ω_v = viscoelastic natural frequency

ω_e = elastic natural frequency established by equation (2-24)

G^0 = the zero frequency, (or elastic) shear modulus

and

$$\bar{G}(\omega_v) = \int_0^{\infty} \dot{G}(s) e^{-i\omega_v s} ds$$

which is the transform of the viscoelastic shear modulus. Equation (2-30) evolves from the following considerations. Using the notation of [39], an operator L_G is defined as

$$L_G g(x, t) = G^0 g(x, t) + \int_0^\infty \dot{G}(s) g(x, t-s) ds \quad (2-31)$$

where G^0 = the shear modulus at zero frequency and $G(s)$ is a real-valued differentiable function on $(0, \infty)$ whose derivative $\dot{G}(s)$ is absolutely integrable. Also, the integral $\bar{G}(\omega_V)$ is defined as

$$\bar{G}(\omega_V) = \int_0^\infty \dot{G}(s) e^{-i\omega_V s} ds \quad (2-32)$$

For solenoidal motion of a homogeneous isotropic viscoelastic solid, the governing equations can be written as

$$-L_G \nabla \times (\nabla \times u) = \frac{\partial^2 u}{\partial t^2} \quad (2-33)$$

where u is the displacement function and

$$G = \text{the shear function} = \frac{G^0 + \bar{G}(\omega_V)}{2\delta}$$

Now if simple free vibrations are assumed, where the definition of simple [39] for solenoidal motion is

$$\nabla \cdot u = 0$$

then $u(x, t) = f(x) e^{i\omega_V t}$, and by making use of equation (2-31) and (2-32), (2-33) becomes

$$\nabla^2 f(x) + \frac{2\delta\omega_V^2}{G^0 + \bar{G}(\omega_V)} f(x) = 0 \quad (2-34)$$

Also for the elastic regime, if $f(x)e^{i\omega t}$ describes a simple free vibration, the resulting equations of motion are

$$\nabla^2 f(x) + \frac{2\delta\omega_e^2}{G^0} f(x) = 0 \quad (2-35)$$

Subtracting (2-35) from (2-34) and simplifying yields

$$\left[\frac{\omega_V}{\omega_e}\right]^2 = 1 + \frac{\bar{G}(\omega_V)}{G^0} \quad (2-36)$$

which is the same relation as (2-30) and means that for a simple free vibration, the mode shapes of the viscoelastic solid are the same as those of the associated elastic solid and the frequencies are related by (2-36). Note that $\bar{G}(\omega_V)$ is the Fourier transform shear modulus and we seek the value in the frequency domain, such that the relation (2-36) is usable in its present form. Now it has been shown that for many filled and unfilled polymers, the storage and loss moduli, G_1 and G_2 , respectively, may be replaced in the expression $\bar{G}(\omega_V) = G_1(\omega_V) + iG_2(\omega_V)$

by

$$G_1 = K_1\omega_V^\kappa \quad (2-37)$$

and

$$G_2 = K_2\omega_V^\epsilon \quad (2-38)$$

where K_1 and K_2 are constants and κ and ϵ are exponents.

It has also been shown that for specific frequency ranges of interest, the ratio of loss modulus to storage modulus is quite small, implying small damping. The assumption will be made at this point,

therefore, that the loss modulus may be neglected. Therefore, replacing $\bar{G}(\omega_V)$ in expression (2-20) with the storage modulus G_1 from (2-21), one obtains

$$\left[\frac{\omega_V}{\omega_e} \right]^2 = 1 + \frac{K_1 \omega_V \kappa}{G_0} \quad (2-39)$$

Note that frequency dependence of the viscoelastic shear modulus is retained with the complex component neglected. This implies that the analysis hereafter is viscoelastic in the sense that the shear storage modulus is frequency dependent, but is quasi-elastic in the sense that damping is neglected. Thus, the free-free propellant shear motion description is complete, with elastic eigenvalues, λ , established by relation (2-24), and elastic frequencies determined by

$$\omega_e^2 = \frac{\lambda^2 G_F}{\delta} ;$$

Viscoelastic frequencies are given by relation (2-39), and viscoelastic (as well as elastic) propellant modes are established by equation (2-29). It is now necessary to develop the systems problem by deriving the governing equations which couple the viscoelastic propellant segment to the launch vehicle cylinder. This derivation is contained in the following chapter.

III. SYSTEMS ANALYSIS

To this point, we have developed the propellant free-free normal mode solution (2-29) and the viscoelastic frequency expression (2-39), both restated here for the purpose of continuity

$$\bar{p}(r) = \frac{\left[\lambda R_1 J_0(\lambda R_1) - 2J_1(\lambda R_1) \right] Y_1(\lambda r) - \left[\lambda R_1 Y_0(\lambda R_1) - 2Y_1(\lambda R_1) \right] J_1(\lambda r)}{\left[\lambda R_1 J_0(\lambda R_1) - 2J_1(\lambda R_1) \right] Y_1(\lambda R_0) - \left[\lambda R_1 Y_0(\lambda R_1) - 2Y_1(\lambda R_1) \right] J_1(\lambda R_0)} \quad (2-29)$$

$$\left[\frac{\omega}{\omega_e} \right]^2 = 1 + \frac{K_1 \omega^k}{G^0} \quad (2-39)$$

These mode and frequency expressions will be used in the development of the systems analysis which follows. In order to develop the governing equations of motion which describe the system dynamics, we will require four basic elements which are as follows:

- (1) Propellant free-free natural modes in shear
- (2) Viscoelastic propellant frequencies
- (3) Vehicle elastic free-free natural modes and frequencies in torsion
- (4) Appropriate physical constraint conditions which couple the propellant and vehicle modes together.

A graphic description of the system physical components is provided in figure 2.

The approach used in developing the coupled system problem is the convenient Lagrange's equations method, with the equations expressed in the general form for dissipative systems

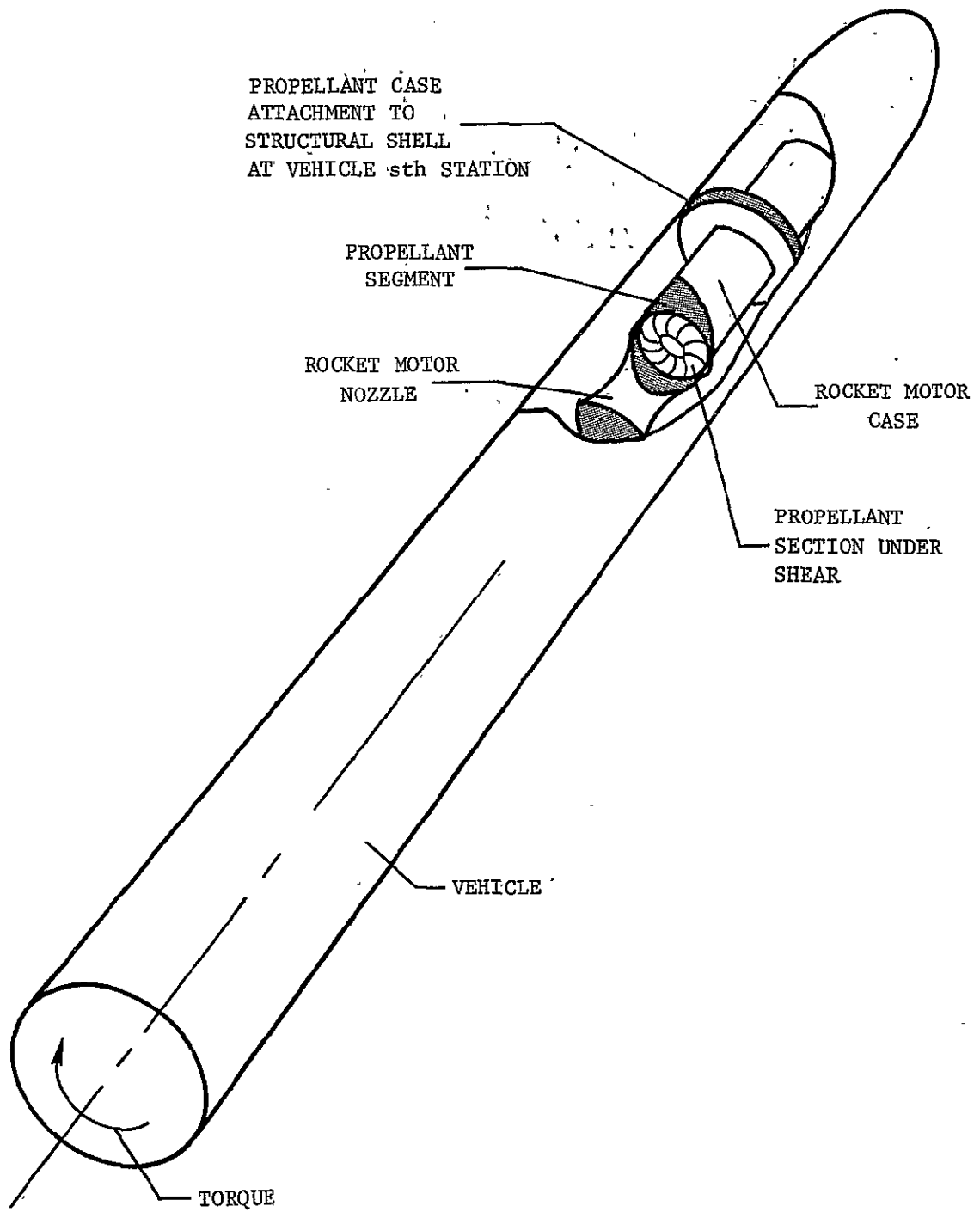


Figure 2.- Launch vehicle system physical components schematic.

$$\frac{d}{dt} \left(\frac{\partial L}{\partial \dot{q}_{ik}} \right) - \frac{\partial L}{\partial q_{ik}} + \frac{\partial \mathcal{F}}{\partial \dot{q}_{ik}} = \sum_l \lambda_l a_{lk} \quad (3-1)$$

where L = the Lagrangian = T (the total system kinetic energy) -
 U (the total system potential energy)

\mathcal{F} = dissipation function (velocity dependent)

λ_l = Lagrange multipliers

a_{lk} = coefficients of the Lagrange multipliers

Dissipation has been considered in order to make the solution more general, even though damping has been considered as negligible in the previous propellant dynamics development.

Now the Lagrangian requires development of the system kinetic and potential energies. The kinetic energy per unit volume for the propellant segment in shear is

$$dT_F = \frac{1}{2} \rho \dot{d}_m^2 \quad (3-2)$$

Now ρ in (3-2) can be expressed in modal series form as

$$\rho = \sum_n \bar{a}_n p_n(r) \quad (3-3)$$

where

$$\bar{a}_n = a_n e^{i\omega t}$$

Therefore, integrating over the propellant volume, $rdrd\theta$, the propellant kinetic energy becomes

$$T_F = \frac{1}{2} l \delta \int_0^{2\pi} \int_{R_i}^{R_o} r \left[\sum_n \dot{a}_n p_n(r) \right]^2 dr$$

or

$$T_F = \pi l \delta \int_{R_i}^{R_o} r \left[\sum_n \dot{a}_n p_n(r) \right]^2 dr \quad (3-4)$$

Also the kinetic energy of the launch vehicle can be expressed as

$$T_{LV} = \frac{1}{2} \int_0^L Z(x) \dot{\theta}_{LV}(x,t)^2 dx \quad (3-5)$$

Again, modal series representation of the angular deflection θ in (3-5) will be used, that is

$$\theta_{LV} = \sum_i \bar{c}_i \zeta_i(s) \quad (3-6)$$

where

$$\bar{c}_i = c_i e^{i\omega t}$$

Therefore, making substitution of (3-6) into (3-5) yields

$$T_{LV} = \frac{1}{2} \int_0^L Z(x) \left[\sum_i \dot{\bar{c}}_i \zeta_i(s) \right]^2 dx \quad (3-7)$$

The total system energy is obtained by adding (3-7) to (3-4), or

$$T = \pi l \delta \int_{R_i}^{R_o} r \left[\sum_n \dot{a}_n p_n(r) \right]^2 dr + \frac{1}{2} \int_0^L Z(x) \left[\sum_i \dot{\bar{c}}_i \zeta_i(x) \right]^2 dx \quad (3-8)$$

Now the potential energy in shear of the propellant per unit volume can be written as

$$\frac{U_F}{\text{vol.}} = \frac{1}{2} \tau_{r\varphi} \gamma_{r\varphi}, \quad (3-9)$$

where the volume is $2rdrd\theta$ as defined before. The shear stress $\tau_{r\varphi}$ has been given in relation (2-7), as

$$\tau_{r\varphi} = G_F r \frac{\partial \varphi}{\partial r}$$

Also, from relation (2-6), the shear strain $\gamma_{r\varphi}$ is

$$\gamma_{r\varphi} = r \frac{\partial \varphi}{\partial r}$$

Substitution of (2-6) and (2-7) into (3-9) and integration over the volume yields

$$U_F = \frac{1}{2} \int_0^{2\pi} \int_{R_1}^{R_0} G_F \left(r \frac{\partial \varphi}{\partial r} \right)^2 r dr d\theta$$

or

$$U_F = \pi l G_F \int_{R_1}^{R_0} r \left(r \frac{\partial \varphi}{\partial r} \right)^2 dr \quad (3-10)$$

But we have shown in relation (2-10) that

$$\frac{\partial \varphi}{\partial r} = \frac{1}{r} \left(\frac{\partial \rho}{\partial r} - \frac{\rho}{r^2} \right) \quad (3-11)$$

and by relation (3-3)

$$\rho = \sum_n \bar{a}_n p_n(r)$$

Therefore

$$\frac{\partial \rho}{\partial r} = \sum_n \bar{a}_n p_n'(r) \quad (3-12)$$

where the prime indicates differentiation with respect to r .

Making substitution of relation (3-3) and (3-12) into (3-11) yields

$$\frac{\partial \rho}{\partial r} = \frac{1}{r} \left(\sum_n \bar{a}_n p_n'(r) - \sum_n \bar{a}_n \frac{p_n(r)}{r} \right) \quad (3-13)$$

Now substituting (3-13) into (3-10) and simplifying results in

$$U_F = \pi \rho G_F \int_{R_i}^{R_o} r \left[\sum_n \bar{a}_n p_n'(r) - \sum_n \bar{a}_n \frac{p_n(r)}{r} \right]^2 dr \quad (3-14)$$

which is the final relation for the potential energy of the propellant.

The potential energy of the launch vehicle can be written as

$$U_{LV} = \frac{1}{2} \int_0^L J_{LV} G_{LV} \frac{\partial \theta_{LV}}{\partial x} (x,t)^2 dx \quad (3-15)$$

But in (3-6) we had

$$\theta_{LV} = \sum_i \bar{c}_i \zeta_i(s)$$

Therefore

$$\frac{\partial \theta_{LV}}{\partial x} = \sum_i \bar{c}_i \zeta_i'(s) \quad (3-16)$$

Substituting (3-16) into (3-15) yields

$$U_{LV} = \frac{1}{2} J_{LV} G_{LV} \int_0^L \left[\sum_i \bar{c}_i \zeta_i'(s) \right]^2 dx. \quad (3-17)$$

The total system potential energy is obtained by adding relations (3-14) and (3-17) yielding

$$U = \pi l G_F \int_{R_i}^{R_o} r \left[\sum_n \bar{a}_n p_n'(r) - \sum_n a_n \frac{p_n(r)}{r} \right]^2 dr + \frac{1}{2} J_{LV} G_{LV} \int_0^L \left[\sum_i \bar{c}_i \zeta_i'(s) \right]^2 dx. \quad (3-18)$$

Thus the Lagrangian L can be obtained by subtracting (3-18) from (3-8) or

$$L = \pi l G_F \int_{R_i}^{R_o} r \left[\sum_n \dot{a}_n p_n(r) \right]^2 dr + \frac{1}{2} \int_0^L Z(x) \left[\sum_i \dot{c}_i \zeta_i(x) \right]^2 dx - \pi l G_F \int_{R_i}^{R_o} r \left[\sum_n \bar{a}_n p_n'(r) - \sum_n a_n \frac{p_n(r)}{r} \right]^2 dr - \frac{1}{2} J_{LV} G_{LV} \int_0^L \left[\sum_i \bar{c}_i \zeta_i'(s) \right]^2 dx \quad (3-19)$$

Now the dissipation function at propellant radius r , assumed to be velocity dependent is

$$\mathcal{F}(r) = \frac{1}{2} K \dot{\rho}(r,t)^2 \quad (3-20)$$

where $K = \sum_n k_n$, the damping coefficient (3-21)

and from (3-3)

$$\rho = \sum_n \bar{a}_n p_n(r)$$

or

$$\dot{\rho} = \sum_n \dot{\bar{a}}_n p_n(r) \quad (3-22)$$

Substituting (3-21) and (3-22) into (3-20) and integrating over the radius of the propellant, the dissipation function \mathcal{F} becomes

$$\mathcal{F} = \frac{1}{2} \int_{R_1}^{R_0} \sum_n k_n \left[\dot{\bar{a}}_n p_n(r) \right]^2 dr \quad (3-23)$$

Now the constraint relations which must be satisfied in coupling the propellant to the launch vehicle at the common interface at R_0 are that displacements and stresses be compatible. The mathematical statement of the displacement condition expressed in Lagrange multiplier form is

$$\lambda_1 \left[\rho - R_0 \theta_{LV} \right] = 0 \quad (3-24)$$

Now making substitution of the modal form relations (3-3) and (3-6) for the propellant and launch vehicle deflections, respectively, yields

$$\lambda_1 \left[\sum_n \bar{a}_n p_n(R_0) - R_0 \sum_i \bar{c}_i \zeta_i(s) \right] = 0 \quad (3-25)$$

Also, the continuity of stresses across the interface can be expressed as

$$\lambda_2 \left[\tau_{R_0\phi} - \tau_{R_0\theta_{LV}} \right] = 0 \quad (3-26)$$

where $\tau_{R_0\phi}$ is obtained from relation (2-7), evaluated at $r = R_0$, or

$$\tau_{r\phi} \Big|_{r=R_0} = G_F r \frac{\partial \phi}{\partial r} \Big|_{r=R_0}$$

or

$$\tau_{R_0\phi} = G_F R_0 \frac{\partial \phi}{\partial r} \Big|_{r=R_0} \quad (3-27)$$

But since modal form series have been used, we can evaluate

$\frac{\partial \phi}{\partial r} \Big|_{r=R_0}$ by using (3-13), or

$$\frac{\partial \phi}{\partial r} \Big|_{r=R_0} = \frac{1}{R_0} \left[\sum_n \bar{a}_n p_n'(R_0) - \sum_n \bar{a}_n \frac{p_n(R_0)}{R_0} \right] \quad (3-28)$$

Substituting (3-28) into (3-27) and simplifying yields

$$\tau_{R_0\phi} = G_F \left[\sum_n \bar{a}_n p_n'(R_0) - \sum_n \bar{a}_n \frac{p_n(R_0)}{R_0} \right] \quad (3-29)$$

Now the shear stress $\tau_{R_0 \theta_{LV}}$ on the launch vehicle side of the interface is in equilibrium with the inertia of the launch vehicle, or

$$\tau_{R_0 \theta_{LV}} = R_0 h \omega^2 \rho_s \theta_{LV} \quad (3-30)$$

By substitution of the modal expression (3-6) for θ_{LV} , we obtain

$$\tau_{R_0 \theta_{LV}} = R_0 h \omega^2 \rho_s \sum_i \bar{c}_i \zeta_i(s) \quad (3-31)$$

Substitution of (3-29) and (3-31) into (3-26) yields

$$\lambda_2 \left\{ G_F \sum_n \bar{a}_n p_n'(R_0) - \sum_n \bar{a}_n \frac{p_n(R_0)}{R_0} - R_0 h \omega^2 \rho_s \sum_i \bar{c}_i \zeta_i(s) \right\} = 0 \quad (3-32)$$

Equations (3-19), (3-23); (3-25), and (3-32) now provide all the essential elements required to develop the system governing equations; by performing the indicated operations of (3-1) on these four relations in the generalized coordinates $q_k = a_m, c_j$, the following equations are obtained. For $q_k = a_m$

$$\begin{aligned} & 2\pi l \delta \int_{R_i}^{R_0} r \left[\sum_n \bar{a}_n p_n(r) \right] p_m(r) dr \\ & - 2\pi l G_F \int_{R_i}^{R_0} r \left[\sum_n \bar{a}_n p_n'(r) - \sum_n \bar{a}_n \frac{p_n(r)}{r} \right] \left[p_m'(r) - \frac{p_m(r)}{r} \right] dr \\ & + \int_{R_i}^{R_0} \left[\sum_n k_n \bar{a}_n p_n(r) \right] p_m(r) dr = \lambda_1 p_m(R_0) + \lambda_2 G_F \left[p_m'(R_0) \frac{p_m(R_0)}{R_0} \right] \end{aligned} \quad (3-33)$$

and for $q_k = c_j$

$$\begin{aligned} & \int_0^L z(x) \left[\sum_i \ddot{c}_i \zeta_i(x) \right] \zeta_j(x) dx \\ & - G_{LV} \int_0^L J_{LV} \left[\sum_i \bar{c}_i \zeta_i'(x) \right] \zeta_j'(x) dx = - \lambda_1 R_0 \zeta_j(s) \\ & - \lambda_2 R_0 h \omega^2 \rho_s \zeta_j(s) \end{aligned} \quad (3-34)$$

Relations (3-25), (3-32), (3-33) and (3-34) completely define the coupled systems problem. In order to simplify and render solvable this system, recourse to orthogonality conditions in the component modes is necessary. These orthogonality conditions are derived for the propellant cylinder in Appendix B, and the elastic vehicle cylinder orthogonality relations are also given therein.

Equation (3-33) can be initially simplified by expanding the second integral to

$$2\pi l G_F \sum_n a_n \left[\int r \left(p_n' - \frac{p_n}{r} \right) p_m' dr - \int r \left(p_n' - \frac{p_n}{r} \right) \frac{p_m}{r} dr \right] \quad (3-35)$$

(where it is understood that the p 's are functions of r only and that the upper and lower integral limits are R_0 and R_1 , respectively). Integrating the first of these expanded integrals by parts by letting

$$r\left(p_n' - \frac{p_n}{r}\right) = u \quad p_m' dr = dv$$

$$\left(rp_n'' + p_n' - p_n\right) dr = du \quad p_m = v.$$

then we have

$$r\left(p_n' - \frac{p_n}{r}\right) p_m \Big|_{R_1}^{R_0} - \int_{R_1}^{R_0} rp_n'' p_m dr \quad (3-36)$$

The first term vanishes identically at the limits by virtue of the free-free boundary conditions (2-17).

Now using the D.E. of motion (eq. (2-14)), we have after rearranging

$$p_n'' = -\frac{p_n'}{r} \left(-\omega_n^2 \frac{\delta}{G_F} + \frac{1}{r^2}\right) p_n \quad (3-37)$$

where the ω_n are the viscoelastic frequencies of the propellant obtained from (2-39).

Making this substitution into equation (3-36), we have

$$-\int rp_n'' p_m dr = \omega_n^2 \frac{\delta}{G_F} \int rp_m p_n' dr + \int p_m p_n' dr - \int \frac{p_m p_n}{r} dr \quad (3-38)$$

Now, substituting the right side of relation (3-38) into equation (3-35) for the first integral and expanding the second integral, we have

$$2\pi l G_F \sum_n a_n \left[\omega_n^2 \frac{\delta}{G_F} \int r p_m p_n dr + \int p_m p_n' dr - \int \frac{p_m p_n}{r} dr \right. \\ \left. - \int p_n' p_m dr + \int \frac{p_n p_m}{r} dr \right] \quad (3-39)$$

which reduces to

$$2\pi l \delta \omega_n^2 \sum_n a_n \int r p_m p_n dr$$

Appendix B relation (B-9) indicates that a value exists only when $m = n$. Therefore, for all terms of the series when $m \neq n$,

$$2\pi l \delta \omega_n^2 \sum_n a_n \int r p_m p_n dr = 0$$

and for $m = n$,

$$2\pi l \delta \omega_n^2 \sum_n a_n \int r p_m p_n dr = a_n \omega_n^2 M_{F_n} \quad (3-40)$$

where ω_n is the viscoelastic component frequency.

Also, it can be shown from more orthodox orthogonality proofs that the second integral of equation (3-34) reduces to

$$c_j \omega_j^2 I_{V_j} \quad \text{for } i = j \quad (3-41)$$

where ω_j is the elastic component frequency.

Now simple harmonic motion in the generalized coordinates a_n and c_i has been assumed. Making use of this fact and relations (3-40) and

(3-41), it can be shown that relations (3-33) and (3-34), after some simplification, reduce to

$$\frac{a_n}{R_0} \left[(\omega_n^2 - \omega^2) I_{F_n} + i\omega R_0^2 \int_{R_1}^{R_0} k_n p_n^2(r) dr \right] + \lambda_2 R_0 G_F \left[p_n'(R_0) - \frac{p_n(R_0)}{R_0} \right] + R_0 \lambda_1 p_n(R_0) = 0 \quad (3-42)$$

and

$$c_i I_{V_i} (\bar{\omega}_i^2 + \omega^2) + \lambda_1 R_0 \zeta_i(s) + \lambda_2 R_0 h \omega^2 \rho_s \zeta_i(s) = 0 \quad (3-43)$$

where $I_{F_n} = M_{F_n} R_0^2$

and ω is the coupled system frequency.

Recasting equations (3-42) and (3-43) to separate system frequency elements from natural component frequency elements,

$$I_{F_n} \frac{a_n}{R_0} \omega^2 - \left[i\omega R_0^2 \int_{R_1}^{R_0} k_n p_n^2(r) dr \right] \frac{a_n}{R_0} = I_{F_n} \frac{a_n}{R_0} \omega_n^2 + R_0 G_F \left[p_n'(R_0) - \frac{p_n(R_0)}{R_0} \right] + R_0 p_n(R_0) \lambda_1 \quad (3-44)$$

and

$$\left[\Gamma_{V_i} c_i + R_o h \rho_s \zeta_i(s) \lambda_2 \right] = \frac{1}{\omega^2} \left[\Gamma_{V_i} c_i \bar{\omega}_i^2 - R_o \zeta_i(s) \lambda_1 \right] \quad (3-45)$$

Also, the constraint relations (3-25) and (3-32) can be rearranged

(remembering that $\bar{a}_n = a_n e^{i\omega t}$ and $\bar{c}_i = c_i e^{i\omega t}$) as follows

$$\left[\sum_n \frac{a_n}{R_o} R_o p_n(R_o) - R_o \sum_i c_i \zeta_i(s) \right] \lambda_1 = 0 \quad (3-46)$$

and

$$R_o h \rho_s \sum_i c_i \zeta_i(s) \lambda_2 \omega^2 = G_F \left[\sum_n \frac{a_n}{R_o} R_o p_n'(R_o) - \sum_n \frac{a_n}{R_o} p_n(R_o) \right] \quad (3-47)$$

Neglecting the second term of equation (3-44) which is the damping of the n th propellant mode, equations (3-44) through (3-47) can be expressed conveniently in matrix form as

$$[M] \{x\} = \frac{1}{\omega^2} [N] \{x\} \quad (3-48)$$

where $[M]$ and $[N]$ are partitioned matrices as follows

$$[M] = \left[\begin{array}{cccc|cccc|cc}
 I_{F_0} & & & & 0 & 0 & \dots & 0 & 0 & 0 \\
 & I_{F_1} & & & 0 & 0 & \dots & 0 & 0 & 0 \\
 & & \ddots & & \vdots & & \ddots & \vdots & \vdots & \vdots \\
 & & & I_{F_n} & 0 & 0 & \dots & 0 & 0 & 0 \\
 \hline
 0 & 0 & \dots & 0 & I_{V_0} & & & & 0 & R_{0h\rho_s}\zeta_0(s) \\
 0 & 0 & \dots & 0 & & I_{V_1} & & & 0 & R_{0h\rho_s}\zeta_1(s) \\
 \vdots & & \ddots & \vdots & & & \ddots & & \vdots & \vdots \\
 0 & 0 & \dots & 0 & & & & I_{V_i} & 0 & R_{0h\rho_s}\zeta_i(s) \\
 \hline
 0 & 0 & \dots & 0 & 0 & 0 & \dots & 0 & 0 & 0 \\
 \hline
 0 & 0 & \dots & 0 & R_{0h\rho_s}\zeta_0(s) & R_{0h\rho_s}\zeta_1(s) & \dots & R_{0h\rho_s}\zeta_i(s) & 0 & 0
 \end{array} \right]$$

(3-49)

and

$$[N] = \begin{bmatrix}
 I_{F_0} \omega^2 & & & & 0 & 0 & \dots & 0 & R_{O P_0}(R_O) & R_{O G_F} \left[P_0'(R_O) - \frac{P_0(R_O)}{R_O} \right] \\
 & I_{F_1} \omega_1^2 & & & 0 & 0 & \dots & 0 & R_{O P_1}(R_O) & R_{O G_F} \left[P_1'(R_O) - \frac{P_1(R_O)}{R_O} \right] \\
 & & \ddots & & \vdots & \vdots & \ddots & \vdots & \vdots & \vdots \\
 & & & I_{F_n} \omega_n^2 & 0 & 0 & \dots & 0 & R_{O P_n}(R_O) & R_{O G_F} \left[P_n'(R_O) - \frac{P_n(R_O)}{R_O} \right] \\
 \hline
 0 & 0 & \dots & 0 & I_{V_0} \bar{\omega}_0^2 & & & & -R_{O \zeta_0}(s) & 0 \\
 0 & 0 & \dots & 0 & & I_{V_1} \bar{\omega}_1^2 & & & -R_{O \zeta_1}(s) & 0 \\
 \vdots & \vdots & \ddots & \vdots & & & \ddots & & \vdots & \vdots \\
 0 & 0 & \dots & 0 & & & & I_{V_1} \bar{\omega}_1^2 & -R_{O \zeta_1}(s) & 0 \\
 \hline
 R_{O P_0}(R_O) & R_{O P_1}(R_O) & \dots & R_{O P_n}(R_O) & -R_{O \zeta_0}(s) & -R_{O \zeta_1}(s) & \dots & -R_{O \zeta_1}(s) & 0 & 0 \\
 \hline
 R_{O G_F} \left[P_0'(R_O) - \frac{P_0(R_O)}{R_O} \right] & R_{O G_F} \left[P_1'(R_O) - \frac{P_1(R_O)}{R_O} \right] & \dots & R_{O G_F} \left[P_n'(R_O) - \frac{P_n(R_O)}{R_O} \right] & 0 & 0 & \dots & 0 & 0 & 0
 \end{bmatrix}$$

(3-50)

and

$$\{x\} = \left\{ \begin{array}{c} \frac{a_0}{R_0} \\ \frac{a_1}{R_0} \\ \cdot \\ \cdot \\ \frac{a_n}{R_0} \\ \hline c_0 \\ \cdot \\ c_1 \\ \cdot \\ \cdot \\ c_i \\ \hline \lambda_1 \\ \hline \lambda_2 \end{array} \right\} \quad (3-51)$$

It should be noted that equation (3-48) represents a coupled viscoelastic-elastic system, because as was stated in equation (2-39) the propellant frequencies, ω_n , are now viscoelastic frequencies. Equation (3-48) is quite general, however, and for the matrices as defined, ω_n could be either elastic or viscoelastic frequencies.

It is important to note here one specific advantage of having selected the Lagrange Multiplier technique. The use of Lagrange Multiplier constraint relations permits the necessary boundary

conditions linking the viscoelastic cylinder to be satisfied on the sum of the modes (rather than on individual modes such as is required in the Rayleigh-Ritz method). This artifice allows the use of free-free modes and the attendant simple boundary conditions to describe the viscoelastic cylinder shear motion. Various slopes of this cylinder at the bonding surface can thus be examined parametrically. The effect is analagous to permitting a rotational spring to exist at the interface.

It should be observed that the order of degeneracy of the systems problem matrix is increased by the inclusion of the multipliers, but this affords no difficulty to the problem solution by modern computational equipment.

Solution of System Equations

It can be noted that presence of the rigid body modes and the Lagrange multiplier relation causes singularity of both matrices $[N]$ and $[M]$, respectively, thus precluding solution of the eigenvalue problem in its present form. An alternate form [reference 41] for the problem is obtained by scaling the eigenvalues as follows:

Equation (3-48) can be written as

$$[[M] \omega^2 - [N] + [\eta M] - [\eta M]] \{y\} = 0 \quad (3-52)$$

where y is a constant scaling factor.

Factoring and rearranging relation (3-52) yields

$$[M] \{y\} = \frac{1}{\eta + \omega^2} [N + \eta M] \{y\} = 0 \quad (3-53)$$

which is valid for

$$\eta > -\omega^2$$

The square matrix on the right-hand side of equation (3-53) is now nonsingular, and equation (3-53) can be written as

$$[H] \{y\} = \lambda' \{y\} \quad (3-54)$$

where

$$[H] = [N + \eta M]^{-1} [M] \quad \text{and} \quad \lambda' = \frac{1}{\eta + \omega^2}$$

Equation (3-54) is now in standard eigenvalue form and is solvable by general iterative procedures and sweeping methods (outlined in Appendix D) for the eigenvectors and respective natural frequencies.

Obvious advantages to this method are that the solution yields all modes, including the rigid body modes, without recourse to sweeping matrices for establishing the lowest system fundamental. There are minor difficulties to be noted in this method of scaling eigenvalues, however. First, lacking prior knowledge as to the lowest frequency, η must be chosen as positive. With positive η close proximity of adjacent latent roots forces slower convergence of the solution than would otherwise occur in the unmodified system. Also, the order of the $[H]$ matrix is larger than required since the rigid body modes are present in the modified form. These minor disadvantages are overshadowed, however, by the fact that the form of equation (3-54) is quite familiar and is easily solved by elementary means.

It is readily recognized that the use of digital computer solution methods are required for expedient solution of matrix expressions such as (3-54). A computer program was developed specifically for the problem described herein and has been supplied in Appendix E.

It will be noted that the eigenvector $\{x\}$ as defined by relation (3-51) represents the modal coefficients of the propellant and vehicle natural modes (also included in the eigenvector are the constraint forces, λ_1, λ_2). Therefore in order to obtain the deflection characteristics of the components at any system frequency, it is necessary to multiply the resulting eigenvalue, $\{x\}$, by a matrix comprised of the component natural modes in the manner following: By selecting the partitioned eigenvector section relevant to propellant modes, that is

$$\{x\} = \begin{Bmatrix} a_0 \\ \frac{R}{R_0} \\ a_1 \\ \frac{R}{R_0} \\ \cdot \\ \cdot \\ \cdot \\ a_n \\ \frac{R}{R_0} \end{Bmatrix}$$

and using the natural modes of the propellant, $p_n(r)$, described by relation (2-29) with the radial coordinate given by

$$r_j, \quad j = 1, 2, \dots, k$$

Then

$$\begin{bmatrix}
 p_0(r_1) & p_1(r_1) & \dots & p_n(r_1) \\
 p_0(r_2) & p_1(r_2) & \dots & p_n(r_2) \\
 p_0(r_3) & p_1(r_3) & \dots & p_n(r_3) \\
 \cdot & \cdot & \cdot & \cdot \\
 \cdot & \cdot & \cdot & \cdot \\
 \cdot & \cdot & \cdot & \cdot \\
 p_0(r_k) & p_1(r_k) & \dots & p_n(r_k)
 \end{bmatrix}
 \begin{Bmatrix}
 \frac{a_0}{R_0} \\
 \frac{a_1}{R_0} \\
 \cdot \\
 \cdot \\
 \cdot \\
 \frac{a_n}{R_0}
 \end{Bmatrix}^{(q)}
 =
 \begin{Bmatrix}
 \cdot \\
 \cdot \\
 \cdot \\
 \cdot \\
 \cdot \\
 \cdot
 \end{Bmatrix}^{(q)}
 = \{y_p\}^{(q)}$$

(3-55)

where $\{y_p\}^{(q)}$ represents the propellant deflection at the qth system frequency. A similar matrix operation which will yield the launch vehicle system deflections is

$$\begin{bmatrix}
 \zeta_0(x_1) & \zeta_1(x_1) & \dots & \zeta_j(x_1) \\
 \zeta_0(x_2) & \zeta_2(x_2) & \dots & \zeta_j(x_2) \\
 \zeta_0(x_3) & \zeta_1(x_3) & \dots & \zeta_j(x_3) \\
 \cdot & \cdot & \cdot & \cdot \\
 \cdot & \cdot & \cdot & \cdot \\
 \cdot & \cdot & \cdot & \cdot \\
 \zeta_0(x_k) & \zeta_1(x_k) & \dots & \zeta_j(x_k)
 \end{bmatrix}
 \begin{Bmatrix}
 c_0 \\
 c_1 \\
 \cdot \\
 \cdot \\
 \cdot \\
 c_i
 \end{Bmatrix}^{(q)}
 =
 \begin{Bmatrix}
 \cdot \\
 \cdot \\
 \cdot \\
 \cdot \\
 \cdot \\
 y_{LV}
 \end{Bmatrix}^{(q)}$$

(3-56)

where the longitudinal coordinate is described by

$$x_j, \quad j = 1, 2, \dots, k$$

and $\{y_{LV}\}^{(q)}$ represents the vehicle deflection at the q th system frequency. The $\zeta_j(x)$ are not developed in the present investigation since methods for establishing natural mode data for launch vehicles in torsion are well documented [42].

The total systems problem has now been cast into matrix form, and appropriate solution methods have been developed. The next logical step in the investigation was to select a satisfactory means of total systems analysis verification. This process is described in the following chapter.

IV. VERIFICATION OF SYSTEMS ANALYSIS

As has been stated, the primary goal in the investigation was to develop a systems analysis which could be applied to a characteristic launch vehicle such as that for Project FIRE shown schematically in figure 2. Prior to application of the analysis to the FIRE system, however, it was deemed important to use an experimental model to verify the fact that the analytical method would correctly predict response characteristics of a system comprised of two components when the modal information for the components had been analytically developed separately and then the components coupled together.

While it would have been very desirable to employ a large-scale dynamic model of a launch vehicle with a solid propellant segment such as that discussed in Chapter I, an appraisal of fabrication and test setup costs required to develop such a model indicated the unfeasibility of doing so. After giving careful consideration to several simpler vehicle system models which could be manufactured, and after noting that the frequency response range of the cylindrical vehicle representations would be unacceptably high, it was obvious that other avenues of experimental verification would have to be explored. It was then observed that in the analytical development of the two boundary conditions for the system (equations (3-25) and (3-32)), the radius of attachment could be changed from the outside to the inside radius with little effort. Although the resulting experimental model then bore little similarity to a launch vehicle system, it was concluded that a neoprene disc could be attached at its inner radius to a brass shaft and by proper selection of

physical characteristics such as radii and lengths, composite system frequencies would be in a sufficiently low range (below 1000 cps) as to be readily measurable. Such a model was subsequently constructed and is described schematically in figure 3. In addition to the neoprene disc fabrication, a steel disc, equal in rigid body inertia to the neoprene item, was made. Use of the steel disc will be discussed subsequently. Physical data for all system components are given in Table I.

Disc modes and frequencies for both the neoprene and steel items were established using the propellant shear mode computer program of Appendix E which was developed to solve equations (2-24) and (2-29) of Chapter II. Elastic assumptions for the neoprene disc were used because it was expected to behave elastically for small-time, short-period frequencies. Shaft modal data were determined by a standard torsional modes analysis not included herein. Coupled neoprene disc-brass shaft and steel disc-brass shaft frequencies and modes were then established via the systems analysis computer program of Appendix E which was written to solve the matrix relation (3-54). The analytical free-free mode shapes of the neoprene disc have been presented in figure 4, and the resulting analytical neoprene disc deflections at system frequencies are shown in figure 5. Steel disc analytical modal data were not plotted, since the more salient information for the steel disc-shaft combination was the frequency spectrum which is discussed later.

Once the analytical information had been established, an experimental program was undertaken to verify the adequacy of the systems

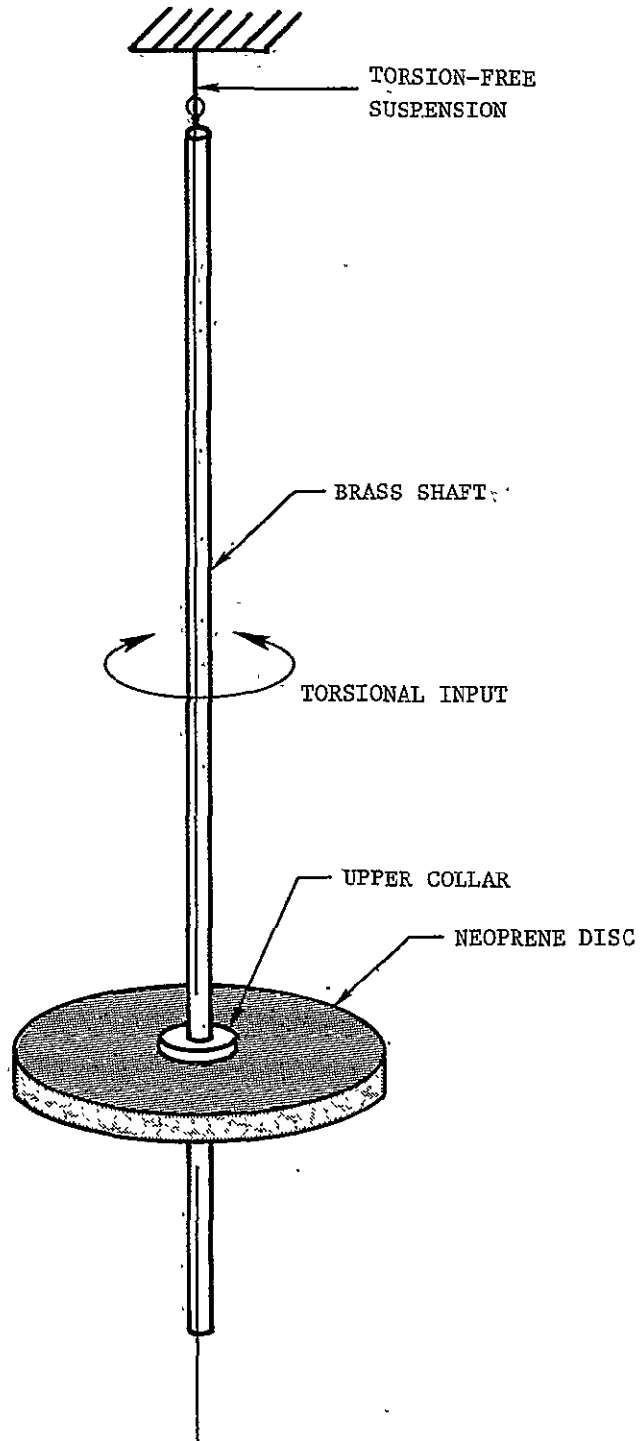
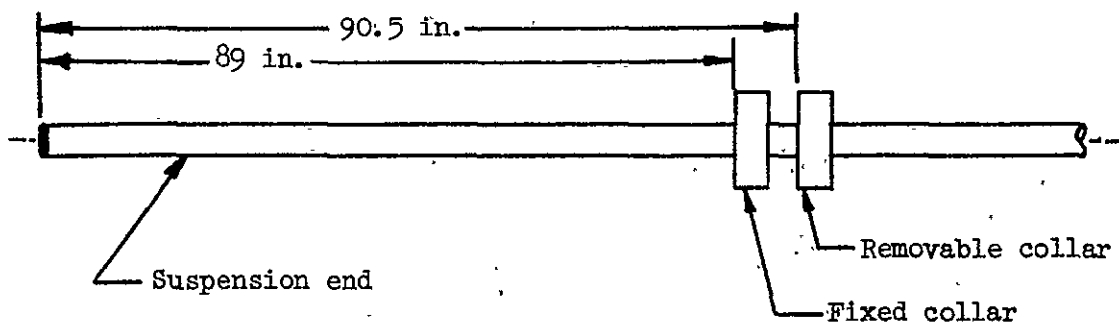


Figure 3.- Disc-shaft experimental model schematic.

TABLE I. - SHAFT-DISC PHYSICAL PARAMETERS

Item	Material	Dimensions	Remarks
Shaft	Red brass	1-in. nominal diameter 100-in. length	Solid rod with two 1/2-in.-thick by 2-in.-diameter brass collars for disc attachment (see sketch)
"Flex" disc	Neoprene	14-in. outside diameter 1-in. inside diameter 1-in. thick	50 durometer Shear modulus = 90 lb/in ² nominal
"Rigid" disc	Steel	8.6-in. outside diameter 1-in. inside diameter 1-in. thick	



Brass shaft configuration

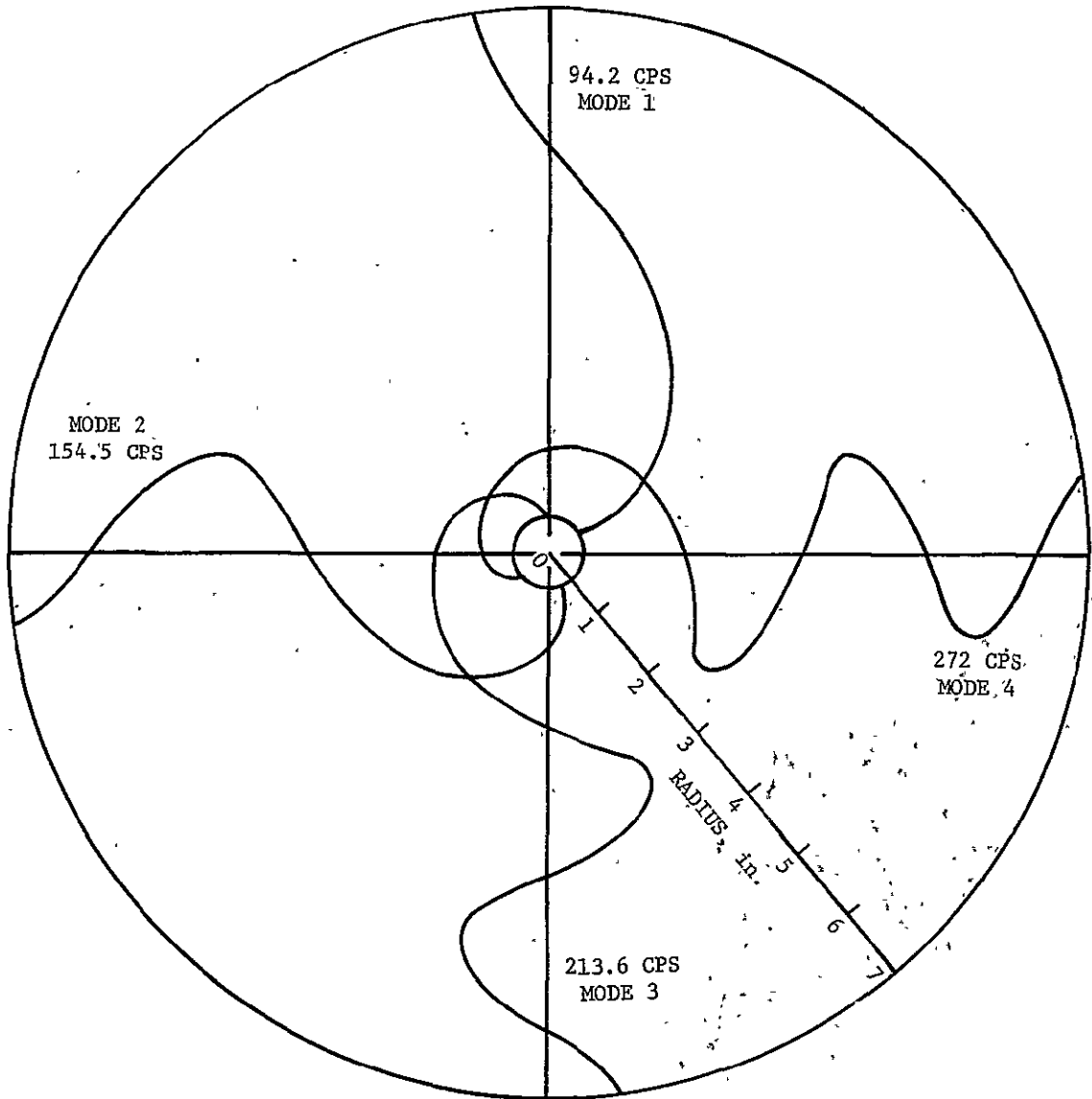


Figure 4.- Analytical disc free-free mode shapes.

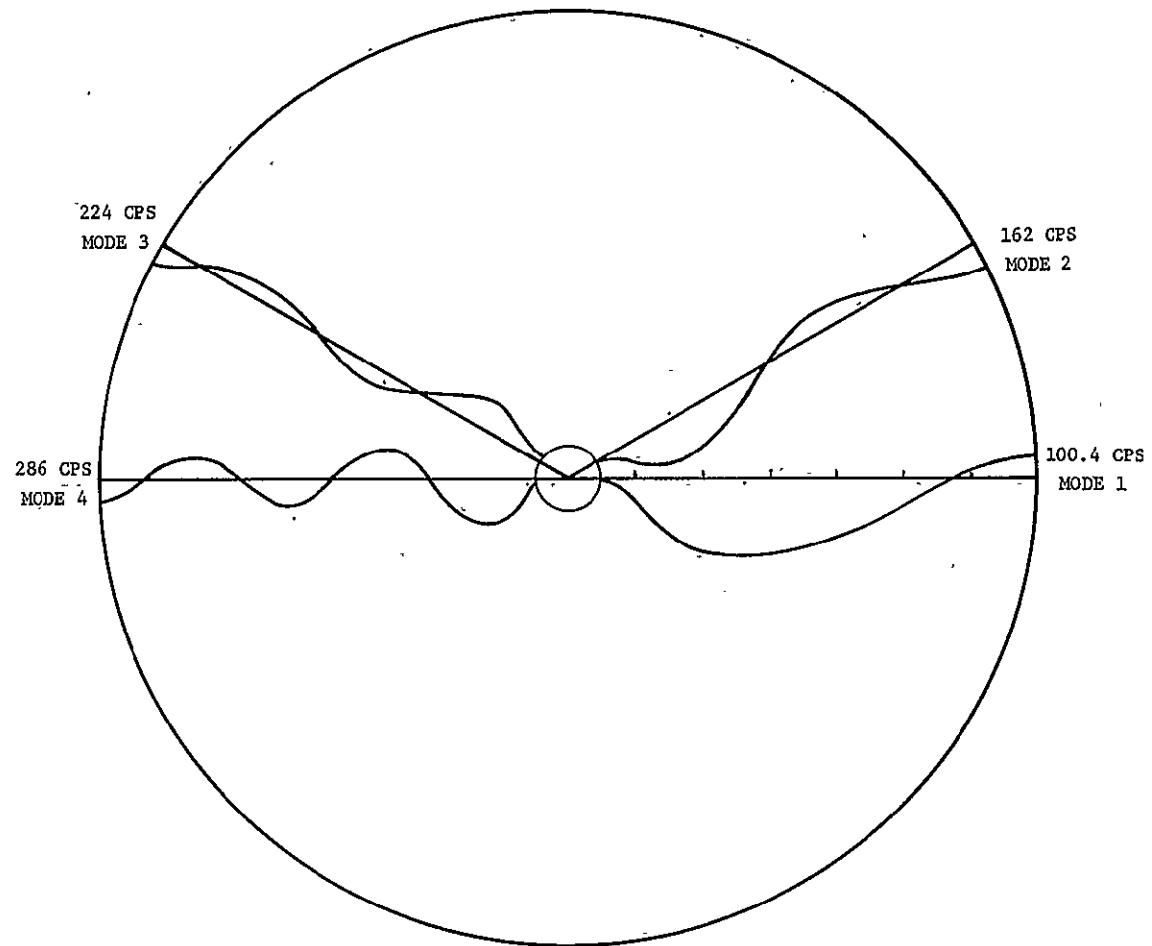


Figure 5.- Analytical neoprene disc characteristics at system frequencies.

analysis. The test setup and apparatus are described in the next section.

Test Method

The boundary conditions simulated for the system were free-free. A small cable sized to ensure negligible torsional restraint was used as the upper end suspension method (fig. 6). The lower end was completely free. Two five-pound shakers (fig. 7) were hooked up 180° out of phase to provide as clean a torsional input as possible to the shaft. The driving point was near a system node such that very small forcing was required to excite system modes. To ensure that only system torsional response characteristics would be measured, a complete transverse modal survey of the shaft was performed prior to the torsional test to identify other modes. Also, several rotational orientations of the accelerometer mount disc radius were evaluated to assess the possibility of spurious mode detection. Minor changes in response measurement were noted after changing the disc position, and the tests were completed with the accelerometers aligned perpendicular to the backboard (fig. 8).

The neoprene disc (fig. 9) was supported prior to testing by a plywood disc covered with teflon to preclude neoprene disc sag (fig. 10). The disc was fixed between two brass collars and double-backed tape between collar and disc on both sides to preclude relative rotation at the interface.

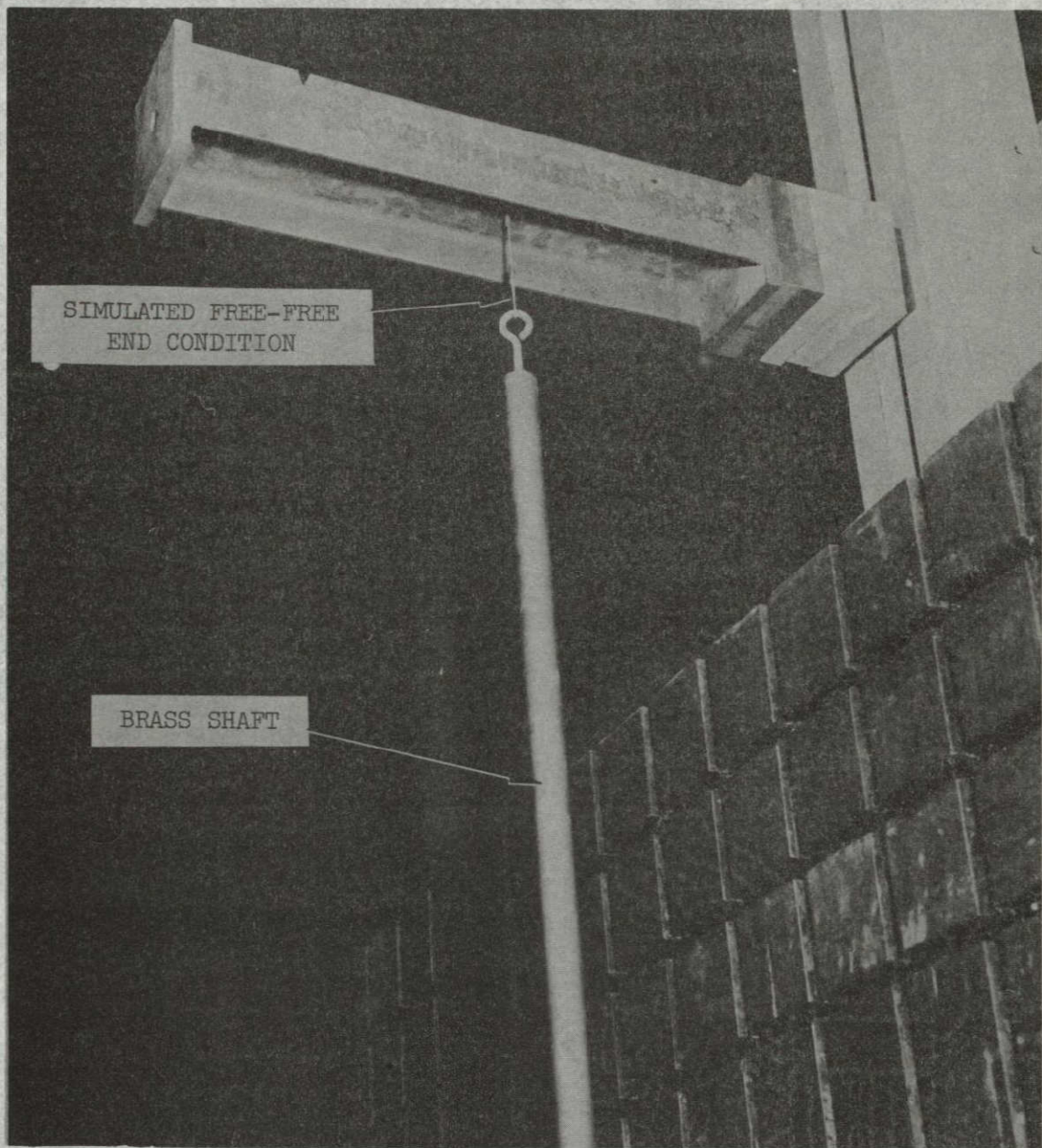


Figure 6.- Free-free suspension for experiment.

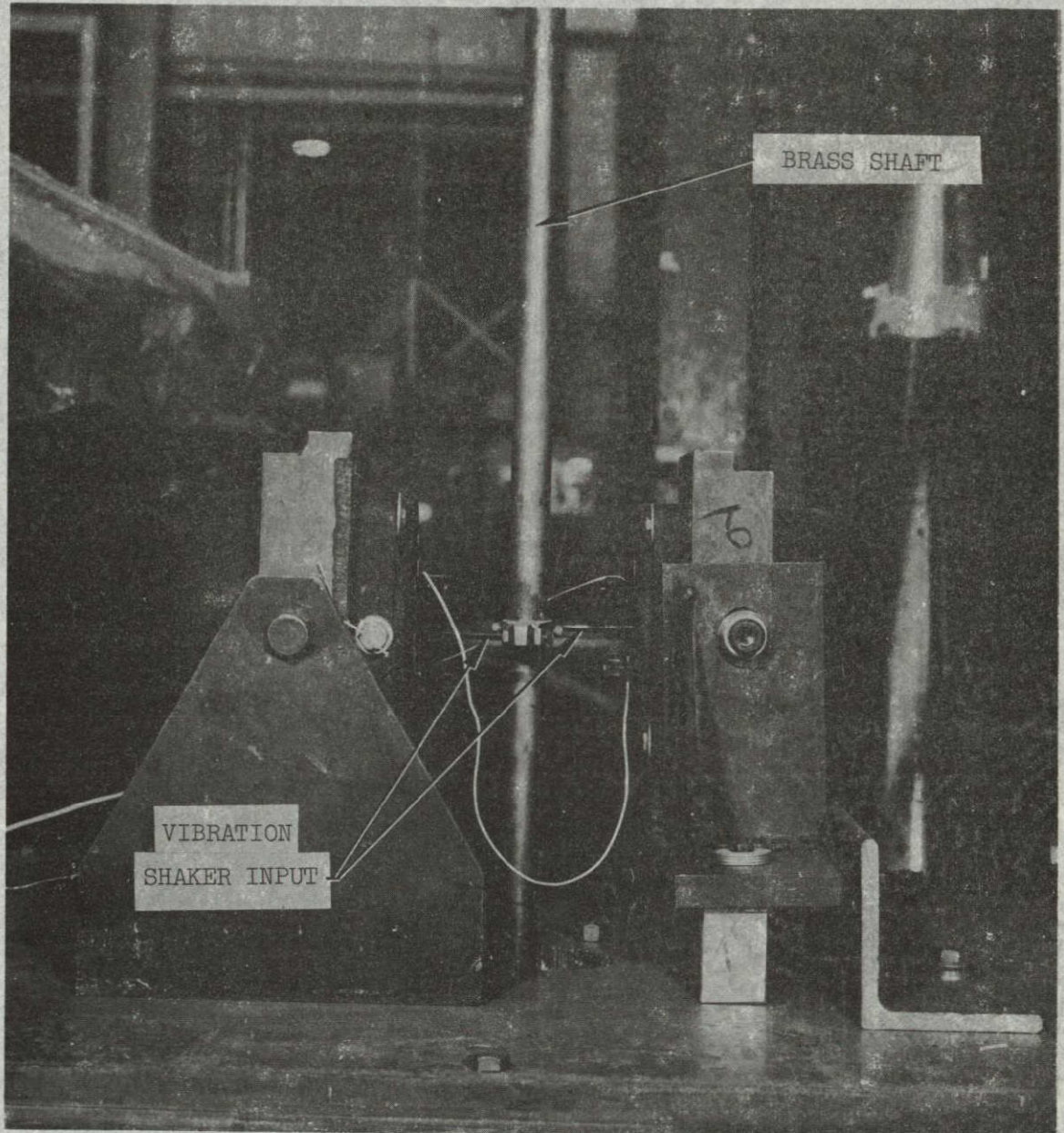


Figure 7.- Vibration shaker mounting for experiment.

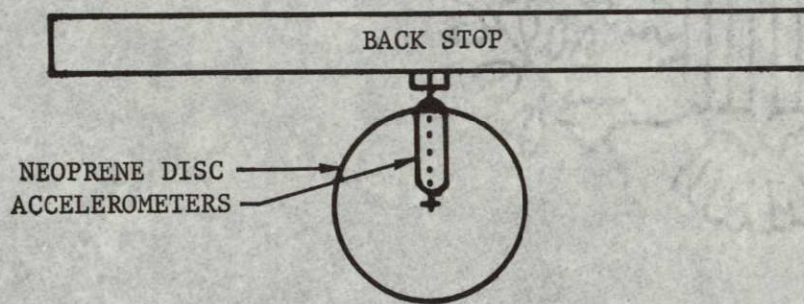
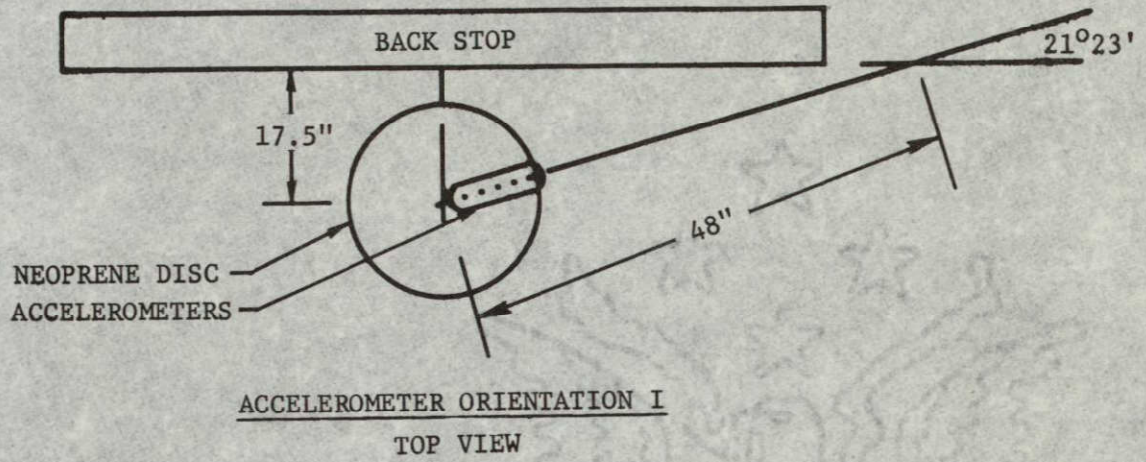


Figure 8.- Radial accelerometer orientation schematic.

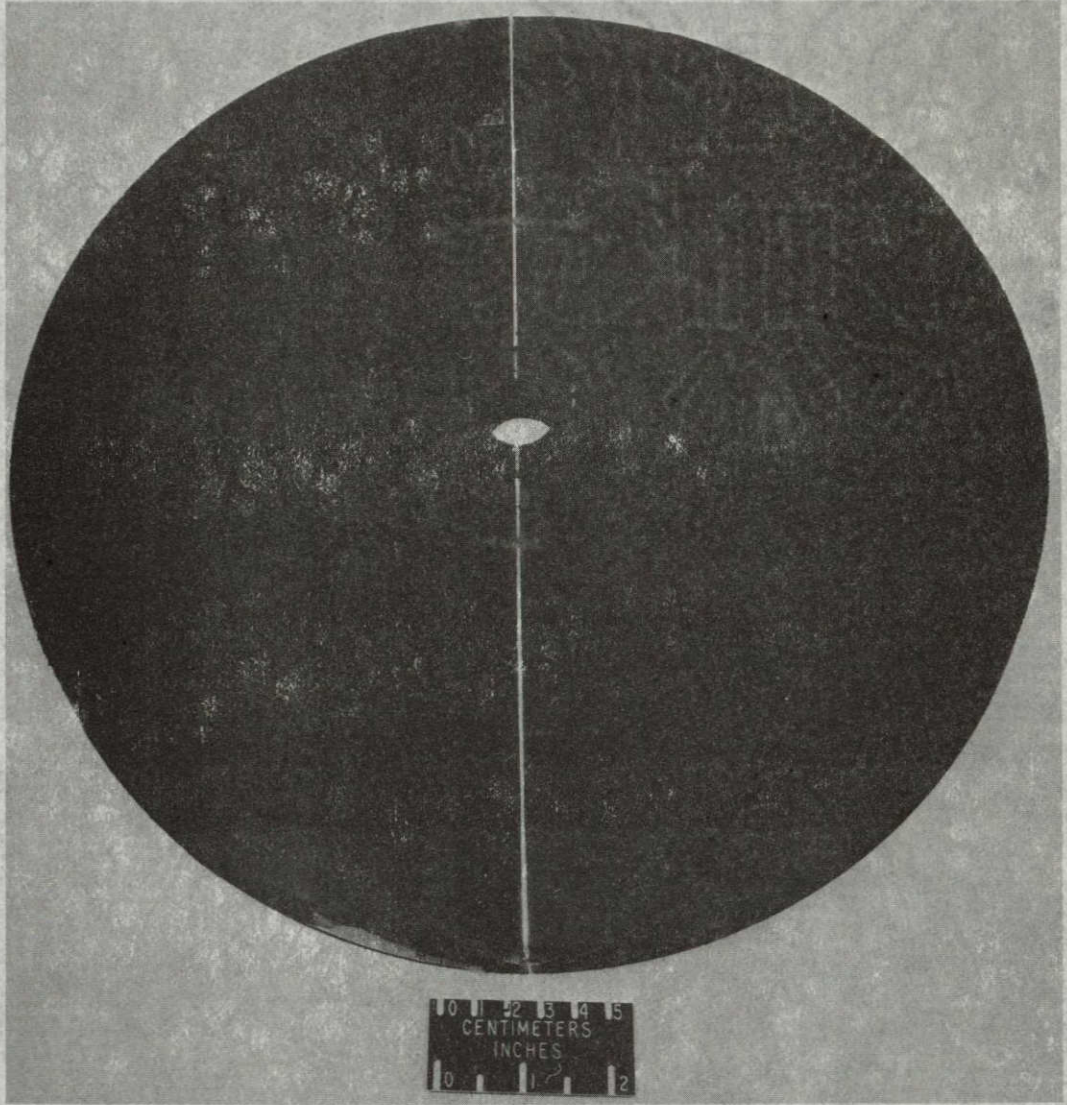


Figure 9.- Neoprene disc.

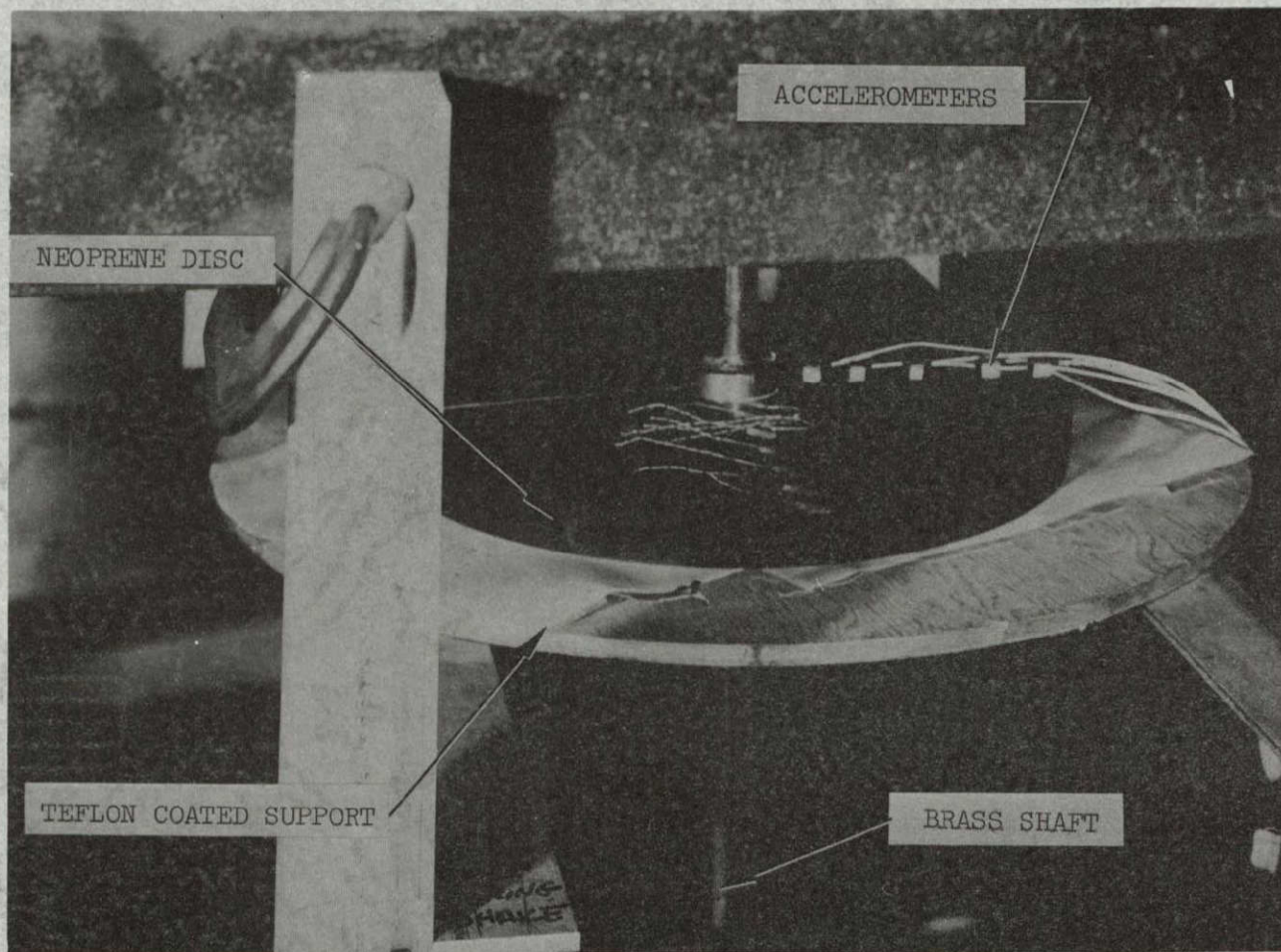


Figure 10.- Neoprene disc location in system.

Measurement data were obtained from five small (5g) Unholtz-Dickie accelerometers mounted across a radius (see fig. 10). All accelerometer readings at each resonant frequency were recorded on an oscillograph. Five runs were made at each resonance allowing resonance verification via oscilloscope monitoring of a separate accelerometer Lissajous pattern for each run. Frequencies of the resonances were read from a digital counter and from the control oscillator. Final determination of frequencies was made later by direct reading of the oscillograph traces.

The complete test setup for the neoprene disc-shaft is shown in figure 11. The setup was identical for subsequent tests with the neoprene disc replaced with the steel disc (fig. 12). For the steel disc modes, only three accelerometers were used.

Test Results

All data are presented in Table II for both shaft-disc systems. The analytical data generated via the systems analysis method developed in Chapter III and discussed in the prior section are also presented for comparison.

The experimental and analytical neoprene disc deflections at the disc-shaft first mode frequency are plotted in figure 13. Frequency agreement was generally acceptable for the experimental setup utilized, but corroboration of the analytical mode shapes was difficult. Several considerations concerning the experimental mode shapes are as follows:

1. Only five accelerometers were used, making node determination at higher frequencies (where nodes are more closely spaced) difficult.

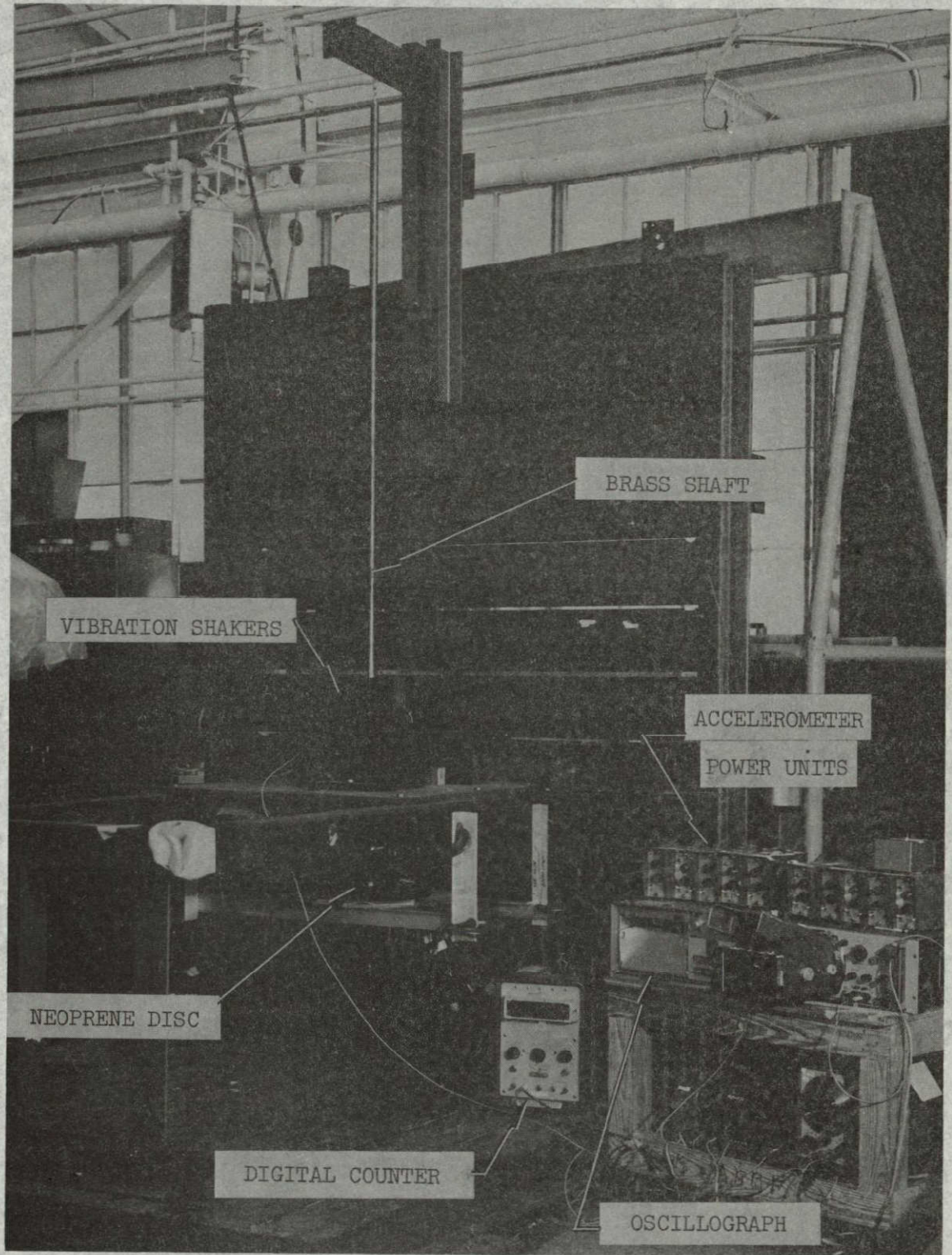


Figure 11.- Complete test setup.

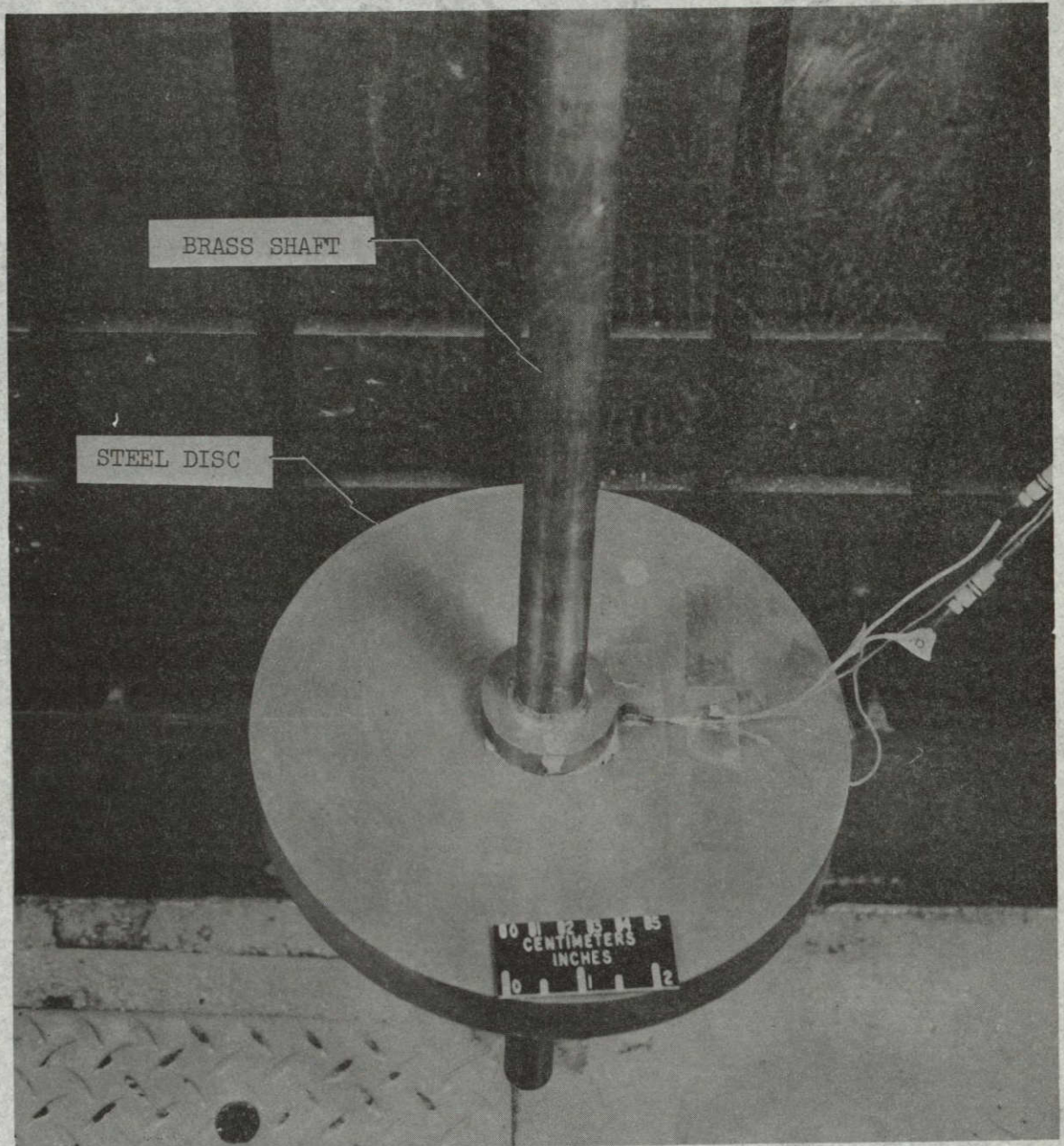


Figure 12.- Experimental steel disc.

TABLE II. - RESULTS OF SHAFT-DISC EXPERIMENT AND ANALYSIS

System	Mode	Frequency, cps	
		Analytical	Experimental
Shaft- neoprene disc	1	100	107
	2	162	162
	3	224	230
	4	286	278
	5	348	350
	6	399	424
Shaft- steel disc	1	266.5	266
	2	741.7	*

*Not included in test equipment frequency span range.

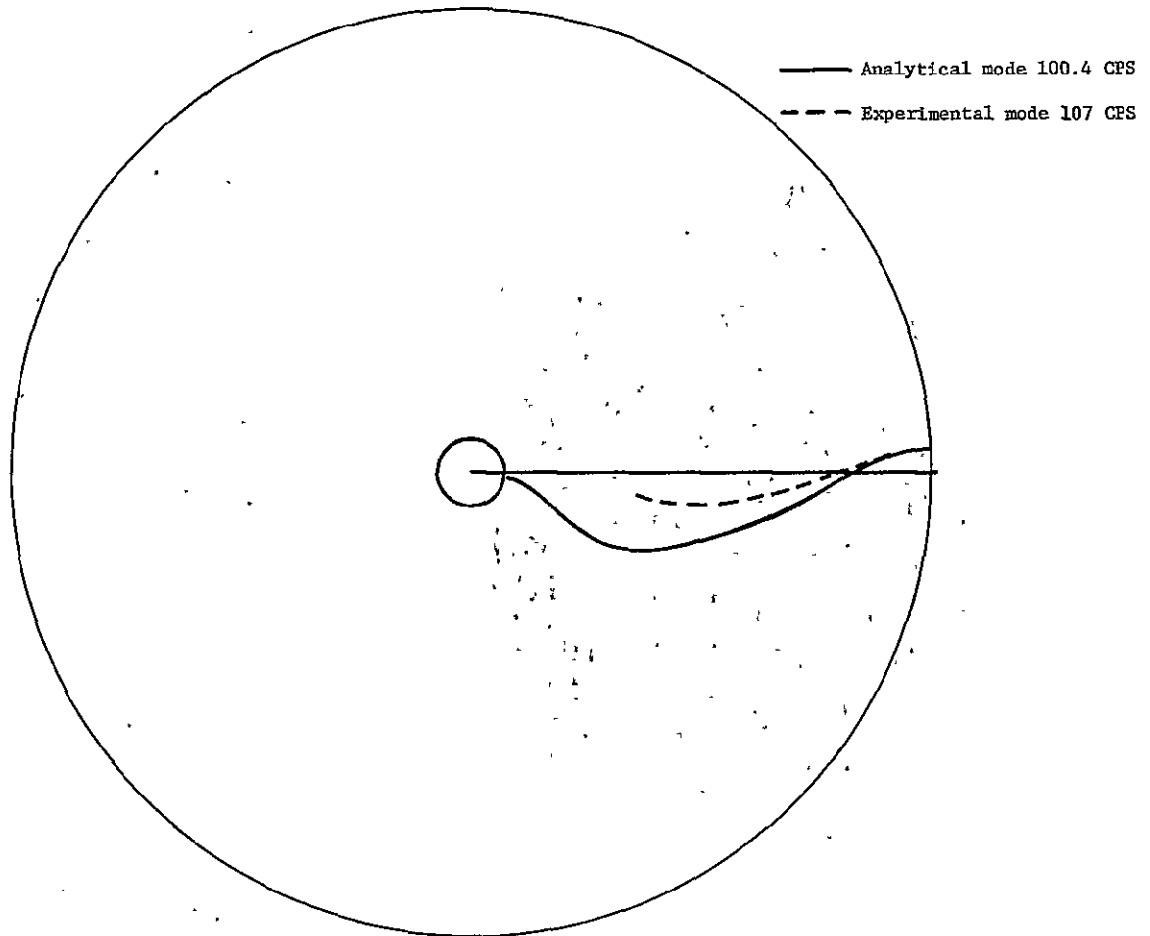


Figure 13.- Analytical vs experimental mode shapes for neoprene disc at system frequencies.

2. Close proximity of several lateral and torsional natural frequencies also hampered mode determination at higher frequencies.

3. The efforts to obtain good fixity at the disc-shaft interface may have affected the modal responses adversely in that there is the possibility that the tightening of the collars may have squeezed the neoprene disc at the inside radius thereby shifting the effective attachment radius outward. Several analytical runs with different attachment radii were made by computer in an attempt to achieve better modal agreement in the higher modes, but better results were not obtained.

With these shortcomings, however, it is felt that the systems analysis predicted the frequency responses well. It should be noted that the frequency spectrum for the rigid steel disc (even though possessing rigid body inertia identical to the neoprene item) differed considerably from that for the neoprene disc thus pointing up the errors to be encountered when flexible body effects are neglected.

Having established what was felt to be satisfactory agreement between analytically predicted and experimentally determined natural system characteristics, particularly in the frequency spectrum, the final step in the investigation was to apply the analytical method to the FIRE vehicle. Details of the example problem are given in the following chapter.

V. EXAMPLE SYSTEMS PROBLEM

The systems analysis developed in Chapter III is applicable to the examination of a wide array of composite systems torsional dynamics problems, including systems such as the experimental model discussed previously. However, it was developed for the specific purpose of describing the torsional motion of a characteristic launch vehicle such as used for project FIRE. The vehicle system is comprised of a near axisymmetric discontinuous thin-walled elastic cylinder with a solid propellant motor attached near the forward end in the payload region (fig. 14). The case examined is not for academic purposes only, it may be noted, since flight data have indicated that the three booster engines which are gimbaled to permit roll control as well as thrust, tend to "chug" on shutdown in a manner which induces a quasi-sinusoidal torsional excitation (fig. 15) devoid of any components which would induce other modes of vibration. This input is in turn transmitted forward through the length of the vehicle, ultimately reaching the propellant attachment station. Since the Young's modulus for a typical propellant casing is $E = 0.6 \times 10^6$, a nominal zero frequency value for the propellant is $E = 500$, and the propellant-length fraction of the total system length is small (approximately 6 percent), classical torsional deflection over the casing length will be neglected for the application of the analytical method. It will also be noted that for the rigid casing assumption, the case responds by undergoing angular rotation constant throughout its length under the influence of

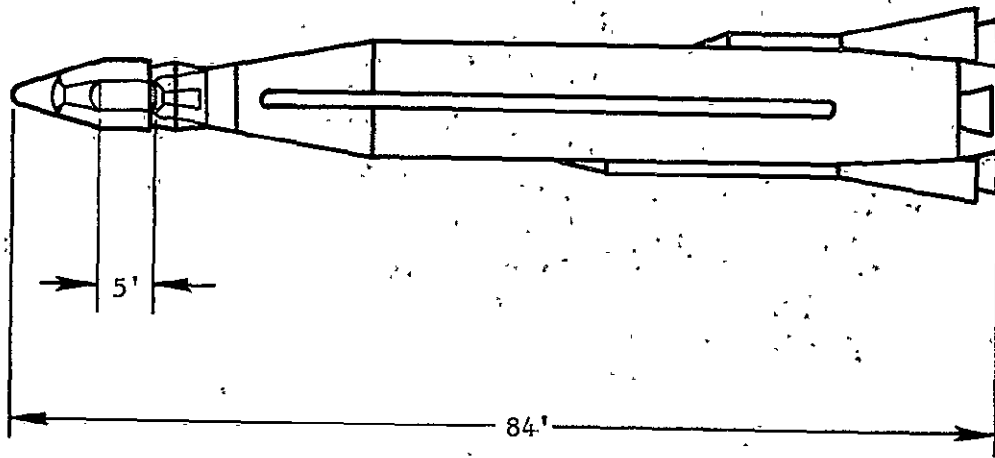


Figure 14.- Atlas FIRE configuration.

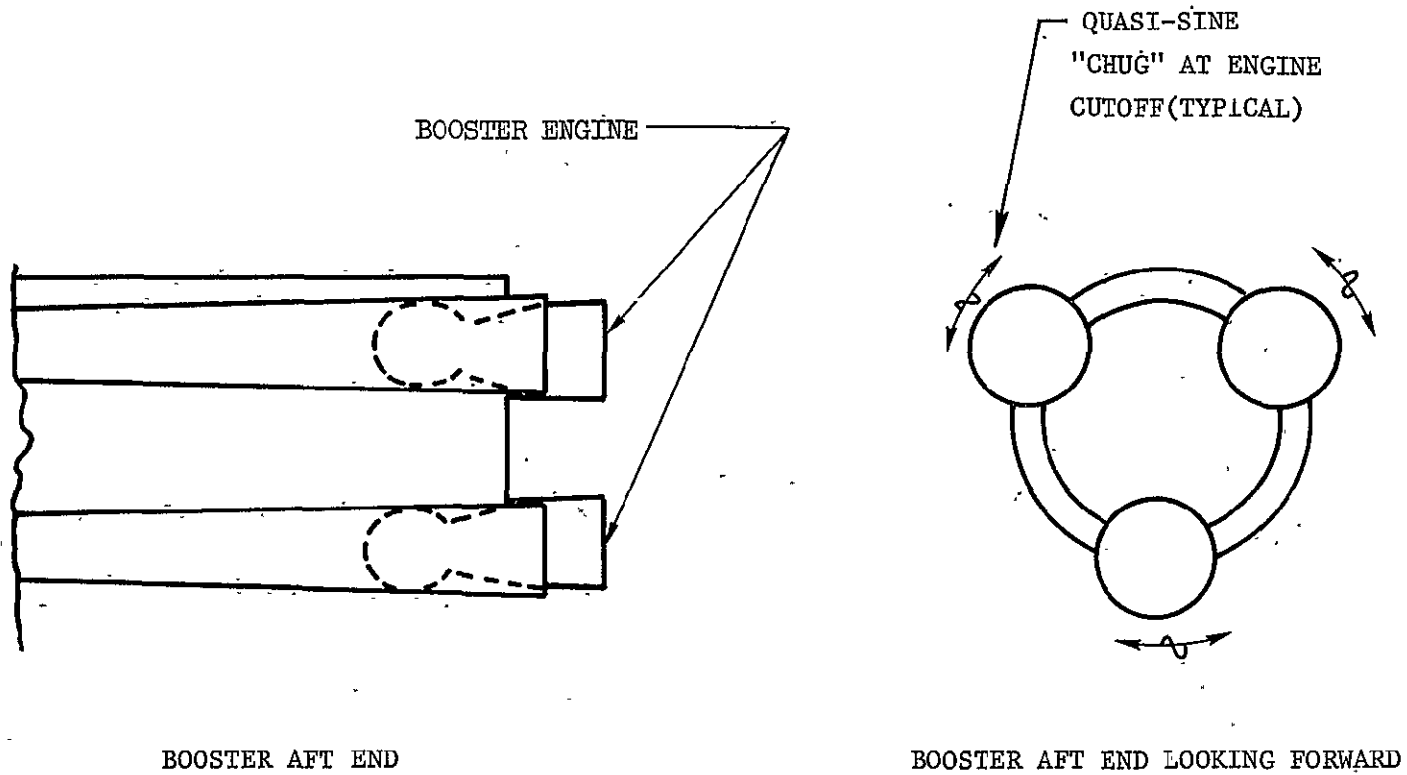
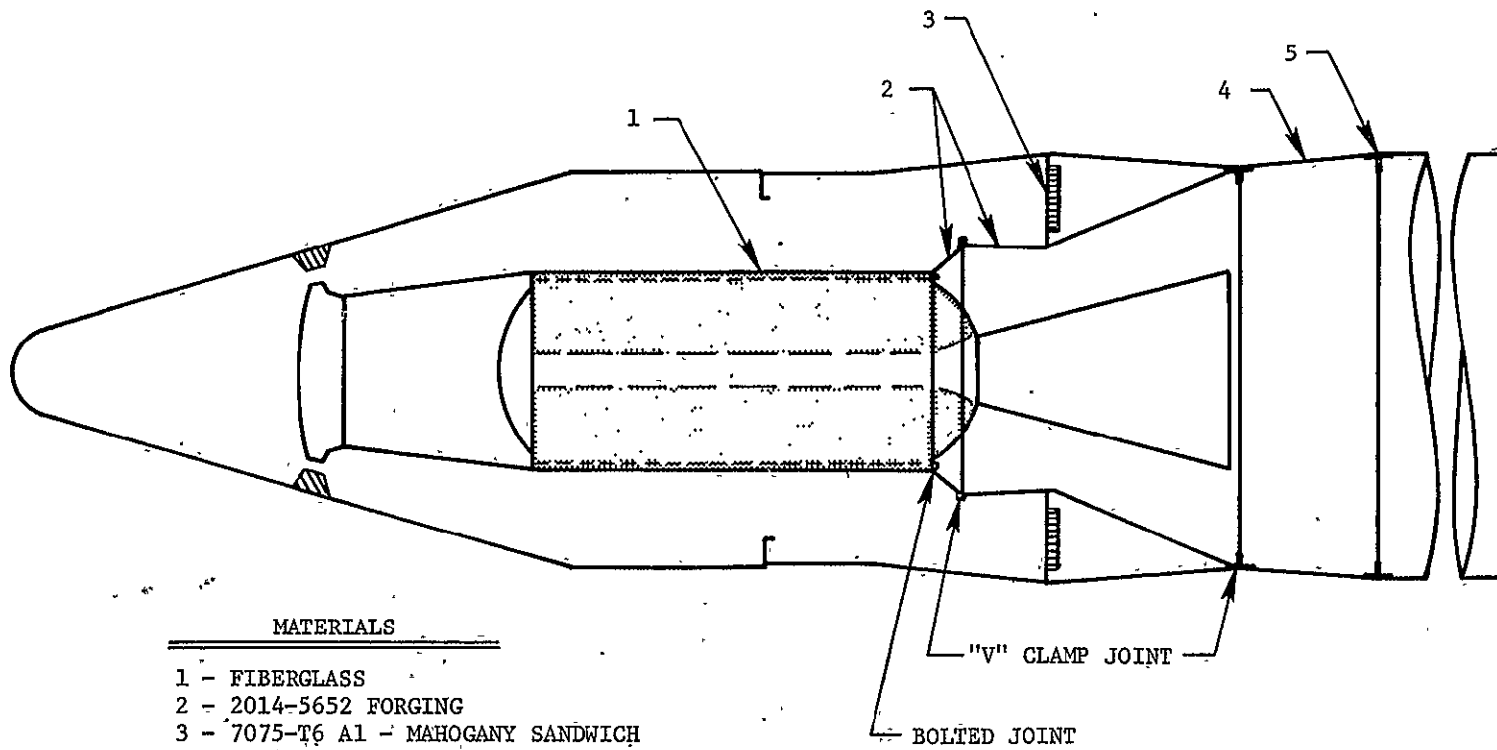


Figure 15.- Booster torsional input.

torsional excitation. Also, when the difference in casing and propellant moduli as well as the mounting arrangement are considered, justification for the assumption that the propellant would behave in pure shear is evident. Figure 16 contains more detailed information about the payload portion and is typical of the mounting arrangement for flight research experiments of this class. The viscoelastic propellant is shown shaded and is encased in a fiberglass-wound casing (item 1). The load path in twist is through a bolted joint near the propellant aft end, via the aluminum forging (item 2) through the "V" clamp joints in the adapter section, then through the aluminum skin structure to the mating joint (item 5). The sandwich structure (item 3) is not intended as a load path and is for the purpose of flight accelerometer mounting only.

Discrete Vehicle Model

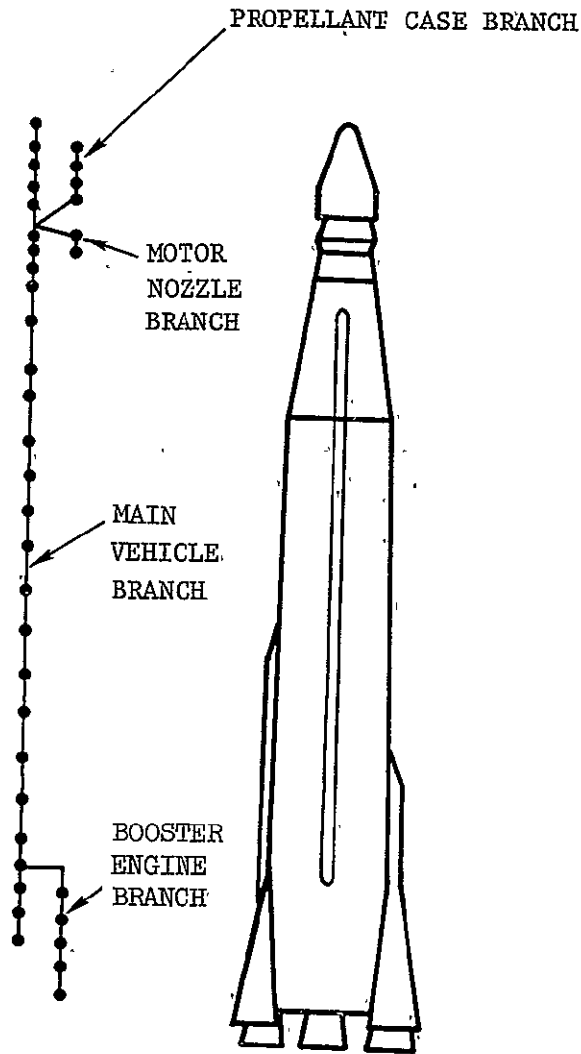
The mathematical model used to describe the longitudinally discontinuous launch vehicle is given in figure 17. The physical attachment station of the propellant is as shown in the figure. The discrete torsional stiffness and inertias are given in Table III. It may be noted that for the vehicle modal deflections and associated generalized inertias computed by standard eigenvalue routines using the discrete data, only the modal deflections of the attachment station (i.e., the launch vehicle-propellant mechanical interface) are required in the systems problem. (Also, the propellant container inertia is lumped at the vehicle attachment point and considered in the vehicle modal data.)



- MATERIALS
- 1 - FIBERGLASS
 - 2 - 2014-5652 FORGING
 - 3 - 7075-T6 AL - MAHOGANY SANDWICH
 - 4 - 2024-T3 AL SKIN
 - 5 - 2014-T652 FORGING

Figure 16.- Solid propellant mounting schematic.

- — ROTATIONAL INERTIAS
- | — ROTATIONAL STIFFNESSES



(DISCRETE BRANCH MODEL)

Figure 17.- Atlas math model.

TABLE III.- TORSIONAL PHYSICAL DATA OF ATLAS STRUCTURE

NODE	x (in.)	I ROLL x 10 ⁻⁶ lb-in. ²	K _T x 10 ⁻⁹ in.-lb/rad
1	98	.202	-
2	120	.224	.80
3	150	.294	2.55
4	177	2.425	12.10
5	210	2.093	13.91
6	250	2.493	10.43
7	290	1.465	10.10
8	340	2.172	7.03
9	390	.805	6.95
10	430	.384	7.74
11	470	.291	7.23
12	510	.276	7.05
13	550	.261	6.42
14	590	.245	5.92
15	630	.276	5.74
16	670	.261	6.25
17	710	.202	5.50
18	750	.204	3.53
19	790	.238	4.36
20	150	1.492	23.10
21	120	2.121	30.70
22	98	5.000	11.60
23	75	2.363	5.67
24	30	2.348	-
4	-	-	-
20	-	-	20.53

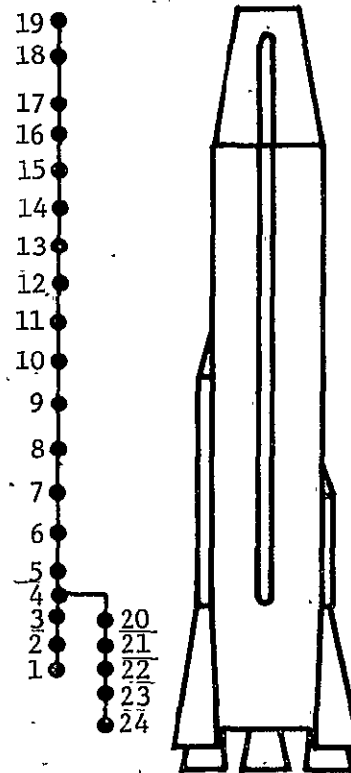
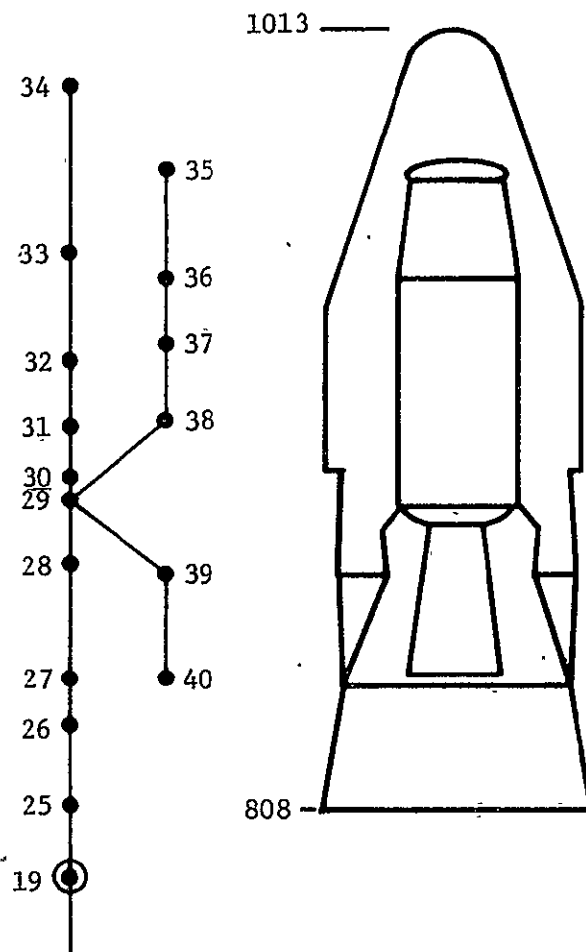


TABLE III.- TORSIONAL PHYSICAL DATA OF ATLAS STRUCTURE = Concluded

Node	x (in.)	I Roll $\times 10^{-4}$ lb-in. ²		$K_T \times 10^{-9}$ in.-lb/rad
		X-259 with solid fuel	X-259 with- out fuel	
19	790	--	--	--
25	808	5.215	5.215	8.660
26	830	5.215	5.215	5.250
27	842	9.310	9.310	7.640
28	872	32.400	32.400	4.290
29	889	8.230	1.840	5.224
30	894	7.600	7.600	17.762
31	908	9.730	9.730	2.214
32	926	4.100	4.100	2.278
33	954	5.910	5.910	1.045
34	996	.860	.860	.213
35	976	1.925	1.925	--
36	948	6.240	1.840	.0681
37	930	10.220	2.660	.167
38	910	10.220	2.660	.150
39	870	.671	.671	--
40	842	.459	.459	.0143
29	889	--	--	--
38	910	--	--	.143
29	889	--	--	--
39	870	--	--	.0183



The launch vehicle torsional modes and frequencies with the propellant excluded are given in figure 18 and differ slightly from those of reference [42] in that the propellant casing is considered rigid in this study.

Propellant Model

Recourse to discrete analysis is not required for the propellant since it can be represented by the continuous deflection result in shear developed by the closed form solution in Chapter II for a visco-elastic thick walled cylinder. Some license was taken, however, in permitting the mathematical model to have a circular cross-section port. In reality this inside port deviates slightly from circularity although it has been assumed that for this study the system dynamic differences due to the assumed and real cross-sections are negligible.

Physical data for the propellant are provided in Table IV.

Vehicle Systems Analysis

The method employed in solving the systems problem was to follow the same analytical steps as described in Chapters II and III. In order to evaluate various propellant assumptions, shear mode shapes with frequencies for an elastic propellant (fig. 19) were first established using equations (2-29) and (2-24) and then combined with launch vehicle torsional modes to develop the systems frequencies. In the systems analysis for this propellant assumption, 9 propellant modes and 12 vehicle modes were used. Modal and frequency results of the

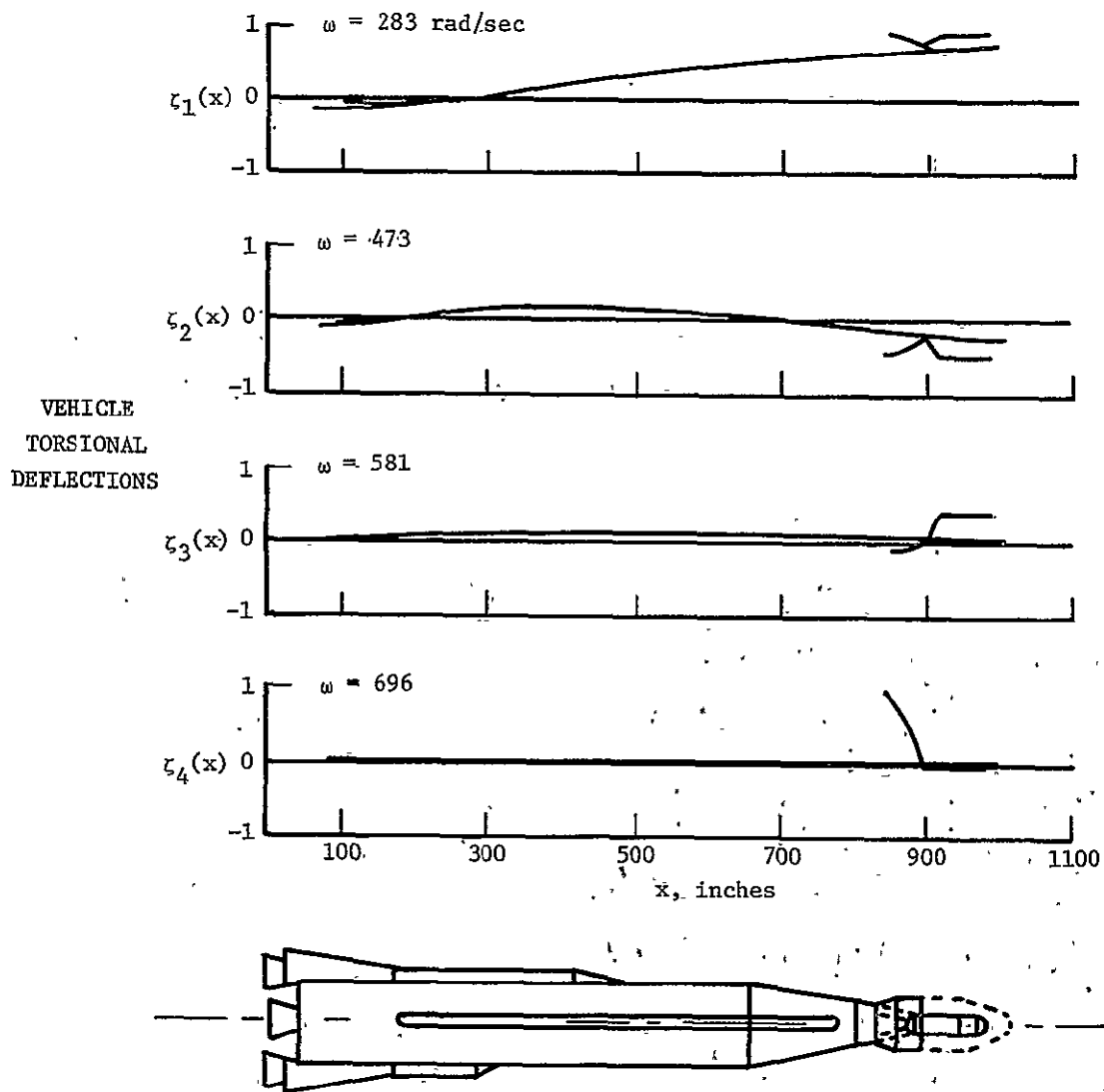


Figure 18.- Launch vehicle torsional modes and frequencies without solid propellant.

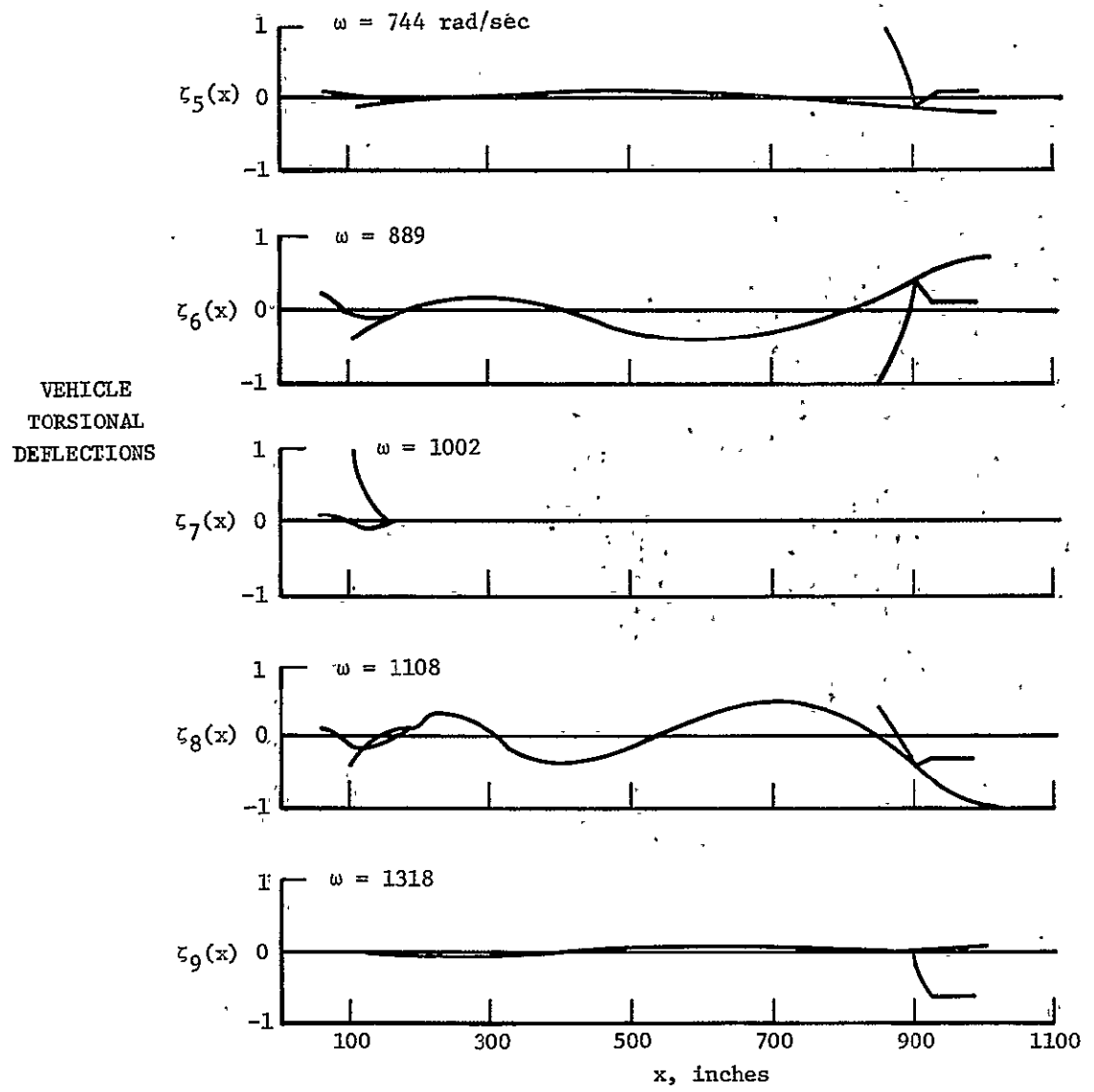


Figure 18.- Concluded.

TABLE IV.- PROPELLANT PHYSICAL DATA

Outside radius	14.85 in.
Inside radius	4.5 in. nominal
Length	56 in. nominal
Density	.0635 lb/in ³
Shear modulus	200 lb/in ² nominal

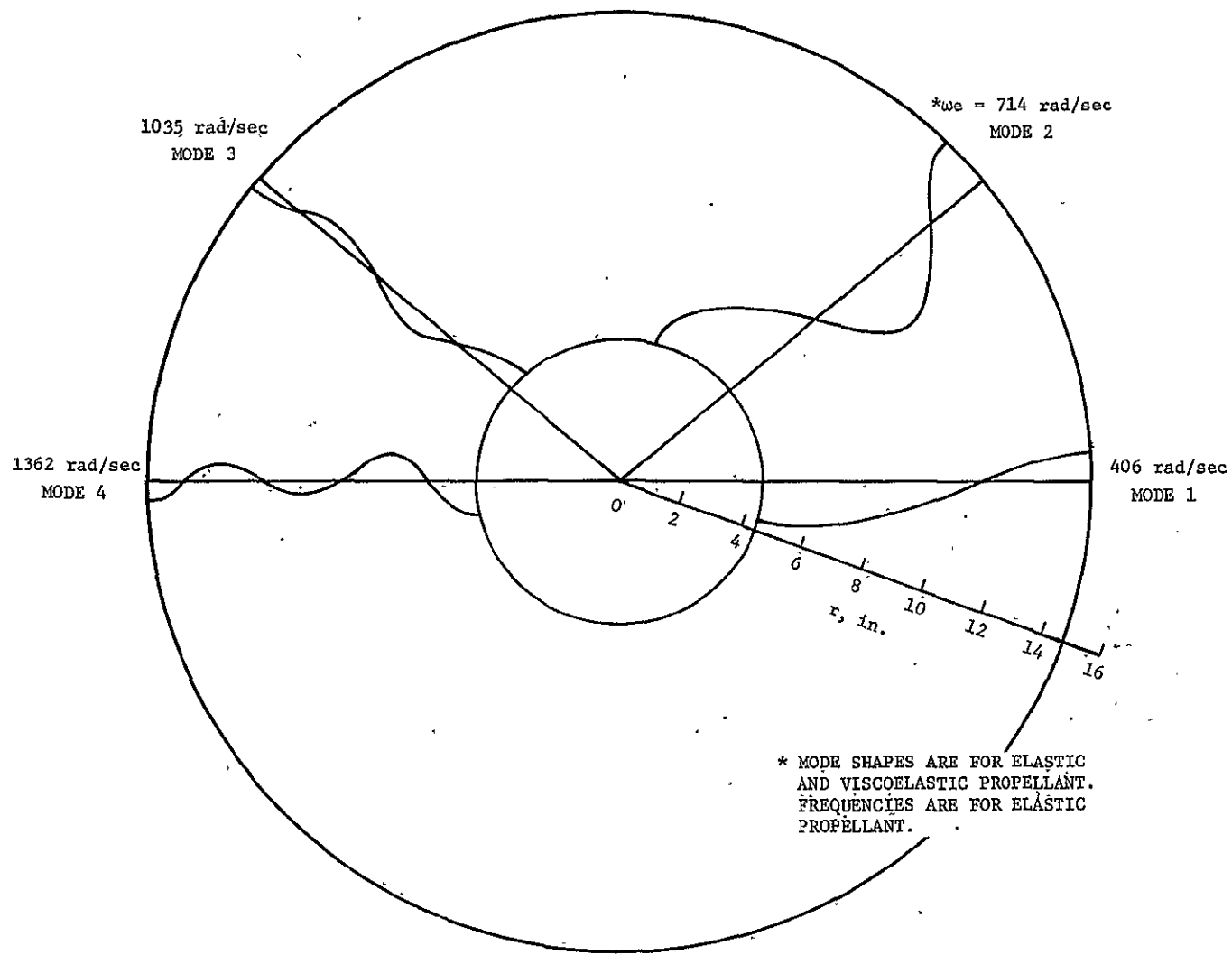


Figure 19.- Propellant shear mode shapes.

coupled system dynamics analysis with the elastic propellant are presented in figure 20 for the propellant and figure 21 for the vehicle.

Next the viscoelastic propellant was considered with frequencies computed from equation (2-39), restated here for clarity

$$\left[\frac{\omega_v}{\omega_e} \right]^2 = 1 + \frac{K_1 \omega_v^\kappa}{G^0} \quad (2-39)$$

Constants were obtained from modulus versus frequency data of reference [21] over the frequency range of 300 to 3000 cps. It was clear that for the storage modulus as herein defined, that is,

$$G_1 = K_1 \omega_v^\kappa$$

selection of $K_1 = 2.47$ and $\kappa = 1$ would appropriately match the referenced data for the frequency range mentioned above.

Propellant manufacturer's data yielded a value of $G^0 = 200 \text{ lb/in}^2$ (G^0 = the shear modulus at zero frequency).

Using the above data, viscoelastic frequencies were computed for the first five propellant modes and the propellant characteristics again coupled to the vehicle modes through the systems equations. The resulting propellant deflections for the viscoelastic assumption and the associated vehicle modes at the system frequencies are presented in figures 22 and 23, respectively.

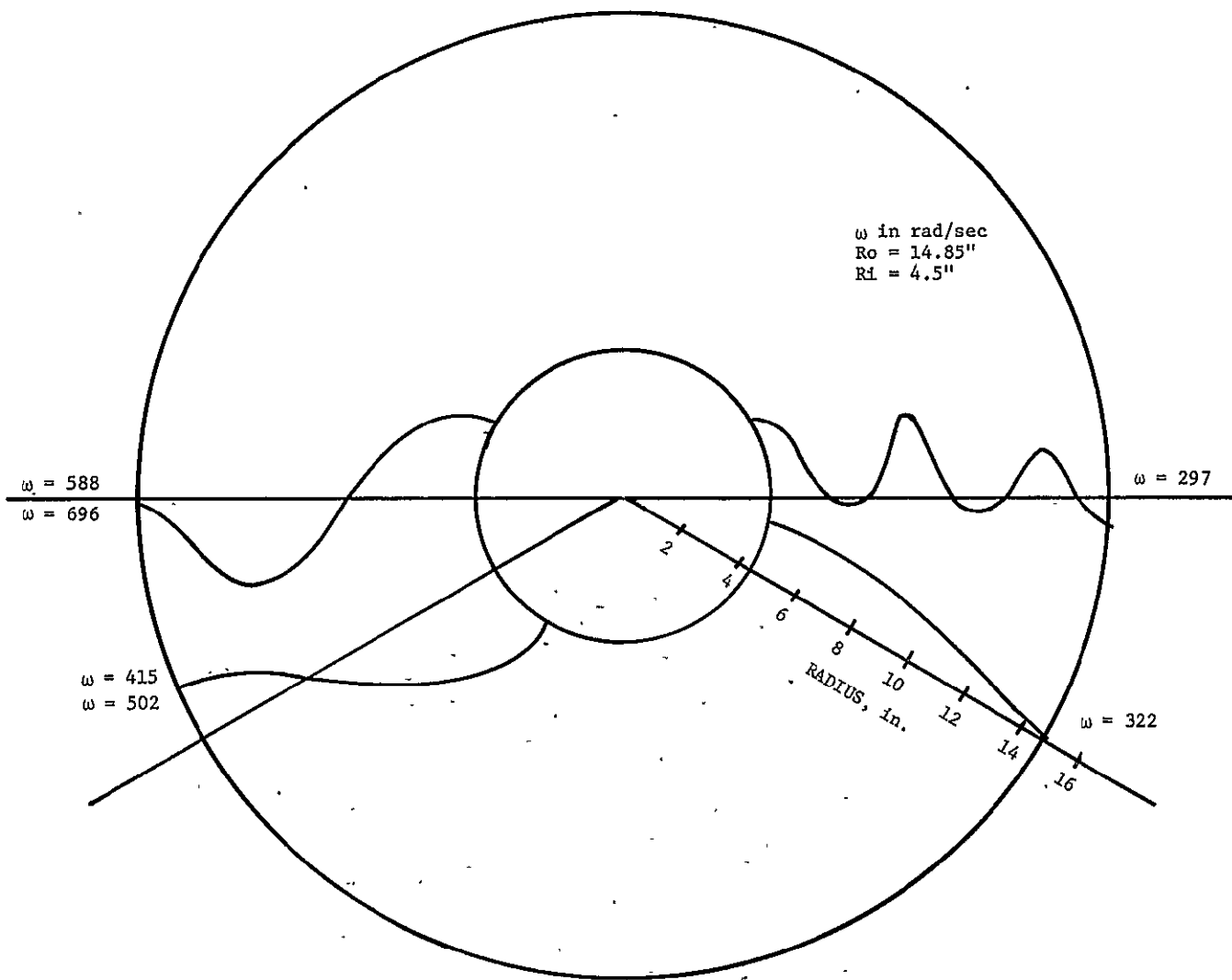


Figure 20.- Elastic propellant shear deflections at system frequencies.

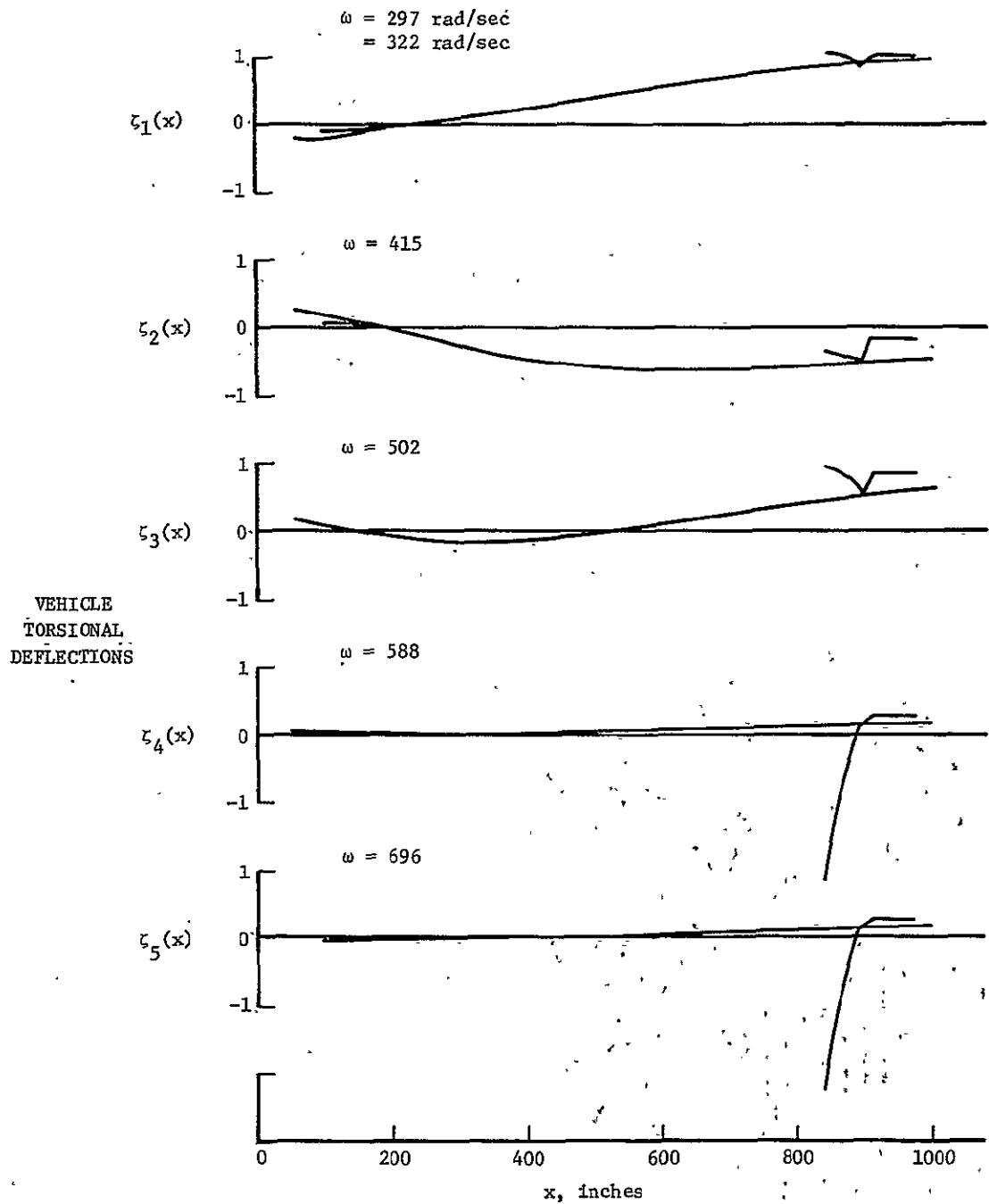


Figure 21.- Launch vehicle deflections at system frequencies with elastic propellant.

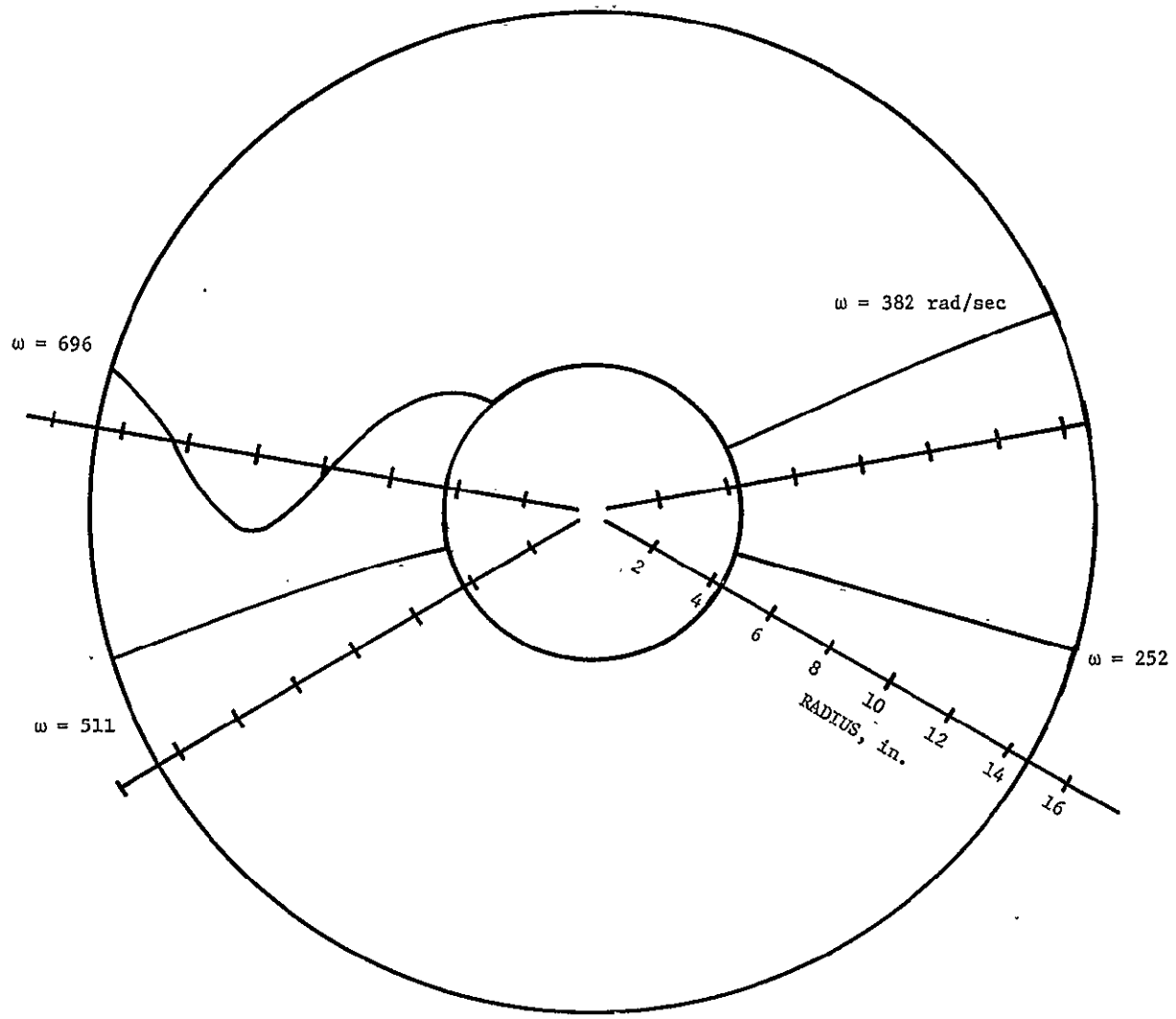


Figure 22.- Viscoelastic propellant shear deflections at system frequencies.

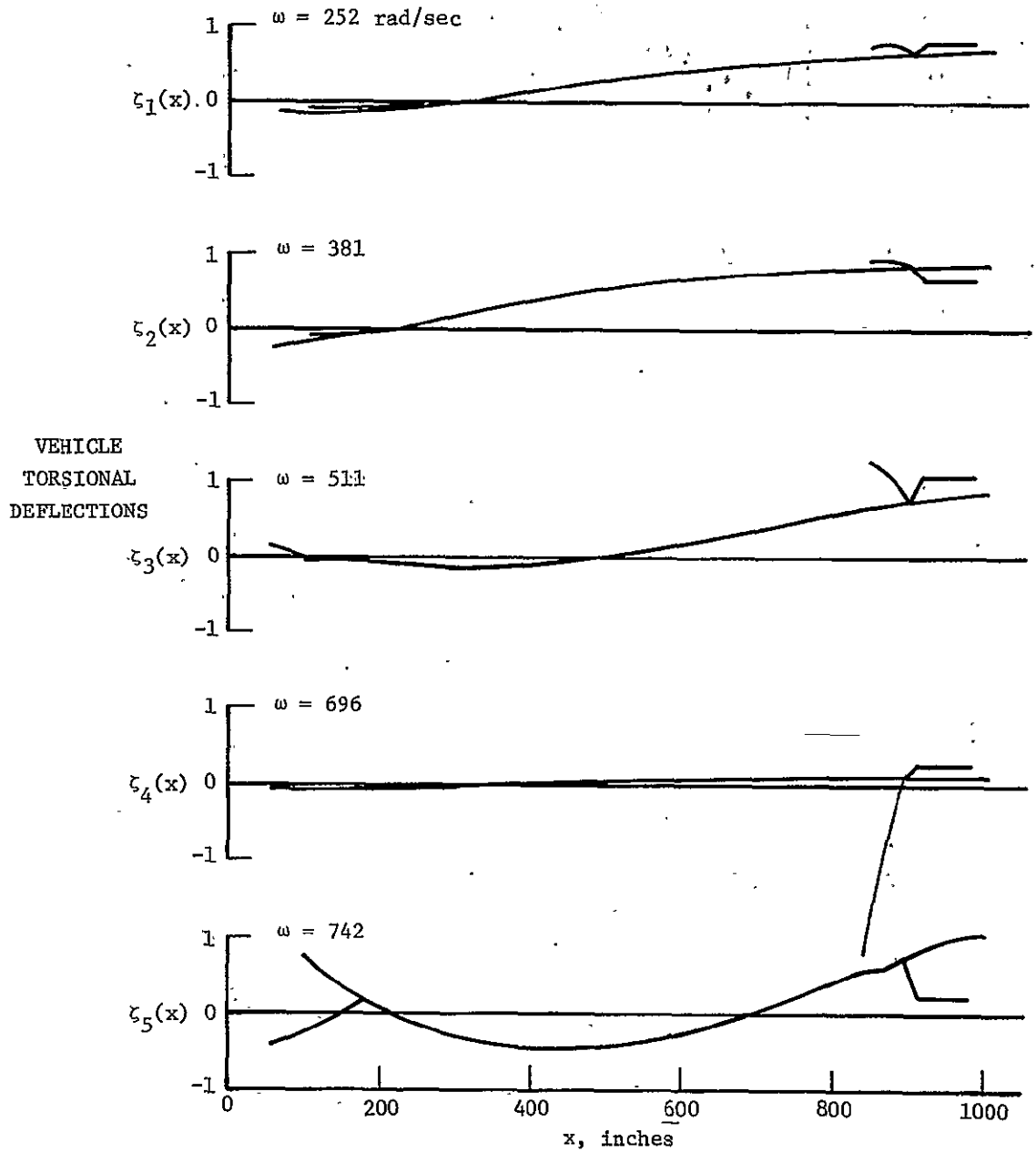


Figure 23.- Launch vehicle deflections at system frequencies with viscoelastic propellant.

Finally, the propellant was assumed rigid and the systems analysis again performed to yield the vehicle deflections at the system frequencies (fig. 24). Because of the simplicity of the propellant assumption, no propellant modes are presented. The results agree well with those of reference [42] even though the method of analysis is quite different.

For comparison, the system frequency spectrum for each of the three propellant assumptions is presented in Table V.

Discussion of Results

It is readily apparent from observing the Table V results that there are essentially no differences in the frequency spectrum between the rigid and viscoelastic propellant-vehicle systems. The differences between the elastic and viscoelastic frequency spectra are more pronounced with six elastic propellant-system modes occurring in the same range (0 to 696 rad/sec) as that in which only four viscoelastic propellant-system modes occur. The mode-by-mode frequency equivalence in the viscoelastic versus rigid propellant vehicle systems results, however, are misleading. Whereas the viscoelastic propellant behaves rigidly through the third system mode (511 rad/sec) (see fig. 20) it will be noted that the propellant responds at 696 rad/sec in quite a flexible manner.

A further observation may be made by comparing the system vehicle response data of figures 21 and 22. It is noted that very little differences occur in these modes with viscoelastic versus rigid propellant assumptions. It appears that the rigid propellant assumption

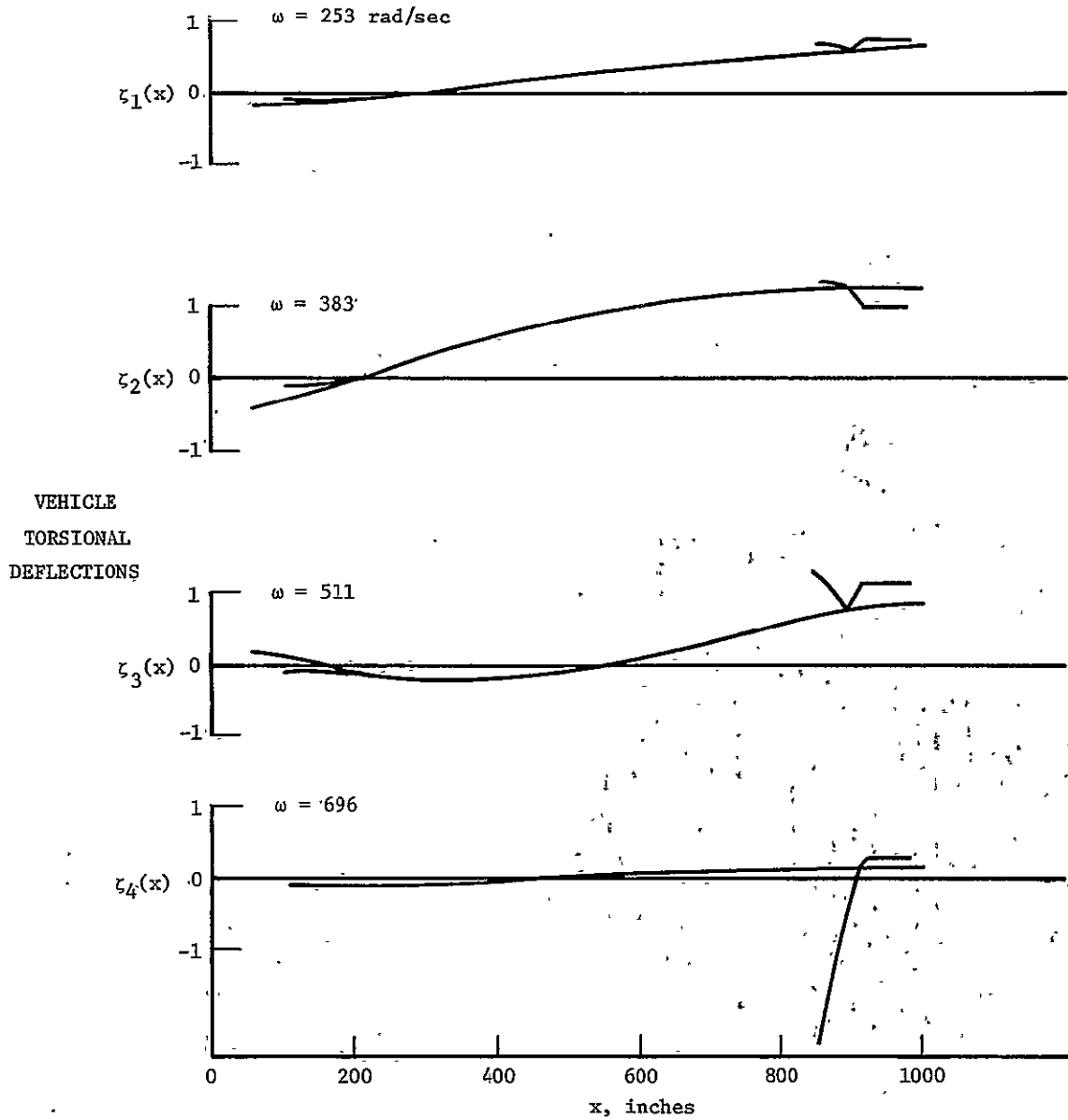


Figure 24.- Launch vehicle deflections at system frequencies with rigid propellant.

TABLE V.- LAUNCH VEHICLE SYSTEM MODES AND FREQUENCIES
FOR VARIOUS PROPELLANT ASSUMPTIONS

Mode	Launch vehicle system frequencies (rad/sec)		
	Elastic propellant	Viscoelastic propellant	Rigid propellant
1	297	252	252
2	322	382	383
3	476	511	511
4	502	696	696
5	588	742	742
6	696	886	886

has small effect on the vehicle responses in a gross sense as compared to the viscoelastic propellant assumption. The appropriate propellant assumption however, is still quite important since it is always necessary to have complete knowledge of key system component natural response characteristics to insure structural design integrity as well as proper guidance system selection.

VI. CONCLUDING REMARKS

The primary objective of the enclosed analysis was to develop a systems analytical method which would permit the examination of various upper stage propellant assumptions and the effect of these assumptions on launch vehicle system dynamics in torsion. As a result of the investigation and in order to meet the objective, a launch vehicle systems analysis has been performed wherein the propellant and vehicle natural modes were generated separately and then coupled together via Lagrange multiplier relations for the appropriate boundary conditions. For the propellant shear displacement, a general closed form Bessel's solution to the governing equations of motion has been developed. Simple harmonic motion was assumed, and general expressions for both the secular equation and the propellant normalized modes have been derived. Also, an orthogonality proof for the propellant free-free modes has been provided. An alternate and concise method for evaluating the normalized free-free propellant modes and frequency expressions using asymptotic approximations to the Bessel's functions has been presented.

The viscoelastic frequencies of the propellant were developed by neglecting loss modulus and using an empirically established frequency-dependent storage modulus in conjunction with an existing frequency correspondence principle relating viscoelastic and elastic frequencies. Since damping was neglected, the analysis may be considered as quasi-elastic but with variable shear modulus. Assumptions that damping was

negligible were justified on the basis of published data on the relation of storage modulus to loss modulus for the frequency range of interest.

In the systems problem development, several convenient mathematical methods were employed which rendered the problem more tractable. First, Lagrange multiplier methods were used to describe the constraint conditions. Boundary conditions could thereby be satisfied on the sum of the vehicle and propellant modes rather than on individual modes such as required in Rayleigh-Ritz procedures. Readily obtained free-free component modes can therefore be used. Also, use of Lagrange multipliers causes convergence on the exact frequency from the lower side as compared to Rayleigh-Ritz procedures which converge from the higher side. Although use of the multiplier relations uncouples the equations of motion for the vehicle and propellant, the effect of the multipliers is to increase the size of and cause singularity of the system matrices. This problem is alleviated by application of a frequency scaling technique which permits even rigid body elements in the system matrices.

Application of the total analytical process was effected in two ways. First, an experimental model consisting of a neoprene disc attached at its inner radius to a brass shaft was built to verify the analytical method. The shaft and neoprene disc analytical modes were generated separately, then coupled together in the systems problem. The experimental frequencies and mode shapes were then obtained and compared with analytical values. Good agreement was obtained in the

frequency spectrum although only the lower modes could be obtained experimentally. It is felt that more accelerometers should have been used, or perhaps other methods should be developed for modal determination of such systems.

The systems analysis was next applied to a characteristic launch vehicle and rigid, elastic, and viscoelastic propellant assumptions were examined. It was found that while the vehicle modal responses at system frequencies differed only slightly for the three assumptions, propellant component natural frequency and responses at system natural frequencies were considerably different. It may be concluded that correct propellant description is more important from the standpoint of its own response at system frequencies rather than from any modifying effect it may have on overall vehicle response.

It is also concluded that appropriate propellant flexibility assumptions are required if correct response characteristics of launch vehicle systems which contain solid propellants as upper stages are to be determined. In this regard, it is felt that the dissertation investigation extends previous work in vehicle torsional dynamics.

A more formidable set of tasks which are recommended to extend the analysis contained herein would include three-dimensional visco-elasticity solutions (which would thereby permit torsional as well as shear deflection throughout the propellant length), elastic propellant case assumptions and the use of noncircular propellant core configurations.

VII. BIBLIOGRAPHY

- Gutowski, R.: Torsional Vibrations of a Nonhomogeneous Cylinder in a Nonstationary Temperature Field. International Union of Theoretical and Applied Mechanics, Symposium Warsaw (September 2 through 9, 1958), Pergamon Press, New York.
2. Achenbach, J. D.: Forced Vibrations of a Burning Rocket. AIAA Journal, vol. 3, No. 7, July 1965.
 3. Shinozuka, M.: Stresses in a Incompressible Viscoelastic-Plastic Thick-Walled Cylinder. AIAA Journal, vol. 2, No. 10, October 1964.
 4. Baltrukonis, J. H.; and Magrab, E. B.: Dynamic Internal Pressurization of an Infinitely-Long, Thick-Walled, Linearly-Viscoelastic Cylinder Case Bonded to a Thin Elastic Tank. The Catholic University of America, Washington, D. C., Tech. Rep. No. 2 to the Hercules Powder Company, Magna, Utah, under Res. Subcont. to No. 177, AF04(647)-243, February, 1964.
 5. Rogers, T. G.; and Lee, E. H.: The Cylinder Problem in Viscoelastic Stress Analysis. Qtr. of Appl. Mech., vol XXII, No. 2, 1964.
 6. Schapery, R. A.: Thermomechanical Behavior of Viscoelastic Media With Variable Properties Subjected to Cyclic Loading. American Society of Mechanical Engineers, Fluids Engineering Conference, Washington, D. C., June 7-9, 1965.
 7. Goldberg, William: Torsional Vibrations of a Hollow Viscoelastic Cylinder. Aberdeen Proving Ground, Maryland, Ballistics Research Laboratories, Memorandum No. 1570, June 1964.
 8. Wolosewick, R. M.; and Gratch, Serge: Transient Response in a Viscoelastic Material With Temperature-Dependent Properties and Thermomechanical Coupling. Journal of Applied Mechanics, September, 1965.
 9. Henry, L. A.; and Freudenthal, A. M.: Standing Waves in a Viscoelastic Cylinder Case-Bonded to a Thin Shell. Preprint 65-173, AIAA Sixth Solid Propellant Rocket Conference. February 1965.
 10. Chree, C.: The Equations of an Isotropic Elastic Solid in Polar and Cylindrical Coordinates, Their Solution and Application. Trans. Cambridge Phil. Soc. 14, 250 (1889).

11. Ghosh, J.: Longitudinal Vibrations of a Hollow Cylinder. Bull. Calcutta Math. Soc., 14, 31 (1923).
12. McFadden, J.A.: Radial Vibrations of Thick-Walled Hollow Cylinders. J. Acoust. Soc. Amer., 26, 714 (1954).
13. Mirsky, I.; and Herrmann, G.: Axially Symmetric Motions of Thick Cylindrical Shells. J. Appl. Mech., 25, 97 (1958).
14. Greenspon, J.E.: Flexural Vibrations of a Thick-Walled Circular Cylinder. Proc. Third U. S. National Congress Applied Mechanics Amer. Soc. Mech. Engrs., New York City (1958), p. 163.
15. Greenspon, J.E.: Flexural Vibrations of a Thick-Walled Circular Cylinder According to the Exact Theory of Elasticity. J. Aero-Space Science, 27, 37, (1960).
16. Bird, J.F.; Hart, R. W.; and McClure, F. T.: Vibrations of Thick-Walled Hollow Cylinders: Exact Numerical Solutions. J. Acoust. Soc. Amer., 32, 1404 (1960).
17. Baltrukonis, J. H.: Forced Transverse Vibrations of a Solid Elastic Core Case-Bonded to an Infinitely-Long, Rigid, Cylinder. The Catholic University of America, Tech. Rep. No. 1 to NASA under Research Grant No. Nsg-125-61 (Aug. 1961).
18. Baltrukonis, J. H.; Gottenberg, W. G.; and Schreiner, R.N.: Dynamics of a Hollow, Elastic Cylinder Contained By an Infinitely-Long, Rigid, Circular-Cylindrical Tank. J. Acoust. Soc. Amer., 32, 1539 (1960).
19. Williams, M.; Blatz, P.J.; and Schapery, R. A.: Fundamental Studies Relating to Systems Analysis of Solid Propellants. Final Report - GALCIT 101 Thiokol Subcontract No. RS-69752, February 1961.
20. Eringen, A.C.; et al.-Editors: Mechanics and Chemistry of Solid Propellants. Proceedings of Fourth Symposium on Naval Structural Mechanics, April 19-21, 1965, Pergamon Press, New York.
21. Baltrukonis, J.H.: A Survey of Structural Dynamics of Solid Propellant Rocket Motors. NASA CR-658, 1966.
22. Achenbach, J. D.: Dynamic Response Problems of Solid Propellant Rockets. Solid Rocket Structural Integrity Abstracts, vol. 5, No. 1, January 1968.

23. Achenbach, J. D.: The Structural Dynamics of Solid Propellant Rockets. Applied Mechanics Reviews, vol. 21, No. 6, June 1968, pp. 549-555.
 24. Kelkar, V. S.: Vibrations of a Hollow Elastic Cylinder Bonded to a Thin Casing of a Different Material. NASA TN D-4221, 1967.
 25. Achenbach, J. D.: Torsional Oscillations of an Encased Hollow Cylinder of Finite Length. J. Spacecraft and Rockets, 3, p. 1637 (1966).
 26. Sann, Robert I.; and Shaffer, Bernard W.: Free Transverse Elastic Vibrations of a Solid Cylinder Bonded to a Thin Casing. SIAM J. Appl. Math., vol. 14, No. 2, March 1966, pp. 266-285.
 27. Baltrukonis, J. H.; Chi, M.; and Gottenberg, W. G.: Free Transverse Vibrations in an Infinitely-Long Layered Elastic Cylinder. TR-3, Catholic Univ. of America, NASA Research Grant NsG-125-61, Suppl. 1-62.
 - *28. Wells, G. R.; and Mitchell, H. P.: Analytical Development of Mathematical Model for Response of Saturn IB Launch Vehicles to Inflight Winds. Ref. [A], pp. 512-528.
 29. Leadbetter, S. A.; Alley, V. A.; Herr, R. W.; and Geringer, A. H.: An Experimental and Analytical Investigation of the Natural Frequencies and Mode Shapes of a Four-Stage Solid Propellant Rocket Vehicle. NASA TN D-1354, August 1962.
 - *30. Jaszlics, I. J.; and Morosow, G.: Dynamic Testing of a 20-Percent Scale Model of the Titan III. Ref. [B], pp. 477-485.
 - *31. Pinson, L. D.; Leonard, H. W.; and Raney, J. P.: Analyses of Longitudinal Dynamics of Launch Vehicles With Application to a 1/10-Scale Saturn V Model. Ref. [A], pp. 502-511.
 32. Rubin, S.: Transient Response Problems of Space Vehicles. Proceedings NASA Symposium on Transient Loads and Response of Space Vehicles, Langley Research Center, November 1967.
 - *33. Leadbetter, S. A.; and Raney, J. P.: Analytical and Experimental Studies of the Dynamics of Launch Vehicles. Ref. [B], pp. 523-527.
- *Ref. [A] Proceedings AIAA/ASME 8th Structures, Structural Dynamics and Materials Conference, Palm Springs, California (1967)
- *Ref. [B] Proceedings AIAA Symposium on Structural Dynamics and Aeroelasticity, Boston, Massachusetts (1965).

34. Alley, V. L., Jr.; Guillotte, R. J.; and Hunter, L. D.: A Method of Determining Modal Data of a Nonuniform Beam With Effects of Shear Deformation and Rotary Inertia. NASA TN D-2930, 1965.
35. Alley, Vernon L., Jr.; and Gerringer, A. Harper: A Matrix Method for the Determination of the Natural Vibrations of Free-Free Unsymmetrical Beams With Application to Launch Vehicles. NASA TN D-1247, 1962.
36. Wingate, R. T.: Matrix Analysis of Longitudinal and Torsional Vibrations in Nonuniform Multibranch Beams. NASA TN D-3844, 1967.
37. Wang, C.: Applied Elasticity, McGraw Hill Book Co., 1953, p. 52.
38. Bland, D. R.: The Theory of Linear Viscoelasticity, Pergamon Press, New York, 1960.
39. Fisher, G. M. C.; and Leitman, M. J.: A Correspondence Principle for Free Vibrations of a Viscoelastic Solid. Journal of Applied Mechanics, Trans. ASME Ser. E., vol. 87, December 1966, pp. 924-926.
40. Dynamic Mechanical Properties of Solid Propellants. Atlantic Research Corp., Alexandria, Virginia. Quarterly Technical Summary, report 3, figs. 4 and 5 (1964).
41. Jennings, A.: Natural Vibrations of a Free Structure, Aircraft Engineering. March 1962, pp. 81-83.
42. Faison, R. W.: An Analysis of the Significance of Booster Engine Cutoff Torsional Transients on the FIRE Vehicle. MS Thesis, Virginia Polytechnic Institute, 1966.

VIII. VITA

The author was born in [REDACTED], in [REDACTED]. He received his elementary education in Daytona Beach and Orlando, Florida and in Savannah, Georgia and graduated from Orlando Senior High School in 1949. He was then employed as a sporting goods store clerk prior to entering the U. S. Navy in 1951. He was married to Mabel M. Fimple in 1954, completed his military service in 1955, and entered Clemson College in the fall of that year. He completed his Bachelor's Degree in Mechanical Engineering in June 1959 and accepted employment with Bell Telephone Laboratories in Whippany, New Jersey as a Member of Technical Staff. He worked in military equipment design at Bell while attending graduate school at the Murray Hill graduate center of New York University. He was then employed with Pratt and Whitney Aircraft as a group coordinator in the Cryogenic Flow Measurement Section from 1960 to 1963. During this period he continued his academic work at the West Palm Beach graduate branch of the University of Florida. He accepted employment with the NASA in 1963 as an aerospace technologist and completed his Master's Degree in Engineering Mechanics in absentia from New York University in October 1964 at Virginia Polytechnic Institute. He returned to residency at Virginia Polytechnic Institute in 1966 to pursue further graduate work in engineering mechanics. He is currently employed as Head of the Design and Structural Integration Section of the Space Systems Research Division of NASA Langley Research Center and resides with his wife and three children in Newport News, Virginia.

Ross I. Goble

IX. APPENDICES

In this chapter are included studies relevant to the foregoing investigation.

Appendix A - General Frequency and Modal Relations for Propellant Shear Dynamics

The general solution to the Bessel's equation (2-15) describing the propellant motion in shear (2-16) was found to be

$$p(r) = AJ_1(\lambda r) + BY_1(\lambda r) \quad (A-1)$$

Free-free boundary conditions were used in Chapter II to establish the natural modes for the investigation. The resulting equation for the frequencies (2-24) was

$$\begin{aligned} & \left[\lambda_n R_0 J_0(\lambda R_0) - 2 J_1(\lambda R_0) \right] \left[\lambda_n R_1 Y_0(\lambda R_1) - 2 Y_1(\lambda R_1) \right] \\ & - \left[\lambda_n R_0 Y_0(\lambda R_0) - 2 Y_1(\lambda R_0) \right] \left[\lambda_n R_1 J_0(\lambda R_1) - 2 J_1(\lambda R_1) \right] = 0 \end{aligned} \quad (A-2)$$

and the expression for the normalized modes (2-29) was established as

$$\bar{p}(r) = \frac{\left[\lambda R_1 J_0(\lambda R_1) - 2 J_1(\lambda R_1) \right] Y_1(\lambda r) - \left[\lambda R_1 Y_0(\lambda R_1) - 2 Y_1(\lambda R_1) \right] J_1(\lambda r)}{\left[\lambda R_1 J_0(\lambda R_1) - 2 J_1(\lambda R_1) \right] Y_1(\lambda R_0) - \left[\lambda R_1 Y_0(\lambda R_1) - 2 Y_1(\lambda R_1) \right] J_1(\lambda R_0)} \quad (A-3)$$

Pinned-Free Modes

For the case of pinned-free boundaries of the propellant, the boundary conditions are expressed as

$$p(r) \Big|_{R_1} = 0, \quad \frac{dp}{dr} \Big|_{R_0} = \frac{p(R_0)}{R_0} \quad (\text{A-4})$$

Making substitution of relation (A-1) into (A-4) and performing the indicated operations yields

$$AJ_1(\lambda R_1) + BY_1(\lambda R_1) = 0 \quad (\text{A-5})$$

and

$$AJ_1'(\lambda R_0) + BY_1'(\lambda R_0) = \frac{AJ_1(\lambda R_0) + BY_1(\lambda R_0)}{R_0} \quad (\text{A-6})$$

from which the transcendental equation is readily developed by rearranging and setting the determinant of the coefficients equal to zero, or

$$\begin{bmatrix} J_1(\lambda R_1) & Y_1(\lambda R_1) \\ J_1'(\lambda R_0) - \frac{J_1(\lambda R_0)}{R_0} & Y_1'(\lambda R_0) - \frac{Y_1(\lambda R_0)}{R_0} \end{bmatrix} = 0 \quad (\text{A-7})$$

Making use of the recurrence relations for the Bessel's functions (2-21) and (2-22) permits (A-7) to be simplified to

$$\begin{aligned} & [\lambda R_0 J_0(\lambda R_0) - 2 J_1(\lambda R_0)] [Y_1(\lambda R_1)] \\ & - [\lambda R_0 Y_0(\lambda R_0) - 2 Y_1(\lambda R_0)] [J_1(\lambda R_1)] = 0 \end{aligned} \quad (\text{A-8})$$

the normalized modes expression is developed in a straightforward manner to yield

$$\bar{p}(r) = \frac{[J_1(\lambda R_1)] Y_1(\lambda r) - [Y_1(\lambda R_1)] J_1(\lambda r)}{[J_1(\lambda R_1)] Y_1(\lambda R_0) - [Y_1(\lambda R_1)] J_1(\lambda R_0)} \quad (A-9)$$

where the normalizing radius is R_0 .

Free-Pinned Modes

For the case of free-pinned modes, the boundary conditions of (A-6) are readily converted simply by interchanging quantities R_0 and R_1 , or

$$\begin{aligned} AJ_1(\lambda R_0) + BY_1(\lambda R_0) &= 0 \\ AJ_1'(\lambda R_1) + BY_1'(\lambda R_1) &= \frac{AJ_1(\lambda R_1) + BY_1(\lambda R_1)}{R_1} \end{aligned} \quad (A-10)$$

which leads directly to the transcendental relation

$$\begin{bmatrix} J_1(\lambda R_0) & Y_1(\lambda R_0) \\ J_1'(\lambda R_1) - \frac{J_1(\lambda R_1)}{R_1} & Y_1'(\lambda R_1) - \frac{Y_1(\lambda R_1)}{R_1} \end{bmatrix} \quad (A-11)$$

The normalized modes relation is readily expressed as

$$\bar{p}(r) = \frac{[\lambda R_1 J_0(\lambda R_1) - 2 J_1(\lambda R_1)] Y_1(\lambda r) - [\lambda R_1 Y_0(\lambda R_1) - 2 Y_1(\lambda R_1)] J_1(\lambda r)}{[\lambda R_1 J_0(\lambda R_1) - 2 J_1(\lambda R_1)] Y_1(\lambda R_0) - [\lambda R_1 Y_0(\lambda R_1) - 2 Y_1(\lambda R_1)] J_1(\lambda R_0)} \quad (A-12)$$

By examination of relations (A-2), (A-3), (A-8), (A-9), (A-11), and (A-12), several observations can be made.

First the transcendental relation can be expressed in general form as

$$\begin{aligned} & \left[a_1 \lambda R_0 J_0(\lambda R_0) - a_2 J_1(\lambda R_0) \right] \left[a_3 \lambda R_1 Y_0(\lambda R_1) - a_4 Y_1(\lambda R_1) \right] \\ & - \left[a_1 \lambda R_0 Y_0(\lambda R_0) - a_2 Y_1(\lambda R_0) \right] \left[a_3 \lambda R_1 J_0(\lambda R_1) - a_4 J_1(\lambda R_1) \right] = 0 \end{aligned} \quad (A-13)$$

and the normalized modes equations can be expressed in general form as

$$\bar{p}(r) = \frac{\left[a_3 \lambda R_1 J_0(\lambda R_1) - a_4 J_1(\lambda R_1) \right] Y_1(\lambda r) - \left[a_3 \lambda R_1 Y_0(\lambda R_1) - a_4 Y_1(\lambda R_1) \right] J_1(\lambda r)}{\left[a_3 \lambda R_1 J_0(\lambda R_1) - a_4 J_1(\lambda R_1) \right] Y_1(\lambda R_0) - \left[a_3 \lambda R_1 Y_0(\lambda R_1) - a_4 Y_1(\lambda R_1) \right] J_1(\lambda R_0)} \quad (A-14)$$

where by appropriate selection of the a coefficients the three cases of free-free, free-pinned, and pinned-free modal characteristics can be established. The proper coefficients are given in the following list.

CASES			
Coefficients	Free-Free	Free-Pinned	Pinned-Free
a_1	1	0	1
a_2	2	-1	2
a_3	1	1	0
a_4	2	2	-1

An additional observation is that the mode shapes (A-14) for the free-free and free-pinned boundary conditions have identical form with $a_3 = 1$ and $a_4 = 2$ for both cases. The identical nature of the modes is due to the selection of the free end condition for both cases to develop the modal expressions. This selection is clarified by the steps required to proceed from relations (2-25) to (2-29) in Chapter II. The transcendental equations for the two cases are of course different.

A general set of equations for free-free, free-pinned, and pinned-free modes and frequencies has thus been developed in this investigation, with free-free modal information being used in the earlier systems analysis.

Appendix B - Orthogonality of the Component Modes

Thick-Walled Cylinder Component

The differential equation of motion for the element of cross section is (from equation (2-14)) for any mode

$$\frac{d^2 p_n}{dr^2} + \frac{1}{r} \frac{dp_n}{dr} + \left(\frac{\omega_n^2 \delta}{G_F} - \frac{1}{r^2} \right) p_n = 0 \quad (B-1)$$

where p_n indicates the normalized nth mode $p_n(r)$.

The same equation written for the normalized mth mode, $p_m(r)$ is

$$\frac{d^2 p_m}{dr^2} + \frac{1}{r} \frac{dp_m}{dr} + \left(\frac{\omega_m^2 \delta}{G_F} - \frac{1}{r^2} \right) p_m = 0 \quad (B-2)$$

Multiplying (B-1) by p_m and (B-2) by p_n , subtracting the two results and simplifying yields

$$\frac{\delta}{G_F} (\omega_n^2 - \omega_m^2) r p_m p_n = r p_n \frac{d^2 p_m}{dr^2} + p_n \frac{dp_m}{dr} - r p_m \frac{d^2 p_n}{dr^2} - p_m \frac{dp_n}{dr}$$

or

$$\frac{\delta}{G_F} (\omega_n^2 - \omega_m^2) r p_m p_n = p_n \frac{d}{dr} (r p_m') - p_m \frac{d}{dr} (r p_n') \quad (B-3)$$

Integrating both sides of equation (B-3) between the limits R_i to R_o yields

$$\frac{\delta}{G_F} (\omega_n^2 - \omega_m^2) \int_{R_i}^{R_o} r p_m p_n dr = \int_{R_i}^{R_o} p_n \frac{d}{dr} (r p_m') dr - \int_{R_i}^{R_o} p_m \frac{d}{dr} (r p_n') dr \quad (B-4)$$

The right side of equation (B-4) can be evaluated by integrating the first of the integrals by parts, letting

$$\begin{aligned} u &= p_n & dv &= \frac{d}{dr} (rp_m') dr \\ du &= p_n' dr & v &= rp_m' \end{aligned}$$

Thus, the first integral on the right side of equation (B-4) becomes

$$rp_n p_m' \Big|_{R_i}^{R_o} - \int_{R_i}^{R_o} rp_m' p_n' dr \quad (B-5)$$

Similarly, the second integral becomes

$$rp_m p_n' \Big|_{R_i}^{R_o} - \int_{R_i}^{R_o} rp_n' p_m' dr \quad (B-6)$$

Substitution of equations (B-5) and (B-6) into equation (B-4), and evaluation of the result at the integral limits yields, after simplification

$$\begin{aligned} \frac{\delta}{G_F} (\omega_n^2 - \omega_m^2) \int_{R_i}^{R_o} rp_m p_n dr &= R_o p_n(R_o) p_m'(R_o) - R_o p_m(R_o) p_n'(R_o) \\ &\quad - R_i p_n(R_i) p_m'(R_i) + R_i p_m(R_i) p_n'(R_i) \end{aligned} \quad (B-7)$$

Substituting into relation (B-7), the following free-free boundary conditions

$$p_n'(R_0) = \frac{p_n(R_0)}{R_0}$$

$$p_n'(R_1) = \frac{p_n(R_1)}{R_1}$$

which are true for all modes, it is seen that the sum of the right-hand terms of (B-7) vanishes, or

$$\left(\omega_n^2 - \omega_m^2\right) \int_{R_1}^{R_0} r p_m p_n dr = 0 \quad (\text{B-8})$$

and, since the ω_n are distinct, then for the total cylinder volume, the orthogonality condition is

$$\left. \begin{aligned} 2\pi\delta \int_{R_1}^{R_0} r p_m p_n dr &= 0, & m \neq n \\ &= M_{Fn}, & m = n \end{aligned} \right\} \quad (\text{B-9})$$

where M_{Fn} is called the generalized mass of the fuel.

Elastic Thin-Walled Cylinder Component

It can readily be shown from established procedures that a like orthogonality relation holds for the thin-walled cylinder. The expression is

$$\int_0^L z(x) \zeta_i(x) \zeta_j(x) dx = 0, \quad i \neq j$$

$$= I_{V_i}, \quad i = j \quad (\text{B-10})$$

Appendix C - Asymptotic Approximations

Unless Bessel's function subroutines are readily available, computation of the generalized mass (equation B-9) in the orthogonality derivation requires cumbersome evaluation of an integral in which the Bessel's functions must be expanded in series form. It is convenient to utilize asymptotic approximations to the Bessel's functions in that computation. The computation of the generalized mass and the associated reevaluation of equations (2-24) and (2-29) follows:

The expression for the effective mass of the fuel as developed in Appendix B is

$$M_{R_n} = 2\pi\delta \int_{R_1}^{R_0} r \left[\bar{P}_n(r) \right]^2 dr \quad (C-1)$$

where $\bar{P}_n(r)$ is obtained from equation (2-29) as

$$\bar{P}_n(r) = \frac{\left[\lambda R_1 J_0(\lambda R_1) - 2J_1(\lambda R_1) \right] Y_1(\lambda r) - \left[\lambda R_1 Y_0(\lambda R_1) - 2Y_1(\lambda R_1) \right] J_1(\lambda r)}{\left[\lambda R_1 J_0(\lambda R_1) - 2J_1(\lambda R_1) \right] Y_1(\lambda R_0) - \left[\lambda R_1 Y_0(\lambda R_1) - 2Y_1(\lambda R_1) \right] J_1(\lambda R_0)}$$

Substitution of the right side of (2-29) for the normalized mode shape $\bar{P}_n(r)$ into equation (C-1) yields

$$M_{F_n} = 2\pi l b \int_{R_1}^{R_0} r \left\{ \frac{\left[\lambda R_1 J_0(\lambda R_1) - 2J_1(\lambda R_1) \right] Y_1(\lambda r) - \left[\lambda R_1 Y_0(\lambda R_1) - 2Y_1(\lambda R_1) \right] J_1(\lambda r)}{\left[\lambda R_1 J_0(\lambda R_1) - 2J_1(\lambda R_1) \right] Y_1(\lambda R_0) - \left[\lambda R_1 Y_0(\lambda R_1) - 2Y_1(\lambda R_1) \right] J_1(\lambda R_0)} \right\}^2 dr \quad (C-2)$$

where $\lambda = \lambda_n$ the eigenvalue of the nth mode.

Using the asymptotic approximations for Bessel's functions of the first and second kinds, which are:

$$J_n(\bar{x}) \cong \frac{\cos\left(\bar{x} - \frac{\pi}{4} - \frac{n\pi}{2}\right)}{\sqrt{\frac{\pi\bar{x}}{2}}} \quad (C-3)$$

$$Y_n(\bar{x}) \cong \frac{\sin\left(\bar{x} - \frac{\pi}{4} - \frac{n\pi}{2}\right)}{\sqrt{\frac{\pi\bar{x}}{2}}} \quad (C-4)$$

and substituting equations (C-3) and (C-4) into equation (C-2) and simplifying, the numerator of the braced quantity becomes

$$\left\{ \frac{2r}{\pi\lambda\sqrt{R_1 r}} \left[\lambda R_1 \sin\left(\lambda r - \frac{3\pi}{4}\right) \cos\left(\lambda R_1 - \frac{\pi}{4}\right) - \lambda R_1 \cos\left(\lambda r - \frac{3\pi}{4}\right) \sin\left(\lambda R_1 - \frac{\pi}{4}\right) \right] + 2 \sin\left(\lambda R_1 - \frac{3\pi}{4}\right) \cos\left(\lambda r - \frac{3\pi}{4}\right) - 2 \cos\left(\lambda R_1 - \frac{3\pi}{4}\right) \sin\left(\lambda r - \frac{3\pi}{4}\right) \right\}^2 \quad (C-5)$$

To simplify notation, let

$$\left. \begin{aligned} \lambda R_1 - \frac{3\pi}{4} &= \beta \\ \lambda R_1 - \frac{\pi}{4} &= \alpha \\ \lambda r - \frac{3\pi}{4} &= \mu \end{aligned} \right\} \quad (C-6)$$

Employing equation (C-6) and simplifying, quantity (C-5) reduces to

$$\frac{4}{(\pi\lambda)^2 R_1 r} \left\{ \lambda R_1 [\sin \mu \cos \alpha - \cos \mu \sin \alpha] \right\}^2 + 2 [\sin \beta \cos \mu - \cos \beta \sin \mu]^2$$

which can be further reduced by use of double angle quadrant relations and simplification, to

$$\frac{4}{(\pi\lambda)^2 R_1 r} \left\{ 2 \sin (\beta - \mu) + \lambda R_1 \sin (\mu - \alpha) \right\}^2 \quad (C-7)$$

Resubstitution of equations (C-6) now provides the desirable form of term (C-7) after simplifying by angle quadrant relations, or

$$\frac{4}{(\pi\lambda)^2 R_1 r} \left\{ 2 \sin \lambda(R_1 - r) - \lambda R_1 \cos \lambda(R_1 - r) \right\}^2 \quad (C-8)$$

Thus, equation (C-2) may now be written as

$$M_{Fn} = 2\pi l \delta \int_{R_1}^{R_0} r \left[\frac{\frac{4}{(\pi\lambda)^2 R_1 r} \left\{ 2 \sin \lambda(R_1 - r) - \lambda R_1 \cos \lambda(R_1 - r) \right\}^2}{\frac{4}{(\pi\lambda)^2 R_1 R_0} \left\{ 2 \sin \lambda(R_1 - R_0) - \lambda R_1 \cos \lambda(R_1 - R_0) \right\}^2} \right] dr$$

which can be simplified to

$$M_{F_n} = \frac{2\pi\lambda\delta R_0}{K_R} \int_{R_i}^{R_0} \left[2 \sin \lambda(R_i - r) - \lambda R_i \cos \lambda(R_i - r) \right]^2 dr \quad (C-9)$$

where

$$K_R = \left\{ 2 \sin \lambda(R_i - R_0) - \lambda R_i \cos \lambda(R_i - R_0) \right\}^2 \quad (C-10)$$

Expanding the integrand of equation (C-9), simplifying, and integrating yields

$$M_{F_n} = \frac{2\pi\lambda\delta R_0}{K_R} \left\{ \begin{array}{l} -\frac{4}{\lambda} \left[\frac{\lambda(R_i - r)}{2} - \frac{\sin 2\lambda(R_i - r)}{4} \right] \Big|_{R_i}^{R_0} \\ -\frac{2\lambda R_i}{-2\lambda} \left[-\cos 2\lambda(R_i - r) \right] \Big|_{R_i}^{R_0} \\ +\frac{\lambda^2 R_i^2}{-\lambda} \left[\frac{\lambda(R_i - r)}{2} + \frac{\sin 2\lambda(R_i - r)}{4} \right] \Big|_{R_i}^{R_0} \end{array} \right\} \quad (C-11)$$

After substitution of the limits and simplifying, the final relation for the generalized mass of the fuel is

$$M_{F_n} = \frac{2\pi\lambda\delta R_0}{K_R} \left\{ R_i \left[1 - \cos 2\lambda(R_i - R_0) \right] + \left(\frac{4}{\lambda} - \lambda R_i^2 \right) \left[\frac{\sin 2\lambda(R_i - R_0)}{4} \right] - \left[\frac{\lambda(R_i - R_0)}{2} \right] \left(\frac{4}{\lambda} + \lambda R_i^2 \right) \right\} \quad (C-12)$$

It is readily seen that expression (C-12) lessens considerably the labor involved in computing the effective inertia as opposed to the use of Bessel's functions. The eigenvalue problem for the approximate solution is developed as follows:

Substituting the equations (C-3) and (C-4) into equation (2-24) for the appropriate order Bessel's functions yield

$$\begin{aligned} & \left[\lambda_n R_0 \frac{\cos\left(\lambda R_0 - \frac{\pi}{4}\right)}{\sqrt{\frac{\pi \lambda R_0}{2}}} - 2 \frac{\cos\left(\lambda R_0 - \frac{3\pi}{4}\right)}{\sqrt{\frac{\pi \lambda R_0}{2}}} \right] \left[\lambda_n R_1 \frac{\sin\left(\lambda R_1 - \frac{\pi}{4}\right)}{\sqrt{\frac{\pi \lambda R_1}{2}}} - 2 \frac{\sin\left(\lambda R_1 - \frac{3\pi}{4}\right)}{\sqrt{\frac{\pi \lambda R_1}{2}}} \right] \\ & - \left[\lambda_n R_0 \frac{\sin\left(\lambda R_0 - \frac{\pi}{4}\right)}{\sqrt{\frac{\pi \lambda R_0}{2}}} - 2 \frac{\sin\left(\lambda R_0 - \frac{3\pi}{4}\right)}{\sqrt{\frac{\pi \lambda R_0}{2}}} \right] \left[\lambda_n R_1 \frac{\cos\left(\lambda R_1 - \frac{\pi}{4}\right)}{\sqrt{\frac{\pi \lambda R_1}{2}}} - 2 \frac{\cos\left(\lambda R_1 - \frac{3\pi}{4}\right)}{\sqrt{\frac{\pi \lambda R_1}{2}}} \right] = 0 \end{aligned} \quad (C-13)$$

or, simplifying (C-13) and rearranging yields

$$\begin{aligned} & \lambda^2 R_0 R_1 \left[\cos\left(\lambda R_0 - \frac{\pi}{4}\right) \sin\left(\lambda R_1 - \frac{\pi}{4}\right) - \sin\left(\lambda R_0 - \frac{\pi}{4}\right) \cos\left(\lambda R_1 - \frac{\pi}{4}\right) \right] \\ & + 2\lambda R_1 \left[\sin\left(\lambda R_0 - \frac{3\pi}{4}\right) \cos\left(\lambda R_1 - \frac{\pi}{4}\right) - \cos\left(\lambda R_0 - \frac{3\pi}{4}\right) \sin\left(\lambda R_1 - \frac{\pi}{4}\right) \right] \\ & + 2\lambda R_0 \left[\sin\left(\lambda R_0 - \frac{\pi}{4}\right) \cos\left(\lambda R_1 - \frac{3\pi}{4}\right) - \cos\left(\lambda R_0 - \frac{\pi}{4}\right) \sin\left(\lambda R_1 - \frac{3\pi}{4}\right) \right] \\ & + 4 \left[\sin\left(\lambda R_1 - \frac{3\pi}{4}\right) \cos\left(\lambda R_0 - \frac{3\pi}{4}\right) - \cos\left(\lambda R_1 - \frac{3\pi}{4}\right) \sin\left(\lambda R_0 - \frac{3\pi}{4}\right) \right] = 0 \end{aligned} \quad (C-14)$$

Again, employing double angle relations, equation (C-14) simplifies to

$$\begin{aligned} & \lambda^2 R_0 R_1 \sin \lambda(R_1 - R_0) + 2\lambda R_1 \sin\left(\lambda R_0 - \lambda R_1 - \frac{\pi}{2}\right) \\ & + 2\lambda R_0 \sin\left(\lambda R_0 - \lambda R_1 + \frac{\pi}{2}\right) + 4 \sin \lambda(R_1 - R_0) = 0 \end{aligned}$$

or

$$[\lambda^2 R_0 R_1 + 4] \sin \lambda(R_1 - R_0) - 2\lambda R_1 \cos \lambda(R_1 - R_0) + 2\lambda R_0 \cos \lambda(R_1 - R_0) = 0$$

or

$$\left[\lambda^2 R_0 R_1 + 4 \right] \sin \lambda(R_1 - R_0) + 2\lambda(R_0 - R_1) \cos \lambda(R_1 - R_0) = 0 \quad (C-15)$$

or, finally

$$\tan \lambda(R_1 - R_0) + \frac{2\lambda(R_0 - R_1)}{4 + R_0 R_1 \lambda^2} = 0 \quad (C-16)$$

which is the transcendental relation, developed from the approximations for the Bessel's function, for the roots λ .

The corresponding normalized mode shape is

$$\bar{P}_n(r) = \sqrt{\frac{R_0}{r}} \left[\frac{2 \sin \lambda(R_1 - r) - \lambda R_1 \cos \lambda(R_1 - r)}{2 \sin \lambda(R_1 - R_0) - \lambda R_1 \cos \lambda(R_1 - R_0)} \right]$$

Appendix D - Method of Obtaining Higher Modes

In order to obtain modes higher than the fundamental in the solution of equation (3-48) an orthogonality sweeping procedure can be used and is developed as follows:

Writing equation (3-48) for the gth and hth modes and rearranging,

$$\omega_g^2 [M] \{y_g\} = [N] \{y_g\} \quad (D-1)$$

$$\omega_h^2 [M] \{y_h\} = [N] \{y_h\} \quad (D-2)$$

Premultiplying (D-1) by y_h and (D-2) by y_g and subtracting the second equation from the first

$$\begin{aligned} & \omega_g^2 [y_h][M] \{y_g\} - [y_h][N] \{y_g\} \\ & - \omega_h^2 [y_g][M] \{y_h\} + [y_g][N] \{y_h\} = 0 \end{aligned} \quad (D-3)$$

By virtue of the symmetry of $[M]$ and $[N]$,

$$[y_h][N] \{y_g\} = [y_g][N] \{y_h\}$$

and a like relation holds for $[M]$ inserted for $[N]$; thus permitting equation (D-3) to be simplified and rearranged to

$$(\omega_g^2 - \omega_h^2) [y_g][M] \{y_h\} = 0 \quad (D-4)$$

and, for distinct ω , then

$$[y_g][M] \{y_h\} = 0, \quad g \neq h \quad \text{Q.E.D.} \quad (D-5)$$

Thus, we have shown that any two eigenvectors of the system are orthogonal with respect to the inertia matrix M . To obtain the explicit relation required, relation (D-5) can be written in expanded form as

$$\begin{array}{c}
 \left(\begin{array}{c|c} \frac{a_0}{R_0} & \frac{a_1}{R_0} \dots \frac{a_n}{R_0} \\ \hline \frac{c_0}{R_0} & \frac{c_1}{R_0} \dots \frac{c_i}{R_0} \end{array} \right) \left(\begin{array}{c} \lambda_1 \\ \lambda_2 \end{array} \right) \quad (g)
 \end{array}
 \left[\begin{array}{ccc|ccc}
 I_{F_0} & & & 0 & 0 & \dots & 0 & 0 & 0 \\
 & I_{F_1} & & 0 & 0 & \dots & 0 & 0 & 0 \\
 & & \ddots & \vdots & \vdots & \ddots & \vdots & \vdots & \vdots \\
 & & & I_{F_n} & & & 0 & 0 & 0 \\
 \hline
 0 & 0 & \dots & 0 & & & I_{V_0} & & 0 & R_0 h p_s \zeta_0(s) \\
 0 & 0 & \dots & 0 & & & & I_{V_1} & & 0 & R_0 h p_s \zeta_1(s) \\
 & & \ddots & & & & & & \ddots & & \vdots \\
 0 & 0 & \dots & 0 & & & & & & I_{V_i} & 0 & R_0 h p_s \zeta_i(s) \\
 \hline
 0 & 0 & \dots & 0 & & & 0 & 0 & \dots & 0 & 0 \\
 \hline
 0 & 0 & \dots & 0 & R_0 h p_s \zeta_0(s) & \dots & R_0 h p_s \zeta_i(s) & & 0 & & 0
 \end{array} \right] \quad (h)
 \left\{ \begin{array}{c} \frac{a_0}{R_0} \\ \frac{a_1}{R_0} \\ \vdots \\ \frac{a_n}{R_0} \\ c_0 \\ c_1 \\ \vdots \\ c_i \\ \lambda_1 \\ \lambda_2 \end{array} \right\} = 0$$

104

By performing the indicated matrix multiplication, equation (D-6) takes the form

$$\begin{aligned}
& \frac{a_0^{(g)}}{R_0} I_{F_0} \frac{a_0^{(h)}}{R_0} + \dots + \frac{a_n^{(g)}}{R_0} I_{F_n} \frac{a_n^{(h)}}{R_0} + \left\{ \left(c_0^{(g)} I_{V_0} + \lambda_2^{(g)} R_0 h \rho_s \zeta_0(s) \right) \right\} c_0^{(h)} \\
& + \dots + \left\{ \left(c_i^{(g)} I_{V_i} + \lambda_2^{(g)} R_0 h \rho_s \zeta_i(s) \right) \right\} c_i^{(h)} \\
& + \dots + \left\{ \left(c_0^{(g)} R_0 h \rho_s \zeta_0(s) + \dots + c_i^{(g)} R_0 h \rho_s \zeta_i(s) \right) \right\} \lambda_2^{(h)} = 0
\end{aligned}$$

Therefore, the solution form for any one of the components of the h th eigenvector, say $\left(\frac{a_0}{R_0} \right)^{(h)}$ is

$$\frac{a_0^{(h)}}{R_0} = \frac{1}{I_{F_0} \frac{a_0^{(g)}}{R_0}} \left\{ \begin{aligned} & \frac{a_1^{(g)}}{R_0} \frac{a_1^{(h)}}{R_0} I_{F_1} + \dots + \frac{a_n^{(g)}}{R_0} \frac{a_n^{(h)}}{R_0} I_{F_n} + \dots + c_i^{(g)} c_i^{(h)} I_{V_i} \\ & + \lambda_2^{(g)} R_0 h \rho_s \zeta_0(s) c_0^{(h)} + \dots + \lambda_2^{(g)} R_0 h \rho_s \zeta_i(s) c_i^{(h)} \\ & + c_0^{(g)} R_0 h \rho_s \zeta_0(s) \lambda_2^{(h)} + \dots + c_i^{(g)} R_0 h \rho_s \zeta_i(s) \lambda_2^{(h)} \end{aligned} \right\} \quad (D-7)$$

or in more general terms

$$y_0^{(h)} = \frac{1}{A_0} \left[A_1 y_1^{(g)} y_1^{(h)} + \dots + A_i y_i^{(g)} y_i^{(h)} \right] \quad (D-8)$$

Now utilizing the fact that

$$\frac{a_1^{(h)}}{R_0} \equiv \frac{a_1^{(h)}}{R_0}, \quad \frac{a_n^{(h)}}{R_0} \equiv \frac{a_n^{(h)}}{R_0}, \quad c_0^{(h)} \equiv c_0^{(h)}, \text{ etc.} \quad (D-9)$$

which can be stated in general form as

$$y_i^{(h)} \equiv y_i^{(h)}$$

A general expression can be written as follows

$$\begin{Bmatrix} y_0 \\ y_1 \\ \cdot \\ \cdot \\ y_i \end{Bmatrix}^{(h)} = \begin{bmatrix} 0 & A_1 y_1^{(g)} & A_2 y_2^{(g)} & \dots & A_i y_i^{(g)} \\ 0 & 1 & 0 & \dots & 0 \\ \cdot & \cdot & \cdot & \cdot & \cdot \\ \cdot & \cdot & \cdot & \cdot & \cdot \\ 0 & 0 & 0 & \dots & 1 \end{bmatrix} \begin{Bmatrix} y_0 \\ y_1 \\ \cdot \\ \cdot \\ y_i \end{Bmatrix}^{(h)} \quad (D-10)$$

or

$$\{y\}^{(h)} = [S] \{y\}^{(h)}$$

where $[S]$ is commonly termed the sweeping matrix and is applied as follows: From equation (3-54) the eigenvalue problem is

$$[H] \{y\} = \lambda' \{y\}$$

therefore

$$[H][S] \{y\}^{(h)} = \lambda' \{y\}^{(h)} \quad (D-11)$$

and since the contribution of the first mode has been removed, iteration on equation (D-11) will force convergence on the second mode and its corresponding frequency. For higher modes, the process is repeated, and the order of the sweeping matrix reduces for each successive operation. Note, however, that because of cumulative errors which are usually incurred in the successive sweeping matrix operation, it is wise to check the highest mode by inversion of the original matrix equation.

Appendix E - Computer Programs

Those computer programs necessary to the solution of the systems problem developed in the investigation, contained herein and developed specifically to support this investigation are presented on the pages following.

Propellant Cylinder Shear Modes

```

PROGRAM A2168 (INPUT,OUTPUT,TAPE5=INPUT,TAPE6=OUTPUT)
DIMENSION ROOT(50),R(700),P(700),PPR(700),XLAMBDA(100),RIJ(700),
1RJ(700),RBRJ(700),SUM(700),RY(1000),RIY(1000),TITLE(8),RBRY(700)
COMMON RZ,RI,IC,A1,A2,A3,A4,A5,A6,A7,A8,
REAL MFN,IFN,
EXTERNAL FOFX,
NAMELIST/NAM1/A,B,DX,RZ,RI,E1,E2,MAXI,RBR,LMAX,RL,DR,RMAX,GF,
1DELTA,EL,RC,FK,A1,A2,A3,A4,A5,A6,A7,A8,GR,
CALL CALCOMP,
CALL LEROY,
70 READ(5,106)TITLE,
READ(5,NAM1),
WRITE(6,NAM1),
WRITE(6,105),
WRITE(6,106)TITLE,
SQ=SQRT(GF*GR/DELTA),
PI=3.14159,
FA=2.*PI*DELTA*EL/GR,
IC=1
DO 30 I=1,LMAX,
DDX=DX
CALL ITR2(X,A,B,DDX,FOFX,E1,E2,MAXI,ICODE),
IF(ICODE)1,2,1,
2 XLAMBDA(I)=X,
A=X+DX,
30 CONTINUE,

```

```

      GO TO 4.
1   PRINT 102, ICODE, I.
102 FORMAT(1X, 8HERROR NO, I4, 2BH IN ITR2 SUBROUTINE, ROOT NO, I4),
      IF(I.GT.1)GO TO 3.
      STOP.
3   LMAX=I-1.
4   DO 40 I=1, LMAX.
      NRR=0.
      K=1.
      R(K)=RL.
      XLRO=XLAMBDA(I)*RI
      XLRBR=XLAMBDA(I)*RBR.
      CALL BSSLS(XLRO, RIJ, 2, IERR).
      ME=1.
      IF(IERR)5, 6, 5.
5   PRINT 100, ME, XLAMBDA(I).
100 FORMAT(1X, 47HERROR IN BSSLS SUBROUTINE USING R AND LAMBDA AS, I3,
      1E15.7).
      STOP.
6   CALL BSSLS(XLRBR, RBRJ, 2, IERR).
      ME=3.
      IF(IERR)5, 8, 5.
8   CALL BF4F(XLRO, RIY, 2, IERR, -1).
      M3=1.
      IF(IERR)9, 10, 9.
9   PRINT 101, IERR, M3, XLAMBDA(I).
101 FORMAT(1X, 8HERROR NO, I4, 42H IN BF4F SUBROUTINE USING R AND LAMBDA
      1 AS, I3, E15.7).
      STOP.
10  CALL BF4F(XLRBR, RBRY, 2, IERR, -1).
      M3=3.
      IF(IERR)9, 12, 9.
12  F1=A3*XLRO*RIJ(1)-A4*RIJ(2).
      F2=F1*RBRY(2).
      F3=A7*XLRO*RIY(1)-A8*RIY(2).
      F4=F2-F3*RBRJ(2).
18  XLR=XLAMBDA(I)*R(K).
      WRITE(6, 110)XLAMBDA(I), R(K), XLR.
110 FORMAT(* LAMBDA =*E15.7, * R =*E15.7, * XLR =*E15.7).
      CALL BSSLS(XLR, RJ, 2, IERR).
      ME=2.
      IF(IERR)5, 13, 5.
13  CALL BF4F(XLR, RY, 2, IERR, -1).
      M3=2.

```

```

      IF(IERR)9,14,9,
14  P(K)=(F1*RY(2)-F3*RJ(2))/F4,
      RDR=R(K)+DR,
      IF(NRR.EQ.1)GO TO 20,
      IF(RDR.LT.RMAX)15,50,
15  K=K+1,
      R(K)=RDR,
      GO TO 18,
50  NRR=1,
      K=K+1,
      R(K)=RMAX,
      GO TO 18,
20  DO 16 M=1,K,
16  PPR(M)=R(M)*P(M)**2,
      CALL TRAP(PPR,R,K,SUM,0),
      MFN=FA*SUM(K),
      OMEG=XLAMBDA(1)*SQ,
      EF=OMEG/(2.*PI),
      IFN=RZ**2*MFN,
      BUF=IFN*OMEG**2,
      PROD=RC*P(K)
      WRITE(6,107),
      WRITE(6,108)XLAMBDA(1),OMEG,EF,MFN,IFN,BUF,PROD,
      CALL PLOT(K,R,P,EF,FK),
40  CONTINUE,
      GO TO 70,
105 FORMAT(1H1,/,15X,*ELASTIC FUEL SHEAR TWIST MODES*)
106 FORMAT(8A10),
107 FORMAT(/,5X,6HLAMBDA,9X,8HFREQ RPS,7X,8HFREQ CPS,7X,8HGEN MASS,
110X,*INF*,.11X,*BUF*,.10X,*PROD*),
108 FORMAT(7E15.7),
      END,
      FUNCTION FOFX(X)
      DIMENSION RANS(700),RIANS(700),RST(700),RIST(700),
      COMMON RZ,RI,IC,A1,A2,A3,A4,A5,A6,A7,A8,
      XR=X*RZ,
      XRI=X*RI,
      CALL BSSLS(XR,RANS,2,IERR),
      IF(IERR)1,2,1,
1  PRINT 101,X,
101 FORMAT(1X,36HERROR IN BSSLS SUBROUTINE, FOFX ROOT,E15.7),
      STOP,
2  CALL BSSLS(XRI,RIANS,2,IERR),
      IF(IERR)1,3,1,

```

```

3 CALL BF4F(XR,RST,2,IERR,-1),
  IF(IERR)5,4,5,
5 PRINT 102,IERR,X,
102 FORMAT(1X,8HERROR NO,14,31H IN BF4F SUBROUTINE, FOFX ROOT,E15.7),
  STOP,
4 CALL BF4F(XRI,RIST,2,IERR,-1),
  IF(IERR)5,6,5,
6 FOFX=(A1*XR*RANS(1)-A2*RANS(2))*(A3*XRI*RIST(1)-A4*RIST(2))-
  (A5*XR
  1*RST(1)-A6*RST(2))*(A7*XRI*RIANS(1)-A8*RIANS(2)),
  IF(IC.EQ.1)20,30,
20 WRITE(6,103)X,FOFX,RIANS(1),RIST(1),
103 FORMAT(/1X,2HX=,E15.7,2X,3HFX=,E15.7,2X,7HJRI(1)=,E15.7,7HYRI(1)=
  1E15.7/)
  IC=IC+1,
30 CONTINUE,
  RETURN,
  END,
  SUBROUTINE TRAP(Y,X,NL,SUM,SUM1),
  DIMENSION Y(NL),X(NL),SUM(NL),
  SUM(1)=SUM1,
  NLM=NL-1,
  DO 1 N=1,NLM,
  NP=N+1,
  1 SUM(NP)=SUM(N)+(Y(NP)+Y(N))*(X(NP)-X(N))/2.,
  RETURN,
  END,
  SUBROUTINE PLOT(K,R,P,EF,FK),
  DIMENSION R(700),P(700),X(702),Y(702),PHI(700),
  DO 10 I=1,K,
  10 PHI(I)=P(I)/R(I),
  PMAX=PHI(1),
  DO 20 I=1,K,
  IF(PHI(I).GT.PMAX)15,20,
  15 PMAX=PHI(I),
  20 CONTINUE,
  F=1./(FK*PMAX),
  DO 40 I=1,K,
  PHI(I)=PHI(I)*F,
  X(I)=R(I)*COS(PHI(I)),
  40 Y(I)=R(I)*SIN(PHI(I)),
  WRITE(6,100)(R(I),P(I),PHI(I),X(I),Y(I),I=1,K),
  100 FORMAT(/7X,*R*,14X,*P*,12X,*PHI*,14X,*X*,14X,*Y*/(5E15.7)),
  CALL GRID(0.,0.,1.,1.,5,5),
  CALL ASCALE(X,5.,K,1,20.),

```

```

CALL ASCALE(Y,5.,K,1,20.),
K1=K+1,
K2=K+2,
Y(K2)=X(K2),
CALL AXES(0.,0.,C.,5.,X(K1),X(K2),1.,2.,1HX.,125,-1),
CALL AXES(0.,0.,90.,5.,Y(K1),Y(K2),1.,2.,1HY.,125,1),
CALL NOTATE(2.,5.5.,14.,11HFREQUENCY =.0.,11),
CALL NUMBER(3.8,5.5.,14, EF,0.,3),
CALL LINPLT(X,Y,K,1,0,0,0,0),
CALL CALPLT(10.,0.,-3),
RETURN,
END,

```

```

PROGRAM A2168      CASE 7CK-1A      FREE-FREE      4-29-70
$NAM1 A=.01,B=20.,DX=.01,RZ=7.,RI=.5,E1=.1E-6,E2=.1E-6,MAXI=100,RBR=7.,
GR=386.,,
LMAX=15,RL=.5,DR=.25,RMAX=7.,GF=90.,DELTA=53.460E-3,EL=1.,RC=.5,A1=1.,
A2=2.,A3=1.,A4=2.,A5=1.,A6=2.,A7=1.,A8=2.,FK=5.73$
-,
-,
-,

```

Systems Eigenvalue Program

```
PROGRAM A0107 (INPUT,OUTPUT,TAPES=INPUT,TAPE6=OUTPUT)
DIMENSION XM(40,40),W(40),XN(40,40),XIF(40),PP(40),V(40),ZI(40),,
1XG(40),WI(40),P(40),
2,FK(40),WV(40),GFV(40),R(10),
DIMENSION HEAD(8),
NAMELIST /NAM1/W,XL,GF,RZ,PP,P,V,WI,ZI,XH,RHO,NN,II,XIF,F1,I4,
1I1,I6,TEST,G,C1,ER1,XG,RN,FK,TA3,DTA3,TF,NROOTS,EPS,ER2,
1 READ(5,103)HEAD,
IF(EOF,5)2,3,
2 STOP,
3 READ(5,NAM1),
WRITE(6,NAM1),
WRITE(6,104)HEAD,
DO 10 I=1,40,
DO 10 J=1,40,
XM(I,J)=0.,
10 XN(I,J)=0.,
PI=3.14159,
NAB=NN+II+2,
NC=NN+II+1,
DO 50 J=1,NN,
IF(W(J).EQ.0.)22,24,
22 R(1)=0.,
NR=1,
GO TO 18,
24 B=-FK(J)*W(J)**2/GF,
C=-W(J)**2,
K=3,
T3=TA3,
DO 15 I=1,NROOTS,
8 CALL SEARCH2(T3,DTA3,TF,ER2,FN2,K,DFN2),
GO TO(4,5,6),K,
4 FN2=T3**2+B*T3**EPS+C,
DFN2=2*T3+EPS*B*T3**(EPS-1),
GO TO 8,
5 R(I)=T3,
15 CONTINUE,
NR=NROOTS,
GO TO 18,
```

CC4

```

6 NR=I-1,
  IF(NR.NE.0)GO TO 18,
  WRITE(6,106)W(J),
106 FORMAT(/* NO ROOTS FOUND FOR W =*E15.7),
  STOP,
18 WRITE(6,105)W(J),(R(I),I=1,NR),
105 FORMAT(/* W =*E15.7,/* ROOTS =*(6E15.7)),
  WV(J)=R(1),
  IF(EPS.EQ.0.)26,28,
26 FA=1.,
  GO TO 32,
28 FA=R(1)**EPS,
32 GFV(J)=FK(J)*FA,
  WRITE(6,107)GFV(J),
107 FORMAT(* GFV =*E15.7),
50 CONTINUE,
  DO 20 N=1,NN,
  XM(N,N)=XIF(N),
  XN(N,N)=WV(N)**2*XIF(N)+F1*2*PI*GFV(N)*(RZ**2)*PP(N)**2,
  XN(N,NC)=RZ*P(N),
  XN(NC,N)=RZ*P(N),
20 XN(NAB,N)=XN(N,NAB)=RZ*GFV(N)*(PP(N)-P(N)/RN),
  NC1=NN+11,
  NN1=NN+1,
  I=1,
  DO 25 N=NN1,NC1,
  XM(N,N)=V(I),
  XN(N,N)=V(I)*WI(I)**2,
  XN(N,NC)=-RN*ZI(I),
  XN(NC,N)=-RN*ZI(I),
  XM(N,NC+1)=XM(NC+1,N)=RZ*XH*RHO*ZI(I),
25 I=I+1,
  DO 30 JJ=1,NAB,
  WRITE(6,100)JJ,(XM(JJ,J),J=1,NAB),
30 CONTINUE,
  WRITE(6,101),
  DO 40 JJ=1,NAB,
  WRITE(6,102)JJ,(XN(JJ,J),J=1,NAB),
40 CONTINUE,
  CALL INVERT(NAB,I4,I1,I6,40,TEST,G,C1,ER1,XM,XN,XG),
  GO TO 1,
100 FORMAT(* M(*,I2,*,1)=*/(8E15.7)),
101 FORMAT(/),
102 FORMAT(* N(*,I2,*,1)=*/(8E15.7))

```

```

103 FORMAT(8A10),
104 FORMAT(/,10X,8A10),
      END,
      SUBROUTINESEARCH2(TA2,DTA2,TF,ER2, FN2,K,DFN2),
      REALLAMA,LAMB,
      GOTO(1,2,3),K,
1   IF(JF.GE.2)GOTO4,
5   TA1=TA2,
      FN1=FN2,
      DFN1=DFN2,
      IE=0,
      FS=0.,
      GOTO6,
2   FN1=(DFN2/ABS(DFN2))*0.00001,
7   DFN1=DFN2,
      TA1=TA2,
      JF=1,
      GOTO8,
3   DFN1=0.,
      FN1=0.,
      TA1=0.,
      JEND=0,
      JF=0,
8   LAMA=0.,
      LAMB=0.,
      JW=0,
      JK=0,
6   TA2=TA2+DTA2,
      JF=JF+1,
9   IF(TA2.GT.TF)GOTO10,
11  K=1,
      RETURN,
10  IF(JEND.EQ.3)GOTO12,
      TA2=TF,
      JEND=JEND+1,
      GOTO11,
12  K=3,
      RETURN,
4   IF(JK.EQ.1)GOTO13,
      IF(FN2/FN1)14,15,16,
16  IF(IE.EQ.0)GOTO17,
18  IF((FN2-FS)/FN2.LE.ER2)GOTO19,
      A1=DFN1,
      A2=(FN2-FN1-DFN1*(TA2-TA1))/(TA2-TA1)**2,

```

```

    TA3=TA1-A1/(2.*A2),
    FS=FN2,
    IF (IE.EQ.1)GOTO20,
    IE=1,
    GOTO25,
20  TA1=TA2,
    FN1=FN2,
    DFN1=DFN2,
25  TA2=TA3,
    GOTO9,
19  FN2=SFN2,
    DFN2=SDFN2,
    TA2=STA2,
    FN1=FN2,
    IE=0,
    FS=0.,
    GOTO7,
17  IF (DFN1/DFN2.GE.0.)GOTO5,
    IF (DFN1*FN1.GE.0.)GOTO5,
    SFN2=FN2,
    SDFN2=DFN2,
    STA2=TA2,
    GOTO18,
14  IE=0,
    FS=0.,
13  A0=FN1,
    A1=DFN1,
    A2=(FN2-FN1-DFN1*(TA2-TA1))/(TA2-TA1)**2,
    TA31=(-A1+SQRT(A1**2-4.*A0*A2))/(2.*A2)+TA1
    TA32=(-A1-SQRT(A1**2-4.*A0*A2))/(2.*A2)+TA1,
    IF (TA1.LE.TA31.AND.TA31.LE.TA2)GOTO22,
    IF (TA1.LE.TA32.AND.TA32.LE.TA2)GOTO23,
    Q=ABS(TA31-TA2),
    R=ABS(TA32-TA2),
    TA3=AMIN1(Q,R),
    IF (TA3.EQ.Q)GOTO22,
    GOTO23,
22  TA3=TA31,
    GOTO24,
23  TA3=TA32,
24  LAMA=LAMB,
    LAMB=TA3,
    JK=1,
    JW=JW+1,

```

```

      IF (JW.LT.2)GOTO20,
      TEST=(LAMB-LAMA)/LAMB,
      IF (ABS(TEST).GE.ER2)GOTO20,
21  K=2,
      TA2=LAMB,
      RETURN,
15  LAMB=TA2,
      GOTO21,
102 FORMAT(1X*INTERPOLATED TIME IS NOT BETWEEN T1 AND T2*),
      END,
      SUBROUTINE INVERT(N,I4,I1,I6,NMAX,TEST,G,C1,ER1,A,B,XG),
C   PROG. NO. 0107 RCM ROSS GOBLE,
      EXTERNALMATINV,
C   IL=LENGTH OF GUFSS VECTOR,
C   I1=0 NORMALIZE ON MAXIMUM ELEMENT,=NO. NORMALIZE ON NO.,
C   I2=ELEMENT WHICH IS NORMALIZED ON,
C   I4=NO. OF MODES WANTED,
      DIMENSIONA(40,40),XB(40),X(40),AH(40,40),B(40,40),C(40,40),
1  INDEX(40,2),AM(40,40),XV(40,40),WB(40,4),I1(3),ERR(4),
1  XG(40),
      I1(1)=I1
      I1(2)=I4
      I1(3)=I6
      ERR(1)=TEST
      ERR(2)=ER1
      ERR(3)=C1
      ERR(4)=G
14  DO15I=1,N,
      DO15J=1,N,
15  AM(I,J)=A(I,J),
      CALLEIGEN(I,I,N,NMAX,I3,ERR,SUM1,A,B,AM,AH,C,XV,INDEX,XG,X,XB,WB,
1  MATINV)
      WRITE(6,110)SUM1,
      WRITE(6,112),
      WRITE(6,113),
      DO1 I=1,I3,
      WRITE(6,109),
      WRITE(6,111)(WB(I,J),J=1,4)
      WRITE(6,109),
1  WRITE(6,106)(XV(J,I),J=1,N),
      RETURN,
100 FORMAT(1X11A6),
106 FORMAT(7E16.8),
109 FORMAT(1X/),

```

```

110 FORMAT(1X4HSUM=,E16.8),
111 FORMAT(4E16.8),
112 FORMAT(6X3HLAM14X1HW15X3HSUM10X2HI5),
113 FORMAT(7X4HX.(I').),
      END,
      SUBROUTINEEIGEN(I1,IL,NX,I3,ERR,SUM1,A,B,MASS,AH,C,XV,INDEX,XG,X,
1XB,WB,MATINV)
      REALMASS,LAM,LAMX
      DIMENSIONA(NX,IL),B(NX,IL),MASS(NX,IL),AH(NX,IL),XV(NX,IL),XG(IL)
1,X(IL),XB(IL),WB(NX,4),C(NX,IL),INDEX(NX,2),I1(3),ERR(4)
      I1=I1(1)
      I4=I1(2)
      I6=I1(3)
      ER=ERR(1)
      ER1=ERR(2)
      C1=ERR(3)
      G=ERR(4)
      DO4I=1,IL,
      DO4J=1,IL
4 B(I,J)=B(I,J)+C1*MASS(I,J),
      DO 60 I=1,IL,
      WRITE(6,100)I,(B(I,J),J=1,IL),
60 CONTINUE,
100 FORMAT(* ADD(*,I2,*+1)=*/(8E15.7)),
      DO11I=1,IL,
      DO11J=1,IL,
11 B(I,J)=B(I,J)/G,
      CALLMATINV(B,IL,C,0,DETERM,X,INDEX,NX,ISCALE)
      DO22I=1,IL,
      DO22K=1,IL,
      C(I,K)=0.,
      DO22J=1,IL,
22 C(I,K)=B(I,J)*MASS(J,K)+C(I,K),
      SUM1=0.,
      DO23I=1,IL,
      DO23K=1,IL,
23 SUM1=SUM1+C(I,K)*C(K,I),
      IF(C1.EQ.0.)GOTO71,
      TEST1=ABS(G/C1),
71 I3=0,
      SUM=0.,
      LAMX=0.,
      DO20I=1,IL,
      DO20J=1,IL,

```

```

20 B (I,J)=0.,
   DO21 I=1,IL,
     J=I,
21 B (I,J)=1.,
   DO19 I=1,IL,
     DO19 J=1,IL,
19 AH(I,J)=C(I,J),
26 I5=0,
   DO31 I=1,IL,
31 XB(I)=XG(I),
   8 DO2I=1,IL,
     X(I)=0.,
     DO2J=1,IL,
   2 X(I)=AH(I,J)*XB(J)+X(I),
     I5=I5+1,
     IF(I5.LT.(I6-I0))GOTO50,
     WRITE(6,103)LAM,
50 IF(I5.LE.I6)GOTO25,
   WRITE(6,105),
   RETURN,
25 IF(I1.NE.0)GOTO1,
   I2=1,
   DO3I=1,IL,
     IF(ABS(X(I2)).GE.ABS(X(I)))GOTO3,
     I2=I,
   3 CONTINUE,
     GOT05,
   1 I2=I1,
   5 LAM=ABS(X(I2)),
     DO6I=1,IL,
   6 X(I)=X(I)/LAM,
     DO18I=1,IL,
18 XB(I)=X(I),
   TLAM=ABS((LAM-LAMX)/LAM),
   IF(TLAM.LE.ER)GOTO7,
   LAMX=LAM,
   GOT08,
   7 Q=ABS((G/LAM)-C1),
     SUM=SUM+LAM**2,
     W=SQRT(Q),
     IF(C1.EQ.0.)GOTO70,
     IF(ABS(LAM-TEST1).GT.ER1)GOTO70,
     W=0.,
70 I3=I3+1,

```

```

WB(I3,1)=LAM
WB(I3,2)=W
WB(I3,3)=SUM
WB(I3,4)=I5
DO9I=1,IL,
9  XV(I,I3)=X(I),
   IF(I3.LT.14.)GOTO30,
   RETURN ,
30  DO10I=1,IL,
     DO10K=1,IL,
     A(I,K)=0.,,
     DO10J=1,IL,
10  A(I,K)=X(I)*X(J)*MASS(J,K)+A(I,K),
     DO12I=1,IL,
     XB(I)=0.,,
     DO12J=1,IL,
12  XB(I)=X(J)*MASS(J,I)+XB(I),
     DENO=XB(I)*X(I),
     DO13I=2,IL,
13  DENO=DENO+XB(I)*X(I),
     DO14I=1,IL,
     DO14J=1,IL,
14  A(I,J)=A(I,J)/DENO,
     DO15I=1,IL,
     DO15J=1,IL,
15  A(I,J)=B(I,J)-A(I,J),
     DO16I=1,IL,
     DO16J=1,IL,
16  B(I,J)=A(I,J),
     DO17I=1,IL,
     DO17K=1,IL,
     AH(I,K)=0.,,
     DO17J=1,IL
17  AH(I,K)=C(I,J)*A(J,K)+AH(I,K),
     GOTO26 ,
103 FORMAT(7E16.8),
105. FORMAT(1X17HDOES NOT CONVERGE),
END,

```